USGS
science for a changing world

Prepared in cooperation with the U.S. Environmental Protection Agency Great Lakes Restoration Initiative; the Michigan Department of Natural Resources; and the Michigan Department of Environment, Great Lakes, and Energy

Development of a Two-Dimensional Hydraulic Model for the Kalamazoo River Between the Trowbridge and Allegan City Dams, Michigan

Scientific Investigations Report 2026–5026

U.S. Department of the Interior
U.S. Geological Survey

Cover. Photograph showing the Trowbridge Dam, taken from downstream on the 26th St. bridge over the Kalamazoo River, Michigan, on June 13, 2024, by Collin Roland, U.S. Geological Survey.

Development of a Two-Dimensional Hydraulic Model for the Kalamazoo River Between the Trowbridge and Allegan City Dams, Michigan

By Collin J. Roland, Angus A. Vaughan, Faith A. Fitzpatrick, Heidi M. Broerman, and J. William Lund

Prepared in cooperation with the U.S. Environmental Protection Agency Great Lakes Restoration Initiative; the Michigan Department of Natural Resources; and the Michigan Department of Environment, Great Lakes, and Energy

Scientific Investigations Report 2026–5026

U.S. Department of the Interior
U.S. Geological Survey

U.S. Geological Survey, Reston, Virginia: 2026

Suggested citation:
Roland, C.J., Vaughan, A.A., Fitzpatrick, F.A., Broerman, H.M., and Lund, J.W., 2026, Development of a two-dimensional hydraulic model for the Kalamazoo River between the Trowbridge and Allegan City Dams, Michigan: U.S. Geological Survey Scientific Investigations Report 2026–5026, 54 p., https://doi.org/10.3133/sir20265026.

Associated data for this publication:
Roland, C.J., Vaughan, A., Broerman, H.M., Lund, J.W., and Fitzpatrick, F.A., 2025, Model application data release for a 2D hydraulic model (HEC–RAS) of the Kalamazoo River Trowbridge Dam to Allegan City Dam reach: U.S. Geological Survey data release, https://doi.org/10.5066/P13CPA5B

U.S. Geological Survey, 2025, USGS water data for the Nation: U.S. Geological Survey National Water Information System database, https://doi.org/10.5066/F7P55KJN.

Vaughan, A.A., Fitzpatrick, F.A., Strange, J.M., Roland, C.J., and Broerman, H.M., 2023, Geomorphic reference reach data for the Kalamazoo River Basin, Michigan Area of Concern (ver. 2.0, October 2024): U.S. Geological Survey data release, https://doi.org/10.5066/P96JBHF4.

ISSN 2328-0328 (online)

Acknowledgments

The authors thank John Riley, Dan Peabody, and Jennifer Tewkesbury (Michigan Department of Environment, Great Lakes, and Energy); Matt Diana, Patrick Ertel, Mark Mills, and Brian Gunderman (Michigan Department of Natural Resources); Paul Ruesch and Susan Virgilio (U.S. Environmental Protection Agency); Keegan Roberts and Jaren Miller (CDM Smith); and Dr. Kenneth M. Kornheiser and Doug McLaughlin (Kalamazoo River Watershed Council) for their thoughtful feedback on this work. Funding provided by the U.S. Environmental Protection Agency Great Lakes Restoration Initiative.

Contents

Figures

Tables

Conversion Factors

U.S. customary units to International System of Units

Multiply	By	To obtain
	Length	
inch (in.)	25.4	millimeter (mm)
foot (ft)	0.3048	meter (m)
mile (mi)	1.609	kilometer (km)
	Area	
square mile (mi^2)	2.590	square kilometer (km^2)
	Volume	
cubic yard (yd^3)	0.7646	cubic meter (m^3)
	Flow rate	
foot per second (ft/s)	0.3048	meter per second (m/s)
cubic foot per second (ft^3/s)	0.02832	cubic meter per second (m^3/s)
	Density	
pound per cubic foot (lb/ft^3)	16.02	kilogram per cubic meter (kg/m^3)
	Hydraulic gradient	
foot per mile (ft/mi)	0.1894	meter per kilometer (m/km)
	Pressure	
pound per square foot (lb/ft^2)	0.04788	kilopascal (kPa)

International System of Units to U.S. customary units

Multiply	By	To obtain
	Length	
millimeter (mm)	0.03937	inch (in.)
meter (m)	3.281	foot (ft)
	Flow rate	
square meter per second (m^2/s)	35.31	square foot per second (ft^2/s)
	Density	
kilogram per cubic meter (kg/m^3)	0.06242	pound per cubic foot (lb/ft^3)

Temperature in degrees Fahrenheit (°F) may be converted to degrees Celsius (°C) as follows:

$$°C = (°F - 32) / 1.8.$$

Datums

Vertical coordinate information is referenced to the National Geodetic Vertical Datum of 1929 (NGVD 29).

Horizontal coordinate information is referenced to the North American Datum of 1983 (NAD 83).

Supplemental Information

Frequency of the velocity sample collection is given in hertz (Hz).

Abbreviations

1D	one-dimensional
2D	two-dimensional
ADCP	acoustic Doppler current profiler
AEP	annual exceedance probability
D	critical grain diameter
GNSS	global navigational satellite system
HEC–RAS	Hydrologic Engineering Center River Analysis System
μ	arithmetic mean
n	Manning's roughness coefficient
NLCD	National Land Cover Database
NRTK	network real-time kinematic
PCB	polychlorinated biphenyl
RMSE	root mean square error
RSS	relative substrate stability
σ	standard deviation
USACE	U.S. Army Corps of Engineers
USGS	U.S. Geological Survey
WSE	water surface elevation

Development of a Two-Dimensional Hydraulic Model for the Kalamazoo River Between the Trowbridge and Allegan City Dams, Michigan

By Collin J. Roland, Angus A. Vaughan, Faith A. Fitzpatrick, Heidi M. Broerman, and J. William Lund

Abstract

The U.S. Geological Survey developed a two-dimensional hydraulic model for a 9.2-mile reach of the Kalamazoo River between the Trowbridge and Allegan City Dams. The model simulates streamflow conditions with spatial coverage and resolution that would be difficult or dangerous to document with field measurements, enabling assessments of habitat connectivity and substrate stability to support dam removal and restoration planning. The model was calibrated with surveyed water surface elevation (WSE) profiles, streamgage WSE time series, and measured depth-average velocities. Modeled WSE profiles had root mean square error (RMSE) values of 0.20 and 0.32 foot. Cross-sectional average velocities were slightly underpredicted, with RMSE of 0.28 and 0.30 foot per second (ft/s). Channel roughness varied with stage, and the high-flow model reproduced streamgage WSE time series with an RMSE of 0.04 foot. Quasi-steady simulations at 4,000 cubic feet per second (ft^3/s), about the 50-percent annual exceedance probability streamflow, indicated that cross-sectional average velocities within 3.4 miles downstream from Trowbridge Dam were commonly between 3 and 4 ft/s, occasionally exceeding 4 ft/s. Farther downstream, velocities seldom exceeded 3 ft/s. Simulated shear stresses were used to estimate substrate stability in the reach. At 4,000 ft^3/s, the minimum stable grain size along most of the main channel was predicted to be in the pebble range (4–64 millimeters), and sands and silts were predicted to be stable in the floodplain and backwaters.

Plain Language Summary

The U.S. Geological Survey built a detailed computer model of how water moves through a 9.2-mile stretch of the Kalamazoo River between the Trowbridge and Allegan City Dams to support dam removal and river restoration planning. Model results were checked against field measurements of water levels and flow speeds, and the model matched water levels very closely (generally within a few inches). Flow speeds were slightly underpredicted, by an average of 0.28 foot per second (ft/s). For a streamflow scenario of 4,000 cubic feet per second (a flow size expected in about half of all years), the model showed that in the first 3.4 miles below Trowbridge Dam, average flow speeds are often 3–4 ft/s and sometimes greater than 4 ft/s. Farther downstream, average speeds rarely exceed 3 ft/s. From the simulated bed shear stresses, the smallest riverbed material likely to stay in place at this flow is mostly pebbles (4–64 millimeters) in the main channel. Finer sands and silts are expected to remain stable in floodplain and backwater areas, where currents are slower. The model gives a high-resolution picture of water levels, currents, and sediment stability in places and at streamflow conditions that are hard to measure in the field. Those insights help decision makers understand habitat connectivity and bed stability as they plan dam removal and river restoration actions.

Introduction

Millions of low-head dams are estimated to exist along rivers across the United States (Graf, 1993), altering river hydraulics, impounding sediment, and affecting aquatic ecosystems (Fencl and others, 2015). As this infrastructure ages and degrades, its utility for its intended function(s) (such as electricity generation, water supply, or navigation) may lapse, and the possibility of catastrophic failure increases, prompting dam owners to consider dam removal as an alternative to continued upkeep (Bellmore and others, 2017). Although dam removal can reestablish natural streamflow regimes and reconnect aquatic habitats, it can also mobilize contaminated sediments that were deposited in impoundments, potentially negatively affecting downstream reaches (Bednarek, 2001; Evans, 2015).

From the mid-1800s through the early 1900s, numerous dams were constructed on the Kalamazoo River and its tributaries for navigation and power generation. At least seven of these dams (Morrow, Plainwell, Otsego City, Otsego Township, Trowbridge, Allegan City, and Calkins Bridge) remained in some form at least through the end of the 20th century (fig. 1). Of these dams, four (Plainwell, Otsego City, Otsego Township, and Trowbridge) were low-head run-of-river dams. About 80 miles (mi) of the Kalamazoo River stretching from Morrow Dam to Lake

Michigan were designated as an Area of Concern under the 1987 Great Lakes Water Quality Agreement because of polychlorinated biphenyl (PCB) contamination. In 1990, the river was designated as a Federal Superfund site. PCBs were historically released in waste discharged to the river during the 1950s–70s from paper mills recycling carbonless copy paper (Blasland, Bouck & Lee, Inc., 1992; Michigan Department of Environmental Quality, 2003). This discharge also contained kaolinite, which sorbed substantial amounts of PCBs and was subsequently deposited in impounded reaches of the river and, to a lesser extent, in the floodplain.

Power generation from the low-head dams ceased in the mid-1960s, and three of the dams (Plainwell, Otsego Township, and Trowbridge) were deeded to the State of Michigan (Rheaume and others, 2002; Arcadis, 2009). Because of their poor condition and lack of continued economic viability, the State of Michigan has worked to progressively decommission and remove the four low-head dams and restore the river to preimpoundment conditions to improve the river's ecological function, recreational value, and human safety. This effort began in the 1970s with the opening of the dams and continued in 1987 with the removal of superstructures including powerhouses, gates, upper abutment walls, and some spillways down to the dam sill. The removal efforts led to a drawdown of water levels by 5−10 feet (ft) in the upstream impoundments, which caused rapid channel incision and bank erosion through the previously submerged, PCB-laden, lacustrine sediment and subsequent deposition of new alluvial material (Rheaume and others, 2002). The mobilization of PCB-laden sediment from previously impounded areas is the principal ongoing source of PCBs to the Kalamazoo River and a primary focus of continued remediation efforts (Arcadis, 2009). The Otsego Township Dam was completely removed during the late 2010s, and its removal was accompanied by excavation of contaminated sediments and channel stabilization to mitigate the sediment transport issues identified with previous dam removal efforts (U.S. Environmental Protection Agency, 2019).

Major channel reconstruction and stabilization projects were conducted to minimize sediment mobilization within the previously impounded reaches. These remediation efforts included construction of grade control structures (engineered riffles) to prevent vertical incision and channel bank stabilization through slope cutbacks, vegetation plantings, and armoring to prevent lateral channel migration (U.S. Environmental Protection Agency, 2019). In preparation for complete removal of the Plainwell, Trowbridge, and Allegan City Dams, the Michigan Department of Environment, Great Lakes, and Energy; the Michigan Department of Natural Resources; the U.S. Environmental Protection Agency; and community organizations are interested in understanding the effects of these structures on streambed substrate habitat quality and fish passage, as well as their similitude with expected predam conditions. To address these concerns, the U.S. Geological Survey (USGS) is focusing studies on free-flowing, unrestored reaches of the Kalamazoo River to characterize their geomorphology and provide reference data that can be used to inform future restoration designs as the State of Michigan continues to pursue complete dam removal. This study uses a two-dimensional (2D) hydraulic model and previously published field observations of sediment size to investigate the distribution of water velocity and substrate stability in a free-flowing, unrestored reach of the Kalamazoo River. The calibrated model provides a means of simulating hydraulic characteristics with high resolution and spatial coverage across the channel and floodplain of the entire study reach. The model was run across a range of streamflow conditions, including high and low flows that would be difficult or dangerous to document via field measurements. The model results are contextualized using threshold velocities for fish passage, and the predicted stability of observed grain sizes is calculated.

Purpose and Scope

This report describes the development of a 2D hydraulic model for a 9.2-mi-long reach of the Kalamazoo River from the Trowbridge Dam to the Allegan City Dam (fig. 1). The primary objective was to produce a hydraulic model that estimates depth-averaged surface water velocity throughout the free-flowing part of the study reach, from just below the Trowbridge Dam to about 42,500 ft (8 mi) downstream, to better understand velocity barriers to fish passage and the hydraulic stability of sediments. In the modeling effort, 11 streamflow scenarios were investigated, including 4 scenarios forced with historical streamflow hydrographs covering March 23–April 14, 2023; January 26–February 14, 2024; June 11–12, 2024; and April 4–6, 2025. These historical scenarios include 50-percent and 20-percent annual exceedance probability (AEP) streamflows, as well as low-flow and bankfull-flow periods during which detailed streamflow velocity and water surface elevation (WSE) observations were collected. The historical streamflow scenarios provided model predictions to inform model calibration and validation against WSE and velocity observations. To improve understanding of more generic streamflow behavior, seven quasi-steady streamflow scenarios, ranging from 1,000 to 7,000 cubic feet per second (ft^3/s) in 1,000 ft^3/s increments, were run. This depth-averaged 2D model does not simulate vertical velocity distributions or rapid velocity fluctuations caused by turbulence, and interpretations of model results are limited to horizontal velocity variability. Furthermore, this model does not simulate rainfall-runoff processes, local contributions to streamflow, or surface water-groundwater interactions.

Previous Studies

The ongoing efforts to remediate PCB contamination and improve aquatic connectivity along the Kalamazoo River have generated studies that are too numerous to fully summarize here (Simard, 2003). These studies have focused on a variety of topics including contaminant distributions in biota,

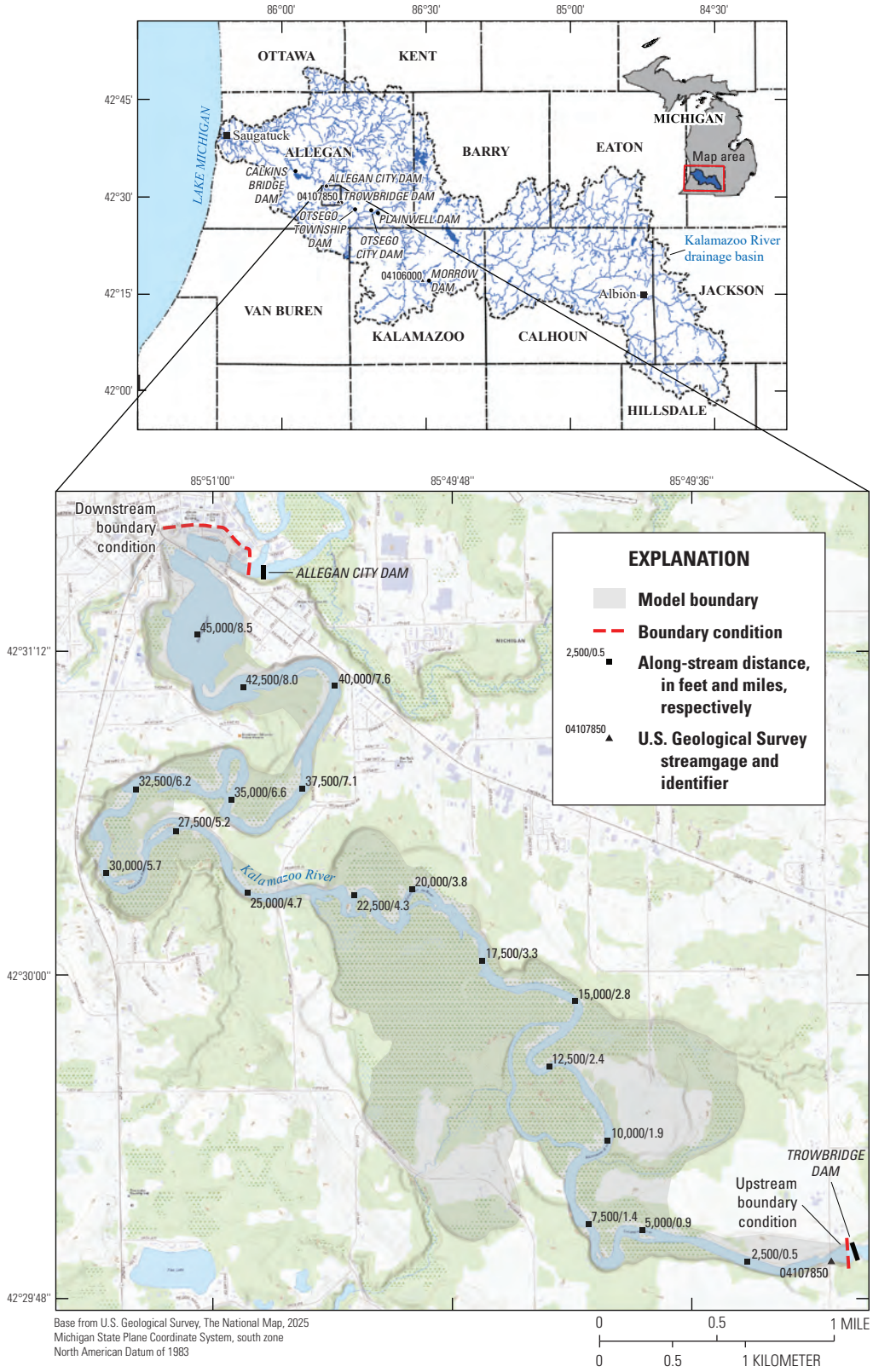

Figure 1. Map showing the Kalamazoo River drainage basin and the model study reach.

sediment, surface water, and groundwater; aquatic ecosystem health; sediment transport; surface water hydraulics; and fluvial geomorphology.

More than 3,000 sediment cores and 6,000 sediment samples have been collected from the river and its floodplains to characterize the horizontal and vertical distributions of sediment size and contaminant concentrations (Arcadis, 2009). In 2000, the USGS and Michigan Department of Environmental Quality collected sediment cores and surveyed transects across the Plainwell, Otsego Township, and Trowbridge impoundments to measure the impounded sediment volumes, investigate their depositional history, and determine contaminant distributions (Rheaume and others, 2002). About 1.2 million cubic yards of accumulated sediment were estimated upstream from the Trowbridge Dam, representing more than 75 percent of the total measured accumulated sediment. In the same study, the researchers identified a distinct depositional sequence within the impoundments, characterized by interbedded lacustrine deposits containing organic-rich silt and clay, fine to medium sand, and minor amounts of gravel overlying predam alluvial deposits consisting primarily of cobbles and gravel. These lacustrine deposits were partially eroded after drawdown of the impoundments as the river channel adjusted toward equilibrium with the increased slope and stream velocity. In some locations, the erosional surface truncating the lacustrine deposits was overlain by alluvial sands and gravels transported by the higher energy conditions postdrawdown (Rheaume and others, 2002). A followup study estimated about 450,000 cubic yards of accumulated sediment in the Otsego City Dam impoundment (Rheaume and others, 2004).

Another study investigated the effects of dam removal on sediment transport in a reach stretching from upstream from the Plainwell Dam to just downstream from the Trowbridge Dam using a calibrated quasi-steady-state one-dimensional (1D) hydraulic and sediment transport model (Syed and others, 2005). The calibrated model indicated that sediment is predominantly transported during high-flow conditions and that mobilized sediments are deposited during the ebb phase of flood peaks. Model results did not indicate a substantial difference in total eroded sediment volume between dam-in and dam-out scenarios. A companion investigation contextualized the Kalamazoo River geomorphological setting, examined planform morphological change using repeat aerial photography and historical surveys, and modeled bank stability using limit equilibrium methods coupled to the previously mentioned 1D hydraulic models (Rachol and others, 2005). The study concluded that the planform of the Kalamazoo River had remained mostly stable over the period of investigation (1830s–1999) and that most planform changes were associated with anthropogenic channelization, inundation because of dam construction, and channel shortening through meander bend cutoffs. The study also identified several channel cross sections with higher stream velocities and shear stresses where banks were predicted to be unstable because of toe erosion.

More recently, AECOM (2023) presented a 100-percent design plan for removal of the Allegan City Dam that included 1D hydraulic modeling results for a 4-mi reach centered on the Allegan City Dam. The plan included dam-in and dam-out scenarios across a wide range of streamflows. The engineering firm WSP (unpub. data) created a 2D hydraulic model reaching from the Trowbridge Dam downstream to the Allegan City Dam for a dam-in scenario and multiple quasi-steady streamflow conditions. This current study builds upon these earlier works by expanding the hydraulic modeling to two dimensions, similar to WSP (unpub. data), and modeling unrestored, free-flowing river reaches to better understand the natural spatial variability in velocities and sediment stability in this river system.

Study Area Description

The Kalamazoo River drains 2,020 square miles (mi^2) of southwestern Michigan and empties into Lake Michigan near Saugatuck (USGS, 2023). The main stem of the river begins in Albion in eastern Calhoun County at the confluence of the north and south branches, and it flows 123 mi to its outlet (USGS, 2024; fig. 1). The drainage basin relief is 686 ft, and the river descends from Albion to Plainwell (the location of the Plainwell Dam) with an average gradient of 3 feet per mile (ft/mi; USGS, 2024). The gradient steepens to 5 ft/mi between Plainwell and Allegan (the location of the Allegan City Dam) as the river passes through the outer Valparaiso Moraine (not shown) and associated glacial outwash deposits. The river gradient then relaxes to about 0.5 ft/mi between Lake Allegan (the impoundment above the Calkins Bridge Dam) and the Lake Michigan outlet (Rachol and others, 2005). Dams and rapids interspersed along the main stem generate deviations from these average gradients.

Southwestern Michigan is covered in ubiquitous glacial drift of variable thickness exceeding 400 ft at places (Leverett and Taylor, 1915). The surficial deposits are typically well-sorted coarse-grained sand and gravel outwash laid down during the late Pleistocene recession of the Michigan and Saginaw lobes of the Laurentide ice sheet. Several moraine systems consisting of poorly sorted rocky debris and glacial drainageways containing well-sorted coarse-grained deposits are also throughout the basin. Underlying the glacial deposits are Mississippian age sedimentary rocks of the Michigan Basin (Deutsch and others, 1960). The central part of the present-day (2026) river occupies a valley formed during the Pleistocene by a much larger river conveying meltwater from the retreating ice sheet and affected by glacial outburst floods (Kozlowski and others, 2005). This ancestral glacial drainage reorganized several times as the lobes retreated, switching outlets and flow directions and developing terraces as it incised through extensive outwash deposits (Gordon, 1898).

The Kalamazoo River Basin land cover was historically dominantly forest and grassland but transitioned to primarily agricultural (47 percent), forested (30 percent), and urban

(8 percent) land cover after European settlement (Kalamazoo River Watershed Council, 2011). Wetlands and lakes compose 15 percent of the drainage basin (Kalamazoo River Watershed Council, 2011). More than 80 percent of the soils in the basin are well drained and sandy (Rachol and others, 2005). The basin has a humid continental climate moderated by a strong lake effect from Lake Michigan. For 1991–2020, average winter temperatures were 27 degrees Fahrenheit (°F) and average summer temperatures were 70 °F. The basin received an average of 37 inches (in.) of annual precipitation (Palecki and others, 2021). For 1981–2010, the most recent period with snowfall climate normals available, the basin averaged 70–80 in. of annual snowfall (Arguez and others, 2010). The USGS streamgage Kalamazoo River at Comstock, Michigan (station 04106000), has been operational from 1931 to present (2026). This upstream site drains 1,010 mi^2. The minimum, 25-percent, median, 75-percent, and maximum recorded average daily streamflows at this location are 190, 580, 810, 1,200, and 6,800 ft^3/s, respectively (USGS, 2025).

This study focuses on a 9.2-mi-long reach of the Kalamazoo River stretching from the Trowbridge Dam to the Allegan City Dam. Here, the river drains about 1,530 mi^2. The river valley constricts as it cuts through the Valparaiso Moraine (not shown) and diverges from the larger ancestral drainage path that flowed south toward the Paw Paw River (not shown; Colgan and others, 2023). The bankfull river width is about 200 ft. During normal streamflow conditions, the average center channel depth is 3–4 ft in the upper reaches and 6–8 ft in the downstream lower gradient reaches that are affected by backwater from the Allegan City Dam. No major tributaries join the river in this section, and the reach includes segments that are straight and tightly confined by valley walls, as well as meandering segments with wider floodplains and meander scars. Within the reach are several islands, and a major channel bifurcation is 1.8 mi downstream from the Trowbridge Dam. The secondary channel rejoins the main channel 2.7 mi downstream from the Trowbridge Dam.

Field Data Collection

WSE profiles and velocity transects were collected during field surveys on June 11–12, 2024, and April 5–6, 2025, to help calibrate the hydraulic model (Roland and others, 2025). The streamflow measured at the USGS streamgage Kalamazoo River near Allegan, Mich. (station 04107850; hereafter referred to as the "Trowbridge streamgage"), just downstream from the Trowbridge Dam, was fairly stable and ranged from 1,020 to 1,120 ft^3/s and from 3,850 to 4,220 ft^3/s during the June 11–12, 2024, and April 5–6, 2025, periods, respectively (USGS, 2025). WSEs were surveyed using a network real-time kinematic (NRTK) global navigational satellite system (GNSS) receiver mounted on a 6.33-ft survey rod. The rod foot was placed at the edge of the water, leveled, and held steady, and the NRTK GNSS position was recorded as the average position of a 5-second data acquisition window. Network corrections were obtained from a nearby Michigan continuously operating reference station in Plainwell, Mich. The accuracy of the NRTK GNSS survey points was assessed to be within 1 in. based on occupation of a benchmark at the beginning and end of the survey. The continuous record of water elevation available from the Trowbridge streamgage was also used for model calibration and validation (USGS, 2025). Survey and streamgage elevation data were converted from the North American Vertical Datum of 1988 to the National Geodetic Vertical Datum of 1929 by adding a uniform offset of 0.433 ft to the measured elevations. This study area offset was determined using VDatum (National Oceanic and Atmospheric Administration, 2022).

Stream velocity measurements were made using downward-facing SonTek M9 and Teledyne RiverPro acoustic Doppler current profilers (ADCPs) rigidly attached to a boat. ADCPs rely on the Doppler principle to measure the velocity of a fluid by transmitting an acoustic pulse and measuring the frequency shift of the pulse reflections off particles suspended in the fluid. The resulting velocity measurements are binned into vertical cells whose height scales as the height of the investigated water column changes. For this reach, cell heights ranged from 0.33 to 0.66 ft (SonTek, 2023). Data were collected along flow-perpendicular transects, as well as longitudinally down the channel, and the position of the ADCP was georeferenced using a GNSS antenna mounted directly above the ADCP that streamed NRTK positions into the data acquisition computer. The immersion depth of the ADCP was measured and assumed to remain constant throughout the survey period(s). The accuracy of the ADCP horizontal positions was assessed to be within 1 ft based on the fixed GNSS solution status present throughout the survey period. Most of the flow-perpendicular transects included two passes, and the ADCP collected velocity samples once per second (1 hertz). Downward-facing ADCPs are unable to measure water velocity near the surface of a waterbody because of the combination of immersion depth and the unmeasurable blanking distance immediately in front of the transducers. Data from cells within 0.52 ft of the ADCP were excluded from the analysis. Additionally, downward-facing ADCPs are unable to measure a part of the velocity profile near the channel bottom. The vertically averaged velocity at each sample point was calculated using the average of cells with observed velocities along with extrapolated velocities for the unmeasured surface and bottom regions. The extrapolation method and parameters for the surface and bottom regions of the velocity profiles were determined with QRev (Mueller, 2013, 2020). The automatic fitting algorithm was used to select between a power law fit through the entire profile or a constant value fit for the surface region and a no-slip condition fit for the bottom region. Power law and no-slip fit exponents were set as the default value of 0.1667 or computed from linear least squares regression to the measured data, depending on the quality of the data in the upper and lower parts of the profile and on the strength of the regression (refer to Mueller [2013] for details).

Distinct extrapolation parameters were determined from the velocity observations for each individual transect and were then applied to the corresponding measurement file in the ADCP data processing software (SonTek, 2023) for exporting the depth-averaged velocity over the entire water column. The complete details regarding the field data collection and the data themselves are available in the accompanying USGS data release (Roland and others, 2025).

Cross-sectional average velocities were calculated for each flow-perpendicular transect measurement by projecting the individual depth-averaged velocity samples onto a straight line that best fit the observation points. If more than one measurement was available for a given transect, the average of the individual cross-sectional averages was computed to obtain a single value for the transect. Additionally, a 5-second rolling average was applied to the individual depth-averaged velocity samples in each measurement, and every fifth sample was extracted to generate a distribution of points to compare against model results. The rolling average and subsampling were applied to smooth the inherently noisy velocity measurements.

Development of a Two-Dimensional Hydraulic Model

We used an open-source numerical model, the Hydrologic Engineering Center River Analysis System (HEC–RAS; ver. 6.6; U.S. Army Corps of Engineers [USACE], 2024), to simulate the flow of water through the study reach. The 2D implementation of HEC–RAS 6.6 solves the unsteady depth-averaged shallow water (Saint-Venant) equations using a combination of finite-difference and finite-volume schemes. The shallow water equations are a simplified version of the Navier-Stokes equations applicable in situations where the horizontal length scales are much greater than the vertical length scales, the pressure is close to hydrostatic, and fluid density is constant. The model computes fluid flow by solving a system of equations incorporating the conservation of mass (eq. 1) and the conservation of linear momentum (eqs. 2 and 3; USACE, 2020).

$$\frac{\partial h}{\partial t} + u\frac{\partial h}{\partial x} + v\frac{\partial h}{\partial y} = 0, \tag{1}$$

$$\frac{\partial u}{\partial t} + \left(u\frac{\partial u}{\partial x} + v\frac{\partial u}{\partial y}\right) = -g\frac{\partial h}{\partial x} - \frac{g n^2 |u| u}{R^{4/3}}, \tag{2}$$

and

$$\frac{\partial v}{\partial t} + \left(v\frac{\partial v}{\partial y} + u\frac{\partial v}{\partial x}\right) = -g\frac{\partial h}{\partial y} - \frac{g n^2 |v| v}{R^{4/3}}, \tag{3}$$

where

h is the height of the fluid column,
t is time,
u is velocity in the x-direction,
v is velocity in the y-direction,
g is gravitational acceleration,
n is the Manning's roughness coefficient,
R is the hydraulic radius, and
$|u|$ and $|v|$ denote the magnitude of the velocity vectors in the x and y directions, respectively.

From left to right in eqs. 2 and 3, the terms represent local acceleration, convective acceleration, acceleration from gravity, and friction. The model described here assumes an incompressible fluid of constant density and neglects turbulent mixing, fluid acceleration from the Coriolis effect, and wind stresses. Pluvial flooding is not simulated. All the input files required to run the models discussed here are available from Roland and others (2025).

Model Geometry and Boundary Conditions

The 2D implementation of HEC–RAS 6.6 permits simulation of fluid flow on an unstructured mesh of variably sized cells, each with as many as eight sides. This approach allows the modeler to efficiently model in-channel streamflow while also incorporating flow through the floodplain by refining a relatively coarser background mesh to a much finer resolution within the channel. This model domain boundary was manually digitized in the companion geographic information system to the HEC–RAS modeling suite, RAS Mapper, to align with the approximate extent of the floodplain throughout the study reach (fig. 1). The extent of surface water inundation computed by the high-flow scenarios was checked to ensure that the model domain encompassed the entire area of potential flow. The background mesh face length was specified as 100 ft. The channel centerline, riverbanks, and island boundaries were manually digitized to support refinement of the mesh within the channel using a 20-ft face length and to enforce the alignment of mesh edges with important topographic features (fig. 2). A 1-ft-resolution seamless topobathymetric digital elevation model derived from airborne light detection and ranging data collected in November 2016 and multibeam sonar data collected in May 2017 was used to define the model surface elevations (Quantum Spatial, unpub. data, 2017). Bridge structures are not explicitly incorporated in the model geometry because all the bridge spans in the study reach are well above the water at the highest flows modeled in this study. The model's vertical datum is the National Geodetic Vertical Datum of 1929, in units of feet, and the horizontal coordinate system is Michigan State Plane South, in linear units of feet (European Petroleum Survey Group code 6499). HEC–RAS 6.6 takes advantage of the higher resolution terrain data relative to the model mesh resolution by incorporating subgrid elevation information in hydraulic property tables for each model cell and face. A streamflow hydrograph (specified flux) was

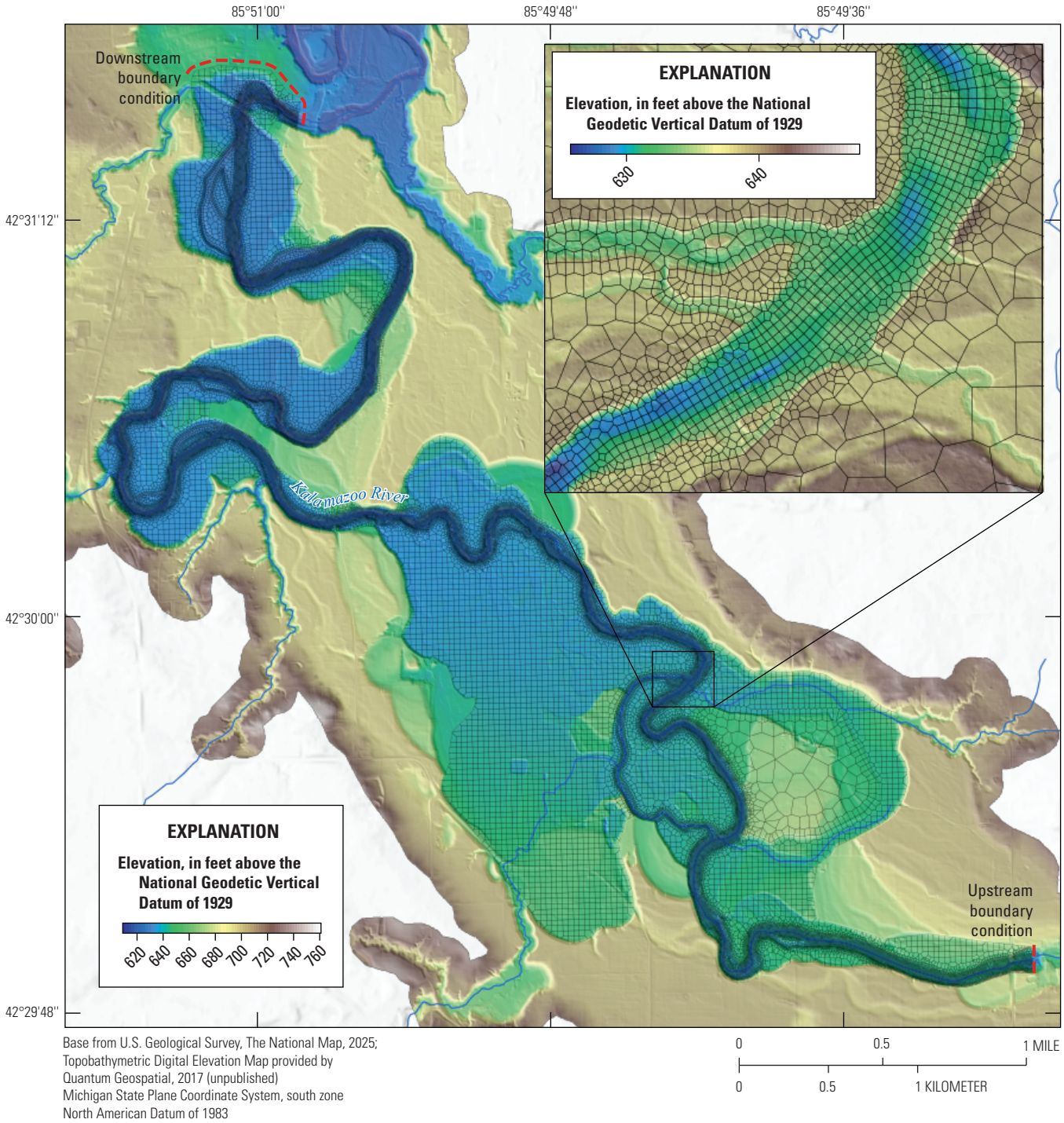

Figure 2. Map showing the Kalamazoo River study reach hydraulic model numerical mesh.

used as the model's upstream boundary condition, and a stage hydrograph (specified elevation) was used as the downstream boundary condition (fig. 1). All other boundaries were zero flux boundaries, but the model domain was large enough to prevent water from interacting with these zero flux boundaries.

Streamflow Simulations

We used streamflow estimates from the Trowbridge streamgage as the inputs to the streamflow hydrograph boundary condition for four unsteady historical simulations across a range of streamflow magnitudes, spanning March 23–April 14 (spring), 2023; January 26–February 14 (winter), 2024; June 11–12 (summer), 2024; and April 4–6 (spring), 2025 (fig. 3*A–D*; USGS, 2025). These streamflow estimates have a 15-minute temporal resolution and are based on a stage-discharge rating curve developed following standard USGS methods (Kennedy, 1983). The peak flows during the spring 2023 event reached 6,800 ft^3/s, which represents about a 10-percent AEP streamflow based on the analysis presented in AECOM (2023). The winter 2024 event peaked at 3,980 ft^3/s, about a 50-percent AEP streamflow magnitude. The streamflows during the spring 2025 observations were similar in magnitude. The summer 2024 scenario streamflows were fairly stable between 1,000 and 1,100 ft^3/s, and this scenario overlaps with the low-flow model validation field data collection period. Additionally, we forced models with seven constant streamflow time series to simulate quasi-steady streamflows ranging from 1,000 to 7,000 ft^3/s in 1,000-ft^3/s increments. The 1,000-, 4,000-, and 7,000-ft^3/s streamflow scenarios are referred to as "low-flow," "bankfull," and "high-flow" scenarios, respectively, in subsequent sections of this report. Emphasis is placed on the 4,000-ft^3/s streamflow scenario because this streamflow is estimated to be about the bankfull or 50-percent AEP streamflow at this site (AECOM, 2023). The downstream elevation boundary was set as 627.8 ft for all simulations except for the spring 2025 streamflow scenario, for which the downstream elevation boundary was set as 628.1 ft based on field survey observations. The downstream Allegan City Dam is operated to maintain stable water elevations in the upstream impoundment and is able to convey the flood flows simulated here (AECOM, 2023).

All simulations used the Eulerian-Lagrangian shallow water equation solver. Each model was initialized in a dry condition and warmed up with a 6-hour period where the input streamflow linearly increases from 0 ft^3/s to the first input streamflow prescribed in the accompanying streamflow scenario during the first 30 minutes of the warmup period. This approach allowed the models to achieve quasi-equilibrium before beginning the unsteady simulations in the case of the historical scenarios. For the quasi-steady simulations, the models were run for an additional 6 hours after the warmup period to ensure steady-state conditions were achieved. Steady-state conditions were verified

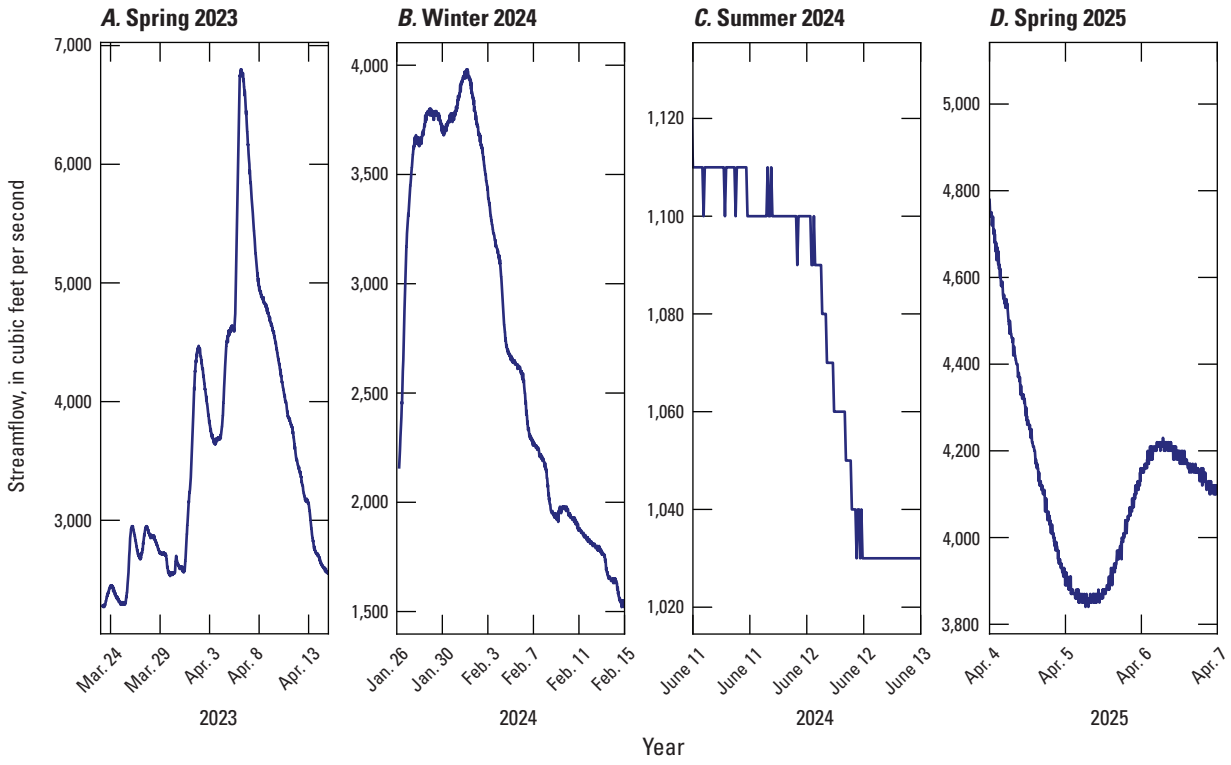

Figure 3. Graphs showing estimated streamflow at the U.S. Geological Survey streamgage Kalamazoo River near Allegan, Michigan (station 04107850), for the four unsteady streamflow scenarios. *A*, March 23–April 14 (spring), 2023; *B*, January 26–February 14 (winter), 2024; *C*, June 11–12 (summer), 2024; *D*, April 4–6 (spring), 2025.

by inspecting the computed water surfaces and velocities for differences between output intervals. All models were run with a 10-second time step, which yielded a median Courant condition value around 0.1 and maximum Courant condition values less than 2; a value of 3 is the maximum allowed by the Eulerian-Lagrangian shallow water equation solver (USACE, 2025). A simulation was also completed using a 2-second time step, and no substantial differences in model results were identified. Model outputs were generated hourly. The water density was assumed to be 62.4 pounds per cubic foot, and the water temperature was assumed to be 55.4 °F.

Roughness Parameterization

In many shallow-flow problems, including streamflow in most rivers, the gravitational and frictional terms are the dominant components of the momentum conservation equation. The Manning's roughness coefficient (n) scales the bed friction, the momentum loss from the flow to the bed, and other sources of drag, and is frequently used as the calibration parameter in hydraulic simulations of open channel flows (USACE, 2020). Manning's roughness coefficient is the primary adjustable parameter in this model formulation. We created an initial spatially distributed n value parameterization using the 30-meter (m) resolution 2021 National Land Cover Database (NLCD; Dewitz, 2023). Manning's roughness coefficients were assigned to the land cover types present in the model domain using default values provided in USACE (2025). The NLCD data had a resolution too coarse to accurately represent the channel and island boundaries of the study reach, so channel and island polygons were manually digitized and were assigned n values overriding the underlying NLCD parameterization (table 1; fig. 4). The n value of the channel polygon was varied from 0.025 to 0.035 during calibration to the historical simulation scenarios. The n values that were used here are similar to those used in the AECOM (2023) and WSP models, and the n value at the cell face centroid was assigned to each cell face.

Table 1. Manning's roughness coefficient parameterization for model land use categories.

[Manning's roughness coefficient (n) values from U.S. Army Corps of Engineers (2025), except channel n values, which were determined through calibration as described in the "Model Calibration" section of this publication]

Land use classification	*n*
No data	0.0356
Developed, medium intensity	0.06
Developed, low intensity	0.06
Developed, open space	0.035
Developed, high intensity	0.1
Deciduous forest	0.06
Open water	0.035
Woody wetlands	0.06
Mixed forest	0.07
Cultivated crops	0.06
Pasture/hay	0.04
Barren land (rock/sand/clay)	0.04
Emergent herbaceous wetlands	0.06
Grassland/herbaceous	0.04
Shrub/scrub	0.06
Evergreen forest	0.08
Channel	0.025–0.035
Island	0.06

Model Calibration

The model was manually calibrated by iteratively simulating historical streamflow scenarios using a range of channel roughness parameterization n values. The model was calibrated for low-flow conditions by running the summer 2024 scenario with channel roughness parameterization n values of 0.025, 0.03, 0.0315, 0.0335, and 0.035. The model was calibrated for higher streamflow conditions by running the spring 2023, winter 2024, and spring 2025 streamflow scenarios with n values of 0.03,0.0315, and 0.0335. The accuracy of the summer 2024 and spring 2025 models was assessed by comparing model elevation and velocity results against the field measurements. The root mean square error (RMSE; eq. 4) and bias (eq. 5) between observed and modeled WSEs, individual velocity samples, and cross-sectional average velocities were used to assess model performance. The spring 2023 and winter 2024 simulations were assessed similarly, but rather than comparing the model results against spatially distributed WSE and velocity observations, we compared the model results against a time series of WSE observations (hydrograph) at the Trowbridge streamgage. For comparison between observed and simulated WSEs and velocities at discrete points, model results were exported from the model output time step nearest the measurement time using the reference points feature in HEC–RAS. Simulated cross-sectional average velocities at the locations of ADCP cross sections were dynamically generated from the HEC–RAS HDF5 results files using Python. The best model parameterizations for the quasi-steady simulations were selected based on best professional judgment and review of the RMSE and bias values for the various calibration datasets. All the models simulated streamflow with less than a 0.001-percent water volumetric error associated with the numerical solution.

$$RMSE = \sqrt{\frac{\sum_{i=1}^{N}(Pred_i - Obs_i)^2}{N}} \quad (4)$$

and

$$bias = \frac{\sum_{i=1}^{N} Pred_i - Obs_i}{N}, \quad (5)$$

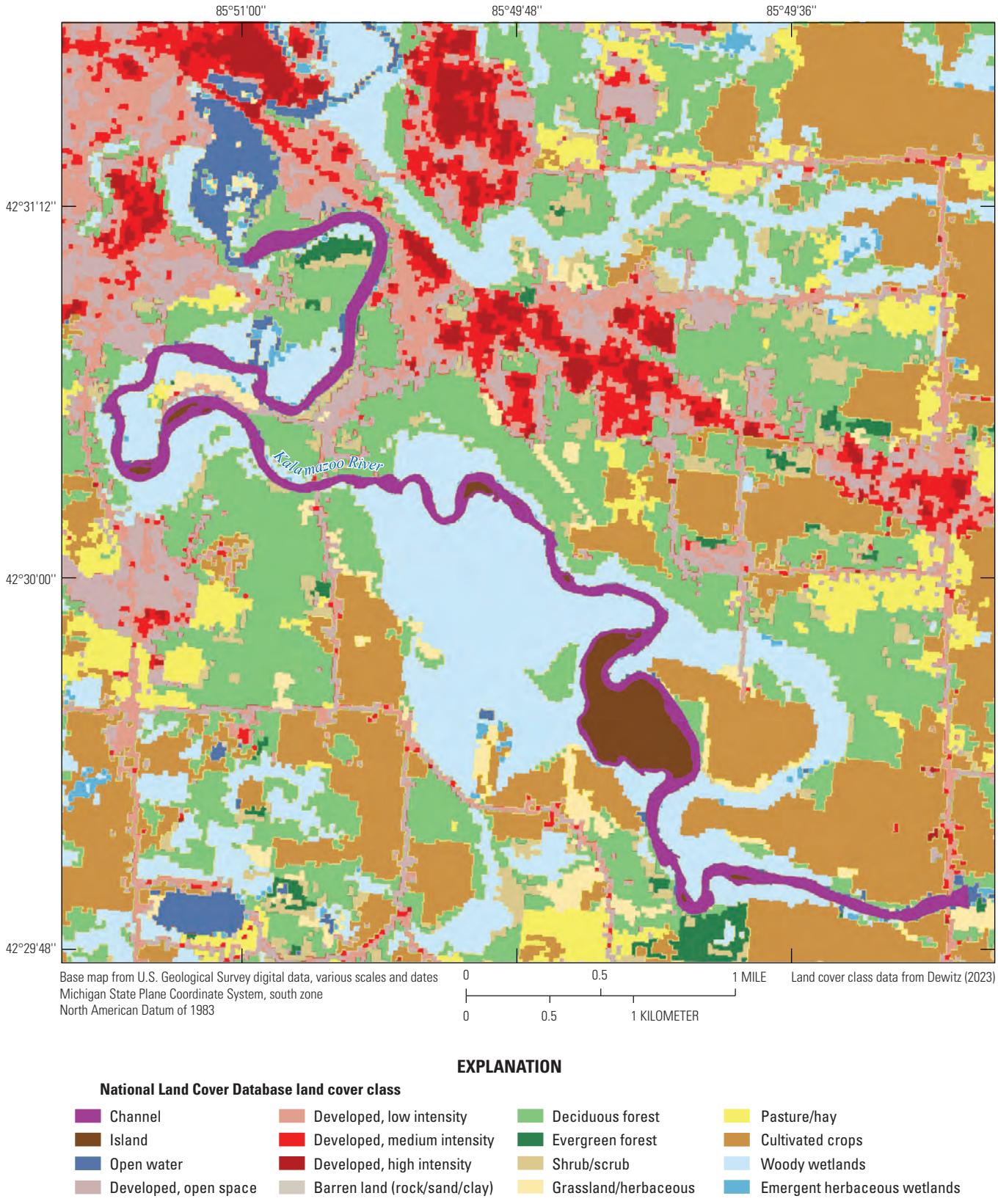

Figure 4. Map showing land cover parameterization for the Kalamazoo River study reach (National Land Cover Database land cover class data from Dewitz [2023]; channel and island classes were manually digitized and are contained in the associated data release [Roland and others, 2025]).

where

$Pred_i$ is the model-predicted value for observation i,
Obs_i is the value measured in the field for observation i,
i is the observation number, and
N is the total number of observations.

Model Outputs and Subsequent Analysis

Gridded outputs of flow depth, depth-averaged velocity, and basal shear stress were generated from the calibrated model for each of the quasi-steady streamflow simulations ranging from 1,000 to 7,000 ft^3/s. The output grid resolution was 3.28 ft across the wetted part of the model domain. These outputs were further analyzed to evaluate hydraulic conditions relevant to ecological thresholds and sediment mobility within the study reach. Longitudinal profiles of channel-average attributes were calculated by casting cross sections across the channel at a 33-ft along-flow spacing. The gridded model outputs were extracted every 3.28 ft along each cross section to compute cross-sectional averages. Cross-sectional average velocities were computed by calculating the total streamflow perpendicular to each cross section and dividing this value by the cross-sectional wetted area. The channel cross-sectional average values were subsequently smoothed using a three-sample rolling average, generating longitudinal profiles representing overlapping reaches about 100 ft long.

Shear stress outputs were used to evaluate channel bed stability and the potential for sediment deposition in the study reach by applying equations for an explicit, empirical Shields diagram presented in Guo (2020). For each output grid cell, the shear stress (taken for this analysis to be the critical shear stress at which sediment motion would be initiated [τ_c]) was related to a corresponding critical grain diameter (D; in other words, the minimum grain size stable at that streamflow) using equation 6. The dimensionless critical shear stress, or Shields parameter (τ_{*c}), was computed according to equation 7, where the dimensionless sediment diameter (D_*) was calculated using equation 8. In equation 9, the critical grain Reynolds number (R_{*c}) was determined from equation 29 in Guo (2020) and was computed by finding the maximum real root of equation 9 with the NumPy function "roots" (Harris and others, 2020).

$$\tau_c = \tau_{*c}(\Delta - 1)pgD, \tag{6}$$

$$\tau_{*c} = \frac{R_{*c}^2}{D_*^3}, \tag{7}$$

$$D_* = D\left[\frac{(\Delta - 1)g}{\nu^2}\right]^{1/3}, \tag{8}$$

and

$$R_{*c}^4 + \frac{195}{7}R_{*c}^3 + \left(\frac{162}{7} - \frac{D_*^3}{18}\right)R_{*c}^2 - \frac{11}{42}D_*^3 R_{*c} - \frac{81}{14}D_*^3 = 0, \tag{9}$$

where

Δ is the sediment specific gravity (2.65),
p is the fluid density (1,000 kilograms per cubic meter),
g is gravitational acceleration (9.81 square meters per second),
R_{*c} is the critical grain Reynolds number, and
ν is the kinematic water viscosity (1.01×10^{-6} square meters per second).

The τ_c values were computed across a range of D values from 0.01 to 128 millimeters (mm), at intervals of 0.01 mm. A D value was then assigned to the nearest corresponding shear stress value of each output raster cell, for each streamflow scenario ranging from 1,000 to 7,000 ft^3/s. For each cell, the D values represent the diameter less than which a grain would be predicted to be mobilized at the simulated streamflow. Any larger grain would be stable at that streamflow. This method is only applicable to noncohesive granular material, which field observations indicate constitutes most of the river bed in the study reach.

Hydraulic Simulation Results

Results from the hydraulic model included simulated WSEs, depth-averaged streamflow velocities, and shear stress. In the following sections, we present results of the model calibration, including evaluation of model performance at replicating observed WSE and velocity; spatial patterns of inundation and velocity across the range of simulated streamflow conditions; and an analysis of shear stress and estimated substrate grain stability in the study reach. All the model outputs discussed here are available in Roland and others (2025).

Model Calibration Results

Comparisons between the observed and modeled WSE profiles for simulations using different channel roughness values are shown in figure 5*A* and *B* for the summer 2024 streamflow simulations. From 0 to 19,500 ft downstream from the Trowbridge Dam, the water surface slope was about 0.003. The water surface slope decreased to about 0.001 from 19,500 to 30,000 ft and then relaxed even farther downstream from this point because of the effect of backwater from the Allegan City Dam. All the modeled water surface profiles matched the general shape of the observed water surface profile (fig. 5*A*) and had an RMSE less than 0.35 ft (table 2). The model slightly underpredicted WSEs from 16,000 to

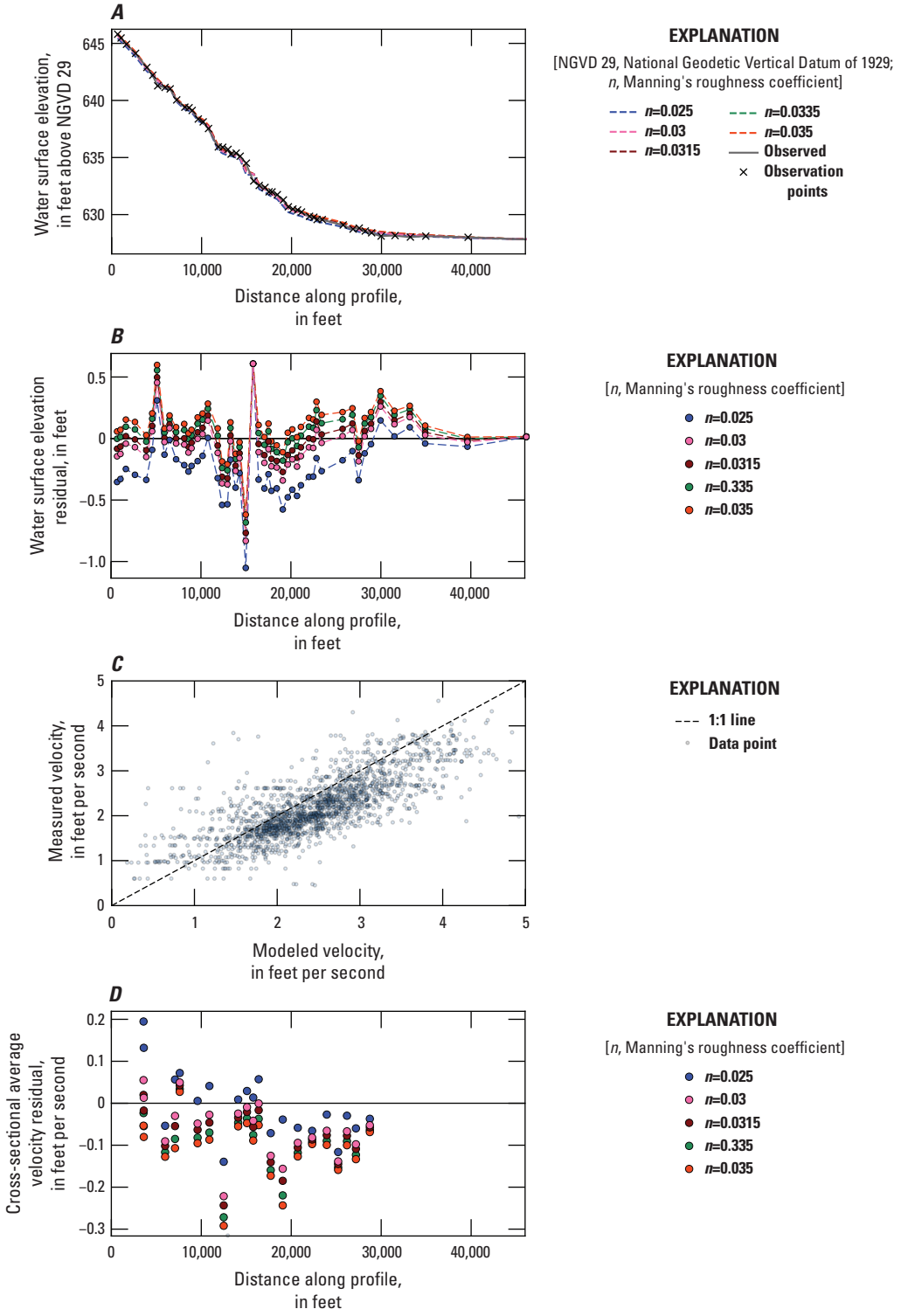

Figure 5. Graphs showing comparison between modeled and observed water surface elevations (WSEs) and velocities for the June 11–12 (summer), 2024, streamflow scenario along the Kalamazoo River, Michigan. *A*, longitudinal profile of modeled and observed WSEs; *B*, differences between the observed and modeled WSEs; *C*, correlation between modeled and measured point velocities for the channel with a Manning's roughness coefficient of 0.315; *D*, differences between observed and modeled cross-sectional average velocities. In *B* and *D*, negative values indicate underprediction, and positive values indicate overprediction.

Table 2. Comparison between observed and modeled water surface elevations and depth-averaged velocities for the June 11–12 (summer), 2024, streamflow scenario parameterizations along the Kalamazoo River, Michigan.

[Data from the associated data release (Roland and others, 2025). *n*, Manning's roughness coefficient; WSE, water surface elevation; RMSE, root mean square error; ft, foot; ft/s, foot per second]

n	WSE RMSE (ft)	WSE bias (ft)	Point velocity RMSE (ft/s)	Point velocity bias (ft/s)	Cross section velocity RMSE (ft/s)	Cross section velocity bias (ft/s)
0.025	0.34	−0.23	0.62	−0.06	0.21	−0.02
0.03	0.22	−0.06	0.59	−0.23	0.23	−0.20
0.0315	0.20	−0.01	0.60	−0.28	0.27	−0.25
0.0335	0.20	0.05	0.63	−0.34	0.32	−0.31
0.035	0.21	0.10	0.65	−0.38	0.36	−0.35

24,000 ft and then slightly overpredicted WSEs between 24,000 and 40,000 ft, although the exact magnitude and direction of the residuals varied as a function of the model channel roughness parameterization. The largest discrepancies between modeled and observed WSEs were at riffles, where local WSE slopes were relatively steep compared to the reach average. WSEs generated by the model with the smallest channel roughness parameterization (n=0.025) were generally less than the observed WSEs, whereas WSEs generated by the model with the highest channel roughness parameterization (n=0.035) were generally higher than the observed WSEs. The models with channel roughness parameterization n values of 0.0315 and 0.0335 each yielded 0.20-ft RMSEs, the smallest of the tested parameterizations (table 2). The n=0.025 model had a −0.23-ft WSE bias, and the n=0.035 model had a 0.10-ft WSE bias; the n=0.0315 model had a WSE bias of only −0.01 ft.

All the model parameterizations underpredicted summer 2024 velocities relative to the ADCP-measured values (table 2 and fig. 5*C* and *D*). The RMSE between the point ADCP measurements and modeled velocities ranged from 0.59 to 0.65 foot per second (ft/s), and the bias ranged from −0.06 ft/s for the n=0.025 channel roughness parameterization model to −0.38 ft/s for the n=0.035 channel roughness parameterization model (table 2). The n=0.025 channel roughness parameterization model had the smallest RMSE and bias between the observed and modeled cross-sectional average velocities at 0.21 and −0.02 ft/s, whereas the n=0.035 channel roughness parameterization model had the largest at 0.36 and −0.35 ft/s (table 2). The n=0.025 channel roughness parameterization model tended to overpredict cross-sectional average velocities upstream from 18,000 ft, whereas other roughness parameterizations slightly underpredicted velocities in this region. Downstream from about 18,000 ft, all the model parameterizations underpredicted cross-sectional average velocities. The n=0.0315 channel roughness parameterization model was chosen as the optimal parameterization for the quasi-steady streamflow simulations from 1,000 to 3,000 ft^3/s based on its minimal WSE bias.

The n=0.03, n=0.0315, and n=0.0335 channel roughness parameterization models were tested for the spring 2023, winter 2024, and spring 2025 streamflow scenarios to evaluate the potential for stage-dependent roughness at higher WSEs relative to the summer 2024 streamflow scenario. As WSEs increase, decreasing composite roughness values are commonly observed (Arcement and Schneider, 1989). Comparisons between the observed and modeled water surface profiles are shown in figure 6*A* and *B* for the spring 2025 streamflow simulations. The water surface slope from 0 to 19,500 ft downstream from the Trowbridge Dam decreased to about 0.002, and the water surface slope from 19,500 to 30,000 ft remained about 0.001. In contrast to WSE observations during the low-flow summer 2024 period, the spring 2025 observations indicate that the water surface slope remained about 0.001 nearly to the downstream extent of the study reach. The differences in the modeled WSE profiles were minor; the n=0.03 and n=0.0315 channel roughness parameterization models yielded WSE RMSEs of 0.32 and biases of −0.05 ft and 0.06 ft, respectively (table 3). WSEs were generally overpredicted upstream from 15,000 ft downstream from the Trowbridge Dam, underpredicted from 15,000 to 32,000 ft downstream from the Trowbridge Dam, and overpredicted for the remainder of the study reach. Similar to the summer 2024 simulations, all the channel roughness parameterizations yielded modeled velocities less than the measured velocities for the spring 2025 simulations (fig. 6*C* and *D*). The n=0.03 channel roughness parameterization model had the smallest point velocity RMSE and bias, at 0.98 ft/s and −0.39 ft/s, respectively (table 3). The model differed in skill at matching the cross section and longitudinal point velocities, with the n=0.03 channel roughness parameterization having an RMSE of 1.09 ft/s and bias of −0.06 ft/s for cross-section points, and an RMSE of 0.88 ft/s and bias of −0.73 ft/s for longitudinal points. The larger negative bias associated with the longitudinal points is potentially caused by the model not resolving the highest channel velocities because of resolution limitations, or the faster boat travel speed during longitudinal measurements affecting the measured velocities. The n=0.03 channel roughness parameterization also yielded the smallest RMSE and bias values for the cross-sectional average velocity comparisons, at 0.27 ft/s and −0.10 ft/s (table 3), respectively. Average absolute differences between the modeled and measured point velocities and cross-sectional average velocities increased slightly from the low-flow to the bankfull-flow models.

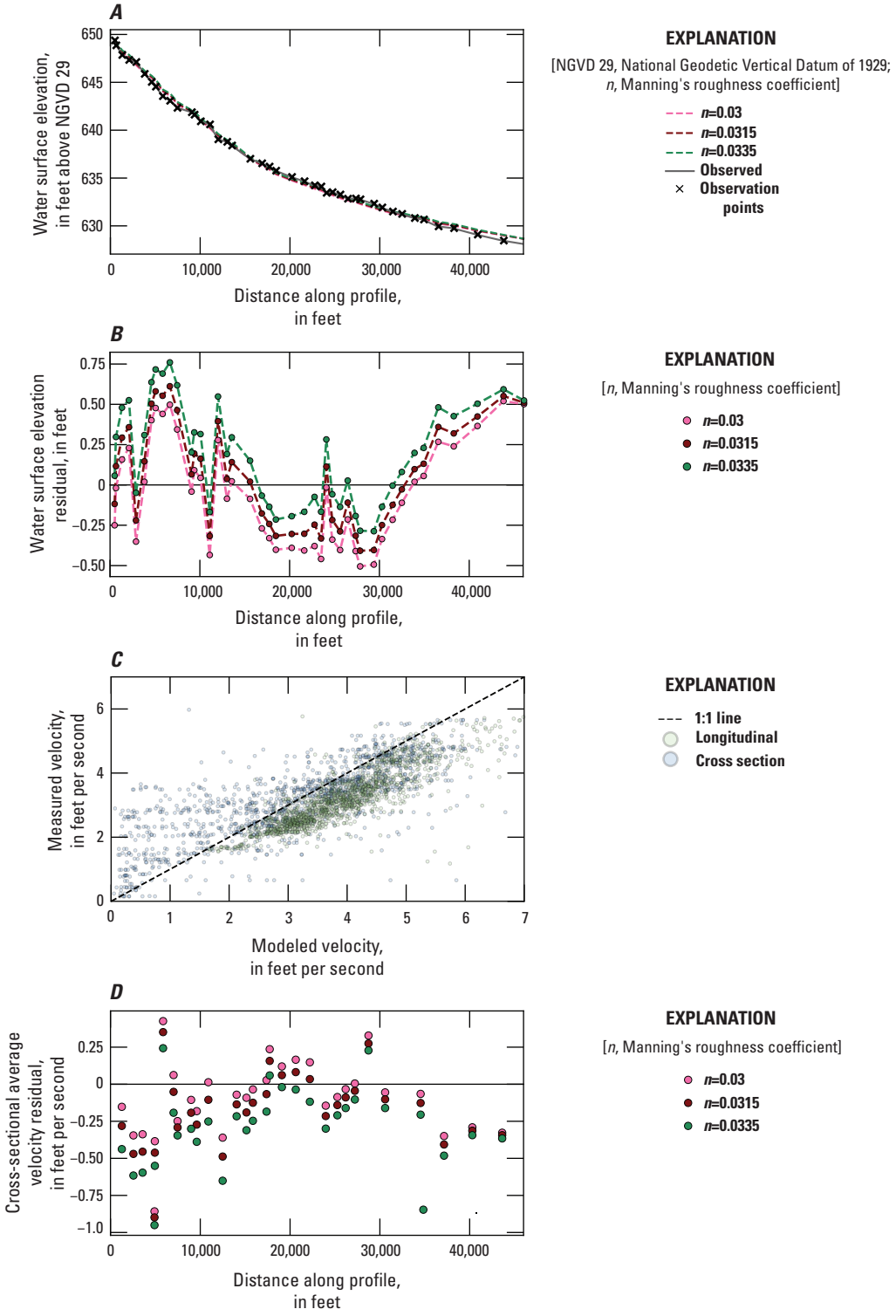

Figure 6. Graphs showing comparison between modeled and observed water surface elevations (WSEs) and velocities for the April 4–6 (spring), 2025, streamflow scenario along the Kalamazoo River, Michigan. *A*, longitudinal profile of modeled and observed WSEs; *B*, differences between the observed and modeled WSEs; *C*, correlation between modeled and measured point velocities for the channel with a Manning's roughness coefficient of 0.315; *D*, differences between observed and modeled cross-sectional average velocities along the Kalamazoo River, Michigan. In *B* and *D*, negative values indicate underprediction, and positive values indicate overprediction.

Table 3. Comparison between observed and modeled water surface elevations and depth-averaged velocities for the April 4–6 (spring), 2025, streamflow scenario parameterizations along the Kalamazoo River, Michigan.

[Data from the associated data release (Roland and others, 2025). *n*, Manning's roughness coefficient; WSE, water surface elevation; RMSE, root mean square error; ft, foot; ft/s, foot per second]

n	WSE RMSE (ft)	WSE bias (ft)	Point velocity RMSE (ft/s)	Point velocity bias (ft/s)	Cross section velocity RMSE (ft/s)	Cross section velocity bias (ft/s)
0.03	0.32	−0.05	0.98	−0.39	0.27	−0.10
0.0315	0.32	0.06	1.02	−0.46	0.30	−0.18
0.0335	0.36	0.19	1.08	−0.56	0.37	−0.27

The *n*=0.0335 and *n*=0.0315 channel roughness parameterization models overpredicted WSEs at the streamgage for the spring 2023 and winter 2024 streamflow scenarios (fig. 7*A* and *B*) with RMSE values of 0.16 and 0.32 ft for the spring 2023 streamflow scenario and 0.14 and 0.28 ft for the winter 2024 streamflow scenario for the *n*=0.0315 and *n*=0.0335 channel roughness models, respectively. The *n*=0.03 channel roughness model indicated close visual correspondence with the observed WSEs at the streamgage and yielded an RMSE of 0.04 ft for the spring 2023 and winter 2024 streamflow scenarios. Based on these results, a channel roughness of 0.03 was selected for the quasi-steady streamflow scenarios from 4,000 to 7,000 ft^3/s. Distributed WSE and velocity observations were not available during any of the simulated high-flow periods, limiting our ability to validate high-flow simulations beyond the immediate area near the streamgage. The parameterizations for the quasi-steady streamflow scenarios are provided in table 4.

Table 4. Calibrated Manning's roughness coefficient channel roughness parameterization for quasi-steady streamflow scenarios along the Kalamazoo River, Michigan.

[Data from the associated data release (Roland and others, 2025). ft^3/s, cubic foot per second; *n*, Manning's roughness coefficient]

Streamflow (ft^3/s)	*n*
1,000	0.0315
2,000	0.0315
3,000	0.0315
4,000	0.03
5,000	0.03
6,000	0.03
7,000	0.03

Channel Velocities and Inundated Area

Maps of modeled flow velocities for the range of streamflow scenarios are provided in appendix 1 (figs. 1.1–1.7). A longitudinal profile of modeled cross-sectional average channel velocities smoothed with a three-sample rolling average for the quasi-steady streamflow scenarios is shown in figure 8*A*. Cross-sectional average channel velocities were the smallest for the 1,000-ft^3/s scenario, which is similar to the summer 2024 streamflow scenario conditions, and cross-sectional average channel velocities were generally greatest for the 7,000-ft^3/s scenario. The longitudinal patterns of cross-sectional average channel velocity are generally similar among the seven streamflow scenarios, having high velocities from 500 to 3,600 ft below the Trowbridge Dam, alternating high and low velocities associated with riffle and pool morphology from 3,600 to 18,000 ft below the Trowbridge Dam, and generally smaller and less variable velocities downstream from this distance. For the 4,000-ft^3/s streamflow scenario, cross-sectional average channel velocities in the 500–3,600-ft reach were about 4 ft/s, and riffle cross-sectional average velocities were between 4 and 5 ft/s. Cross-sectional average channel velocities decreased to about 2.5–3 ft/s from 18,000 to 23,000 ft because of the valley constriction about 1,000 ft upstream from the Bridge Road crossing. Below the 23,000-ft reach, cross-sectional average channel velocities were variable but generally decreased from 3 to about 2 ft/s.

The Michigan Department of Natural Resources uses guideline flow velocity thresholds for fish passage of 3 and 4 ft/s for *Percina caprodes* (logperch) and *Micropterus dolomieu* (smallmouth bass), respectively (M. Diana, Michigan Department of Natural Resources, oral commun., 2024). These thresholds are displayed in figure 8*A*. In the 4,000-ft^3/s scenario, the cross-sectional average channel velocities in the upper reaches of the river upstream from 18,000 ft below the Trowbridge Dam generally exceeded the 3-ft/s velocity threshold associated with logperch, but the 4-ft/s velocity threshold used for smallmouth bass was only exceeded at riffles. Downstream from the 18,000-ft reach, the threshold for both species was generally not exceeded.

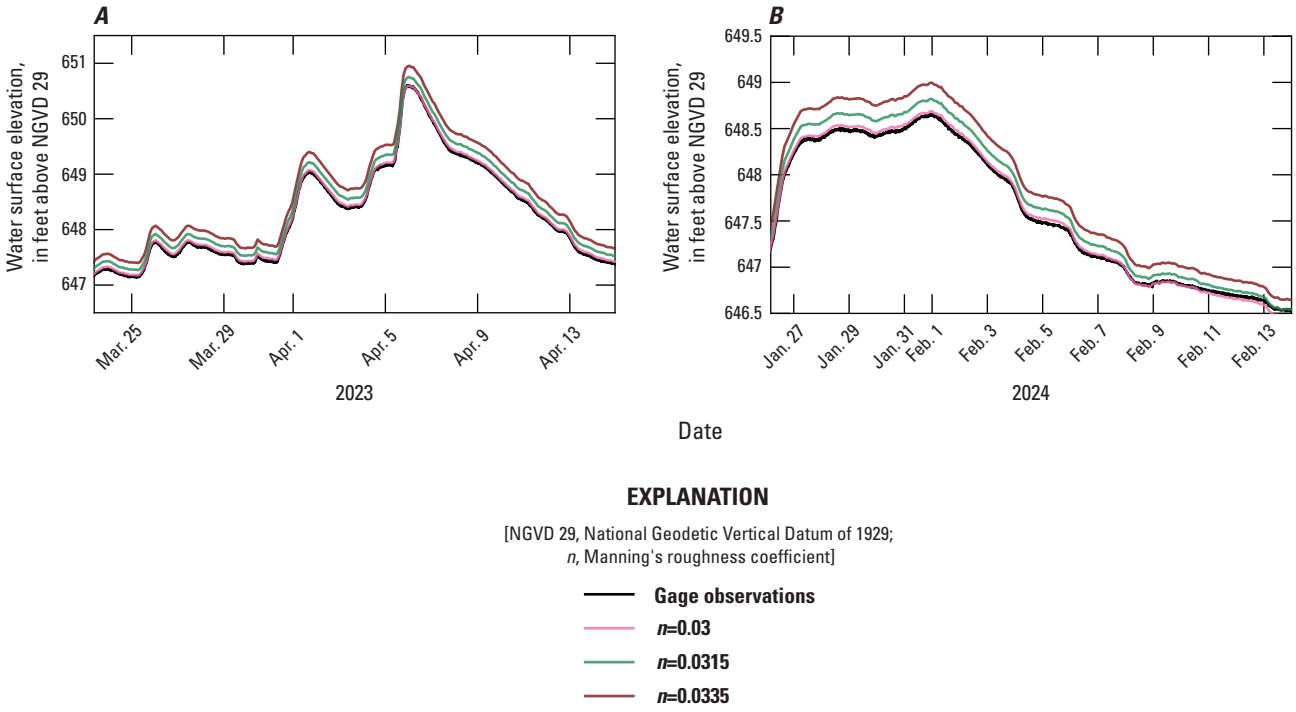

Figure 7. Graphs showing comparison between modeled and observed water surface elevations at the Trowbridge streamgage along the Kalamazoo River, Michigan. *A*, for the March 23–April 14 (spring), 2023, streamflow scenario; *B*, for the January 26–February 14 (winter), 2024, streamflow scenario.

Maps of modeled flow depths are provided in appendix 2 (figs. 2.1–2.7). At 1,000 ft^3/s, flow is contained within the channel, and the large oxbow about 35,000 ft downstream from the Trowbridge Dam is inundated (app. 2, fig. 2.1). As streamflow increases to 3,000 ft^3/s, water enters meander scars and other low-lying areas on the floodplain from 9,000 to 24,000 ft downstream from the Trowbridge Dam and begins to fill the narrow valley 30,000 ft downstream from the dam. Inundation in the reach from 9,000 to 24,000 ft expands at 4,000 ft^3/s streamflow, especially in the reach from 15,000 to 24,000 ft (app. 2, fig. 2.4). Streamflows greater than 4,000 ft^3/s lead to continuous inundation in this region, and the valley downstream from 25,000 ft becomes completely inundated. Additionally, for streamflows of 6,000–7,000 ft^3/s, water begins to flow out of the channel on the river right bank about 5,000 ft downstream from the Trowbridge Dam, bypassing the major bend in the river near 6,000 ft. Planform heterogeneity in the modeled velocities at high streamflows is substantial, with smaller velocities toward the channel margins, in the floodplain, and in secondary channels (app. 1, figs. 1.4–1.7). Fish may seek refuge in these low velocity regions during high-flow events to minimize energy expenditures and then return to main channel habitats as floods recede. Increases in the downstream boundary water elevation would cause increases in inundation depths and extents in the lower reaches of the model and alter velocity distributions.

Shear Stress and Grain Stability

Maps of the modeled basal shear stresses are provided in appendix 3 (figs. 3.1–3.7). Modeled shear stresses within the channel ranged from 0 to 0.81 pound per square foot (lb/ft^2; arithmetic mean [μ]: 0.050, standard deviation [σ]: 0.062) in the 1,000-ft^3/s scenario and from 0 to 0.92 lb/ft^2 (μ: 0.13, σ: 0.062) in the 7,000-ft^3/s scenario. At the approximate bankfull flow of 4,000 ft^3/s, shear stress ranged from 0 to 0.89 lb/ft^2 (μ: 0.10, σ: 0.086).

Maps of modeled minimum stable grain sizes are provided in appendix 4 (figs. 4.1–4.7). Values within the channel ranged from 0.01 to 43.3 mm (μ: 2.98, σ: 3.31) in the low-flow 1,000-ft^3/s scenario (app. 4, fig. 4.1). Grains in the fine gravel size range and coarser (4–64 mm) were stable throughout most of the reach at this streamflow. Sand and silt grains were predicted to be mobile through most of the reach, even under low-flow conditions; however, in certain pools, channel margins, and the lower reach affected by the Allegan City Dam impoundment, sand was predicted to be stable. In small areas along channel margins and in off-channel areas in the impoundment-affected zone, silt-sized particles were immobile at this streamflow. Cross-sectional averages of estimated channel minimum stable grain size are variable but indicate a general decrease along the longitudinal profile from 0 to 23,000 ft downstream from Trowbridge Dam, at which point the trend flattens out (fig. 8*B*).

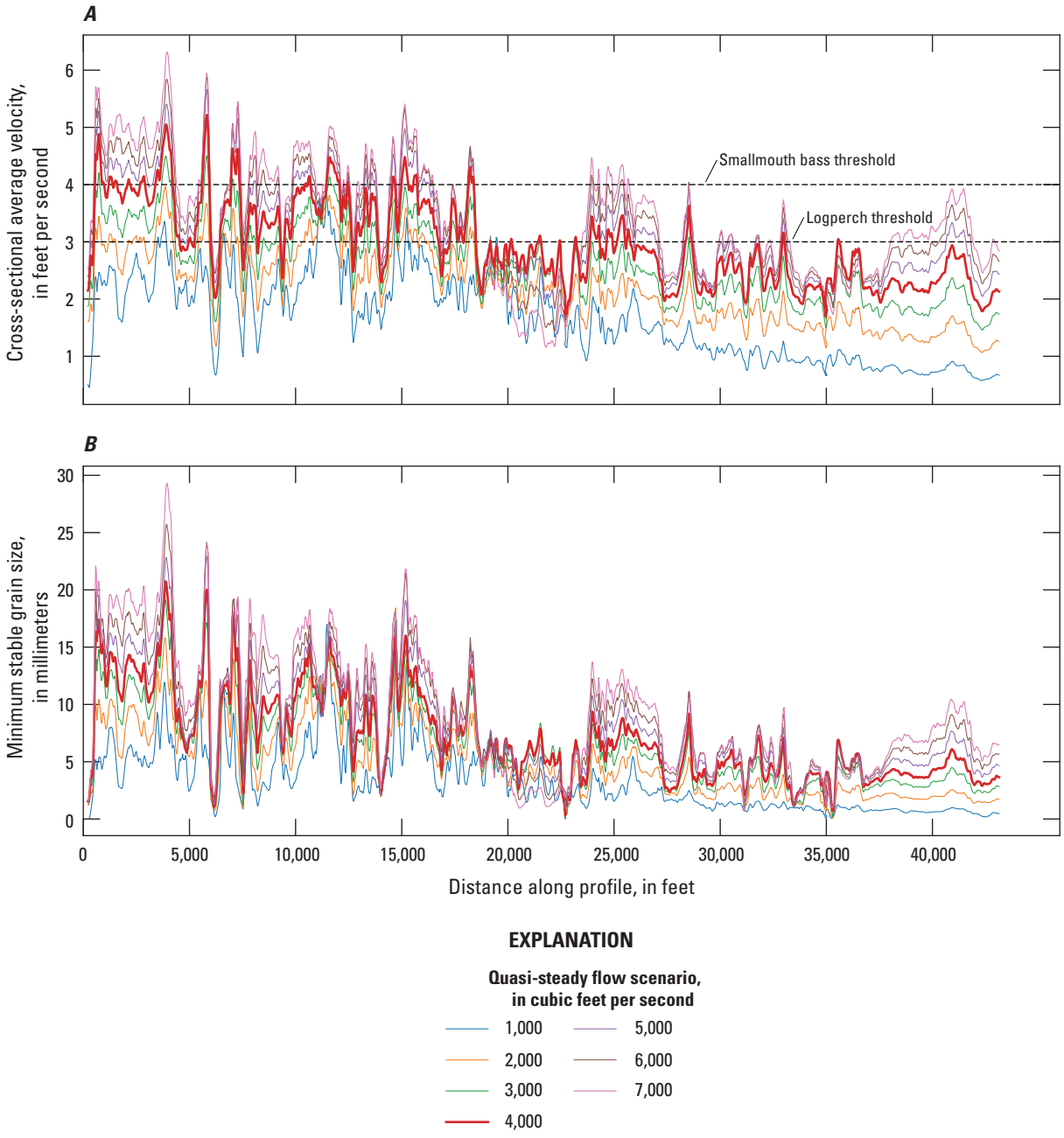

Figure 8. Graphs showing longitudinal profiles of hydrodynamic model results for seven quasi-steady streamflow scenarios in the Kalamazoo River, Michigan. Values are cross-sectional averages smoothed with a three-sample rolling average. *A*, modeled flow velocities; *B*, minimum stable grain sizes. [*Micropterus dolomieu*, smallmouth bass; *Percina caprodes*, logperch]

At the approximate bankfull streamflow of 4,000 ft^3/s, minimum stable grain size ranged from 0.01 to 47 mm (μ: 5.72, σ: 4.56; app. 4, fig. 4.4). Grains finer than gravel (*D* less than 2 mm) were predicted to be mobile through the entire main channel under this streamflow condition, including through the main channel of the impoundment. Areas of predicted sand and silt stability were within side channels and some channel margins in the upper reaches of the study area, and in broader off-channel areas with predicted overbank flooding in the lower reaches.

In the high-flow scenario of 7,000 ft^3/s, minimum stable grain sizes ranged from 0.01 to 49.3 mm (μ: 7.20, σ: 6.08; app. 4, fig. 4.7). Fine and medium gravel (*D*=4–16 mm) were predicted to be transported through most of the main channel, and coarse gravel was predicted to be mobile in riffles at this streamflow. The floodplain was almost completely inundated in this simulation, and substantial zones of the floodplain had predicted stability of grains in the sand and silt size range.

Minimum stable grain size results were compared with substrate size measurements made in the study reach in 2023 and 2024 (Vaughan and others, 2023; Roland and others, 2025) to evaluate the degree to which existing substrates may be mobile under a range of streamflow conditions. A total of 2 pebble counts consisting of 100 grain size observations were done on riffles within the study area, along with 3 reach-composite counts of 50, 76, and 51 observations evenly spaced along reaches 0.87-, 0.75-, and 0.75-mi long, respectively.

Observations in the reach-composite pebble counts were geolocated and could therefore be compared directly to the raster outputs. For each streamflow scenario, a stability index (relative substrate stability [RSS]) was computed for each grain size observation (171 total observations across three study reaches) as the ratio of the modeled shear stress at that location to the critical shear stress computed for the grain. RSS values greater than 1 indicate shear stress greater than the critical shear stress for a grain of the observed size, whereas values less than 1 indicate insufficient shear stress to mobilize the grain. The reach-composite observations consisted of one randomly selected grain at each preselected sample location. The randomly selected grains are not a representative grain size selected from a distribution (for example, the median, which is commonly used for bed material transport modeling). Therefore, results should be interpreted with caution because any particular observation (and therefore, substrate stability metric) may not be fully representative of the grain size distribution at the sample location.

For the low-flow 1,000-ft^3/s scenario, about the top quartile of observed grains across the three reach-composite pebble counts had estimated RSS values greater than 1 (fig. 9*A*). The median RSS value at that streamflow was 0.41. RSS values increased steadily with increasing streamflow until the bankfull-flow scenario of 4,000 ft^3/s, at which point they continued to increase, but more gradually (fig. 9*A*). At streamflows greater than bankfull, the bed shear stress increases more gradually with increasing streamflow as water spreads out across the floodplain. The median RSS value for the 4,000-ft^3/s scenario was 0.81, indicating that slightly less than one-half of the observed grains were predicted to be mobile at the bankfull streamflow. For the high-flow scenario, the median RSS value was 0.95.

RSS values had a strong negative relation with grain size (fig. 9*B*). For the 4,000-ft^3/s scenario, most grains smaller than 8 mm (fine gravel and smaller) were estimated to be mobile (RSS greater than 1), whereas larger grains were predicted to remain stable at the bankfull streamflow.

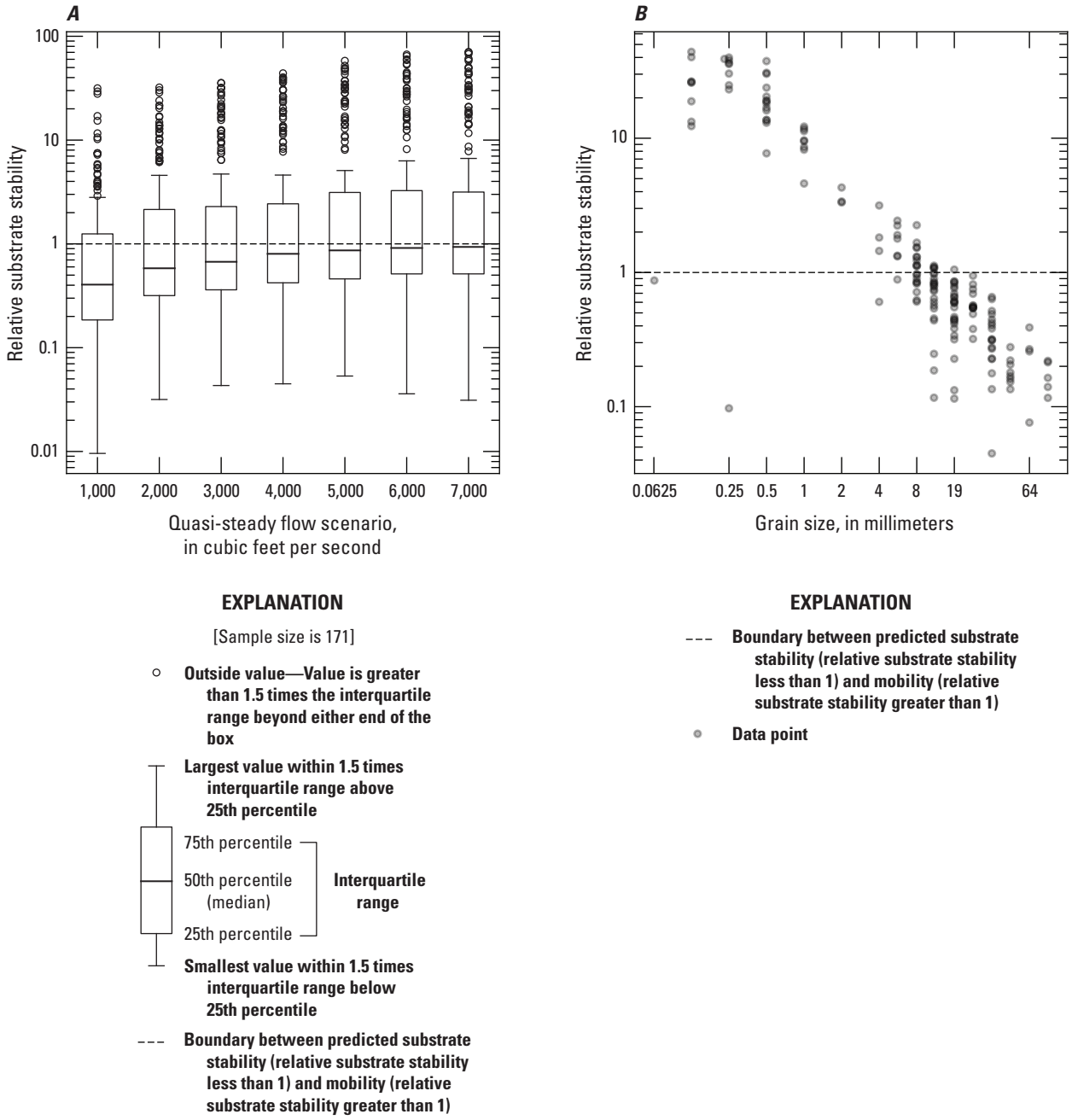

Figure 9. Boxplot (*A*) showing relative substrate stability distributions for the seven quasi-steady streamflow scenarios and a scatterplot (*B*) showing relative substrate stability versus grain size for the bankfull scenario along the Kalamazoo River, Michigan.

Summary and Conclusions

Dam removal has the potential to release contaminated sediments deposited in upstream impoundments, sometimes motivating restored channel designs that are narrow and deep to minimize the transport of contaminated sediment. Beginning in the 1960s, several low-head dams along the Kalamazoo River in southwestern Michigan were progressively removed to improve fish passage and recreational opportunities. The area of dam removals overlaps with the Kalamazoo River Area of Concern, a stretch of the Kalamazoo River and tributaries that is about 80 miles (mi) long and is a designated Superfund site because of polychlorinated biphenyl contamination associated with paper processing during the 1950s–70s. Complete removal of the Trowbridge and Allegan City Dams and restoration of the impounded channels are planned during the next few years. To aid the Michigan Department of Natural Resources; Michigan Department of Environment, Great Lakes, and Energy; and the U.S. Environmental Protection Agency's understanding of reference hydraulic conditions in an unrestored, free-flowing reach of the Kalamazoo River, the U.S. Geological Survey constructed a two-dimensional hydraulic model of the reach between the Trowbridge and Allegan City Dams using specified streamflow and specified water surface elevation (WSE) upstream and downstream boundary conditions, respectively.

The channel roughness parameterization of the two-dimensional U.S. Army Corps of Engineers Hydrologic Engineering Center River Analysis System model was calibrated by simulating a low-flow period (June 11–12 [summer], 2024) and a bankfull-flow period (April 4–6 [spring], 2025) coincident with the collection of spatially distributed WSE and velocity measurements. Additional calibration was performed for two higher streamflow periods (March 23–April 14 [spring], 2023, and January 26–February 14 [winter], 2024) during which time series WSE observations were available from the U.S. Geological Survey streamgage Kalamazoo River near Allegan, Michigan (station 04107850), at the upstream end of the reach. The optimum low-flow model with a channel roughness (Manning's roughness coefficient [n]) of 0.0315 yielded a WSE root mean square error (RMSE) and bias of 0.20 and −0.01 foot (ft), respectively. This model underpredicted cross-sectional average velocities with an RMSE and bias of 0.27 and −0.25 foot per second (ft/s), respectively. The model with the n=0.03 channel roughness parameterization closely matched the WSE and cross-sectional average velocity observations during the spring 2025 simulation, yielding RMSEs of 0.32 ft and 0.27 ft/s and biases of −0.05 ft and −0.10 ft/s. The n=0.03 channel roughness model reproduced the streamgage hydrograph with RMSEs of 0.04 ft for the spring 2023 and winter 2024 streamflow scenarios. Based on the results of the calibration exercise, quasi-steady streamflow simulations were run for input streamflows ranging from 1,000 to 7,000 cubic feet per second (ft^3/s) in 1,000-ft^3/s increments with a channel roughness parameterization of n=0.0315 for models with input streamflows less than 4,000 ft^3/s and a channel roughness parameterization of n=0.03 for models with input streamflows equal to or greater than 4,000 ft^3/s.

The bankfull streamflow is frequently chosen as the upper limit design scenario for fish passage evaluation, which for this reach of the Kalamazoo River is about 4,000 ft^3/s. For the 4,000 ft^3/s model scenario, the cross-sectional average channel velocities for most of the upper 18,000 ft of this reach of the Kalamazoo River exceeded 3 ft/s, a rule-of-thumb velocity threshold for *Percina caprodes* (logperch) passage. At this 4,000 ft^3/s streamflow, only the cross-sectional average velocities at riffles exceeded the 4 ft/s rule-of-thumb velocity threshold for *Micropterus dolomieu* (smallmouth bass) passage. Downstream from 18,000 ft below the Trowbridge Dam, these velocity thresholds are rarely exceeded at the 4,000-ft^3/s streamflow magnitude.

The shear stresses simulated by the quasi-steady streamflow scenarios were used to assess the potential stability of substrate within the study reach across a range of streamflows. At the approximate bankfull streamflow of 4,000 ft^3/s, the minimum stable grain size along most of the main channel is predicted to be in the pebble (4–64-millimeter) range, whereas fine gravels, sands, and silts are expected to be transported through the channel and potentially deposited in the floodplain and backwaters. Comparison of modeled shear stresses with observed grain size data indicated that at low streamflow, most grains observed in the study reach are predicted to be stable. At the bankfull streamflow, a substantial part of the observed grain sizes, particularly those in the fine gravel and smaller size range, are predicted to be mobile.

Hydraulic models provide a means of simulating distributed streamflow conditions with a spatial coverage and resolution that would be difficult or dangerous to document via field measurements, facilitating improved understanding of aquatic habitat connectivity and substrate stability to inform management decisions regarding river restoration.

References Cited

AECOM, 2023, Allegan City Dam removal—100 percent design report: Southfield, Mich., AECOM, 281 p., accessed March 12, 2025, at https://www.cityofallegan.org/Allegan%20City%20Dam%20Removal%20Final%20Design%20Report.pdf.

Arcadis, 2009, Generalized conceptual site model: Brighton, Mich., Arcadis, 77 p., accessed March 12, 2025, at https://semspub.epa.gov/work/05/424157.pdf.

Arcement, G.J., and Schneider, V.R., 1989, Guide for selecting Manning's roughness coefficients for natural channels and flood plains: U.S. Geological Survey Water Supply Paper 2339, 38 p., accessed March 12, 2025, at https://doi.org/10.3133/wsp2339.

Arguez, A., Durre, I., Applequist, S., Squires, M., Vose, R., Yin, X., and Bilotta, R., 2010, U.S. monthly climate normals (1981–2010): National Centers for Environmental Information digital data, accessed March 12, 2025, at https://www.ncei.noaa.gov/access/metadata/landing-page/bin/iso?id=gov.noaa.ncdc:C00822.

Bednarek, A.T., 2001, Undamming rivers—A review of the ecological impacts of dam removal: Environmental Management, v. 27, no. 6, p. 803–814, accessed March 12, 2025, at https://doi.org/10.1007/s002670010189.

Bellmore, J.R., Duda, J.J., Craig, L.S., Greene, S.L., Torgersen, C.E., Collins, M.J., and Vittum, K., 2017, Status and trends of dam removal research in the United States: WIREs Water, v. 4, no. 2, article e1164, 13 p., accessed March 12, 2025, at https://doi.org/10.1002/wat2.1164.

Blasland, Bouck & Lee, Inc., 1992, Allied Paper, Inc./Portage Creek/Kalamazoo River Superfund site—Description of the current situation: Kalamazoo River Study Group, v. I of VII, [variously paged; 293 p.], accessed March 12, 2025, at https://semspub.epa.gov/work/05/165898.pdf.

Colgan, P.M., Erber, N.R., Esch, J.M., Yellich, J.A., and Anderson, G.P., 2023, Surficial geology of Allegan County, Michigan: Michigan Geological Survey Map, 2 sheets, various scales, accessed March 12, 2025, at https://michigan-geological-survey-hub-wmugeography.hub.arcgis.com/datasets/b119af024e9d4148bd407314e336fccb/about.

Deutsch, M., Vanlier, K.E., and Giroux, P.R., 1960, Ground-water hydrology and glacial geology of the Kalamazoo area, Michigan: Lansing, Mich., Michigan Geological Survey Progress Report 23, 22 p., accessed March 12, 2025, at https://www.michigan.gov/documents/deq/GIMDL-PR232162057.PDF. [Also available at https://www.michigan.gov/-/media/Project/Websites/egle/Documents/Programs/GRMD/Catalog/06/GIMDL-PR23.PDF?rev=93765989cdb344edae273c662af2f37c.]

Dewitz, J., 2023, National Land Cover Database (NLCD) 2021 products: U.S. Geological Survey data release, accessed March 12, 2025, at https://doi.org/10.5066/P9JZ7AO3.

Evans, J.E., 2015, Contaminated sediment and dam removals—Problem or opportunity?: Eos (Washington, D.C.), v. 96, p. 12–17, accessed March 12, 2025, at https://doi.org/10.1029/2015EO036385.

Fencl, J.S., Mather, M.E., Costigan, K.H., and Daniels, M.D., 2015, How big of an effect do small dams have? Using geomorphological footprints to quantify spatial impact of low-head dams and identify patterns of across-dam variation: PLoS One, v. 10, no. 11, article e0141210, 22 p., accessed March 12, 2025, at https://doi.org/10.1371/journal.pone.0141210.

Gordon, C.H., 1898, Notes on the Kalamazoo and other old glacial outlets in southern Michigan: The Journal of Geology, v. 6, no. 5, p. 477–482, accessed March 12, 2025, at https://www.journals.uchicago.edu/doi/pdf/10.1086/608147. https://doi.org/10.1086/608147

Graf, W.L., 1993, Landscapes, commodities, and ecosystems—The relationship between policy and science for American rivers, chap. 2 *of* Sustaining our water resources: Washington, D.C., National Academy Press, p. 11–42, accessed March 12, 2025, at https://nap.nationalacademies.org/read/2217/chapter/4.

Guo, J., 2020, Empirical model for shields diagram and its applications: Journal of Hydraulic Engineering (New York), v. 146, no. 6, article 04020038, 8 p., accessed March 12, 2025, at https://doi.org/10.1061/(ASCE)HY.1943-7900.0001739.

Harris, C.R., Millman, K.J., van der Walt, S.J., Gommers, R., Virtanen, P., Cournapeau, D., Wieser, E., Taylor, J., Berg, S., Smith, N.J., Kern, R., Picus, M., Hoyer, S., van Kerkwijk, M.H., Brett, M., Haldane, A., del Río, J.F., Wiebe, M., Peterson, P., Gérard-Marchant, P., Sheppard, K., Reddy, T., Weckesser, W., Abbasi, H., Gohlke, C., and Oliphant, T.E., 2020, Array programming with NumPy: Nature, v. 585, no. 7825, p. 357–362, accessed March 12, 2025, at https://doi.org/10.1038/s41586-020-2649-2.

Kalamazoo River Watershed Council, 2011, Kalamazoo River Watershed Management Plan: Michigan Nonpoint Source Program [Michigan Department of Environmental Quality and the U.S. Environmental Protection Agency], 174 p., accessed March 12, 2025, at https://kalamazooriver.org/wp-content/uploads/2018/02/KRWMP_final_textonly_2015.pdf.

Kennedy, E.J., 1983, Computation of continuous records of streamflow: U.S. Geological Survey Techniques of Water-Resources Investigations, book 3, chap. A13, 53 p., accessed March 12, 2025, at https://doi.org/10.3133/twri03A13.

Kozlowski, A.L., Kehew, A.E., and Bird, B.C., 2005, Outburst flood origin of the central Kalamazoo River Valley, Michigan, USA: Quaternary Science Reviews, v. 24, no. 22, p. 2354–2374, accessed March 12, 2025, at https://doi.org/10.1016/j.quascirev.2005.03.016.

Leverett, F., and Taylor, F.B., 1915, The Pleistocene of Indiana and Michigan and the history of the Great Lakes: U.S. Geological Survey Monograph 53, 529 p., 8 pls., accessed March 12, 2025, at https://doi.org/10.3133/m53.

Michigan Department of Environmental Quality, 2003, Final (revised) baseline ecological risk assessment, Allied Paper, Inc./Portage Creek/Kalamazoo River Superfund site: Lansing, Mich., Michigan Department of Environmental Quality, prepared by CDM, [variously paged; 265 p.], accessed March 12, 2025, at https://archive.epa.gov/reg5sfun/ecology/web/pdf/allied_paper_bera.pdf.

Mueller, D.S., 2013, extrap—Software to assist the selection of extrapolation methods for moving-boat ADCP streamflow measurements: Computers & Geosciences, v. 54, p. 211–218, accessed June 13, 2025, at https://doi.org/10.1016/j.cageo.2013.02.001.

Mueller, D.S., 2020, QRev, version 4.38: U.S. Geological Survey software release, accessed October 15, 2024, at https://doi.org/10.5066/P9OZ8QDL.

National Oceanic and Atmospheric Administration, 2022, VDatum, version 4.4.2: National Oceanic and Atmospheric Administration software release, accessed August 11, 2022, at https://vdatum.noaa.gov/welcome.html.

Palecki, M., Durre, I., Applequist, S., Arguez, A., and Lawrimore, J., 2021, U.S. Climate normals 2020—U.S. hourly climate normals (1991–2020): National Centers for Environmental Information digital data, accessed March 12, 2025, at https://www.ncei.noaa.gov/metadata/geoportal/rest/metadata/item/gov.noaa.ncdc:C01619/html.

Rachol, C.M., Fitzpatrick, F.A., and Rossi, T., 2005, Historical and simulated changes in channel characteristics of the Kalamazoo River, Plainwell to Otsego, Michigan: U.S. Geological Survey Scientific Investigations Report 2005–5044, 59 p., accessed March 12, 2025, at https://doi.org/10.3133/sir20055044.

Rheaume, S.J., Hubbell, D.L., Rachol, C.M., Simard, A., and Fuller, L.M., 2004, Sediment characteristics and configuration within the Otsego City Dam impoundment on the Kalamazoo River, Michigan, 2001–02: U.S. Geological Survey Water-Resources Investigations Report 2003–4218, 54 p., accessed March 12, 2025, at https://doi.org/10.3133/wri034218.

Rheaume, S.J., Rachol, C.M., Hubbell, D.L., and Simard, A., 2002, Sediment characteristics and configuration within three dam impoundments on the Kalamazoo River, Michigan, 2000: U.S. Geological Survey Water-Resources Investigations Report 2002–4098, 58 p., accessed March 12, 2025, at https://doi.org/10.3133/wri024098.

Roland, C.J., Vaughan, A., Broerman, H.M., Lund, J.W., and Fitzpatrick, F.A., 2025, Model application data release for a 2D hydraulic model (HEC–RAS) of the Kalamazoo River Trowbridge Dam to Allegan City Dam reach: U.S. Geological Survey data release, https://doi.org/10.5066/P13CPA5B.

Simard, A., 2003, Annotated bibliography of selected references on PCB and the Kalamazoo River Superfund site, Michigan, 1982–2002: U.S. Geological Survey Open-File Report 2003–338, 25 p., accessed March 12, 2025, at https://doi.org/10.3133/ofr2003338.

SonTek, 2023, RiverSurveyor S5/M9 system manual: San Diego, Calif., SonTek, 236 p., accessed March 12, 2025, at https://www.xylem.com/siteassets/brand/sontek/resources/manual/rsl-manual.pdf.

Syed, A.U., Bennett, J.P., and Rachol, C.M., 2005, A pre-dam-removal assessment of sediment transport for four dams on the Kalamazoo River between Plainwell and Allegan, Michigan: U.S. Geological Survey Scientific Investigations Report 2004–5178, 37 p., accessed March 12, 2025, at https://doi.org/10.3133/sir20045178.

U.S. Army Corps of Engineers [USACE], 2020, HEC–RAS hydraulic reference manual: USACE website, accessed March 12, 2025, at https://www.hec.usace.army.mil/confluence/rasdocs/ras1dtechref/latest.

U.S. Army Corps of Engineers [USACE], 2024, HEC–RAS, version 6.6: U.S. Army Corps of Engineers software release, accessed March 12, 2025, at https://www.hec.usace.army.mil/software/hec-ras/download.aspx.

U.S. Army Corps of Engineers [USACE], 2025, HEC–RAS 2D user's manual: USACE website, accessed March 12, 2025, at https://www.hec.usace.army.mil/confluence/rasdocs/r2dum/latest.

U.S. Environmental Protection Agency, 2019, Otsego Township Dam area—Time critical removal action—Final report: Chicago, Ill., U.S. Environmental Protection Agency, prepared by Wood Environment & Infrastructure Solutions, Inc., accessed March 12, 2025, at https://response.epa.gov/sites/11006/files/FINAL%20OTDA%20TCRA%20Final%20Report_072619.pdf.

U.S. Geological Survey [USGS], 2023, Watershed boundary dataset (WBD)—USGS National Map downloadable data collection: U.S. Geological Survey digital data, accessed February 11, 2025, at https://www.usgs.gov/national-hydrography.

U.S. Geological Survey [USGS], 2024, National Hydrography Dataset Plus High Resolution (NHDPlus HR)—USGS National Map downloadable data collection: U.S. Geological Survey digital data, accessed February 11, 2025, at https://www.usgs.gov/national-hydrography.

U.S. Geological Survey [USGS], 2025, USGS water data for the Nation: U.S. Geological Survey National Water Information System database, accessed February 11, 2025, at https://doi.org/10.5066/F7P55KJN.

Vaughan, A.A., Fitzpatrick, F.A., Strange, J.M., Roland, C.J., and Broerman, H.M., 2023, Geomorphic reference reach data for the Kalamazoo River Basin, Michigan Area of Concern (ver. 2.0, October 2024): U.S. Geological Survey data release, accessed March 25, 2025, at https://doi.org/10.5066/P96JBHF4.

Appendix 1. Quasi-Steady Streamflow Scenario Velocity Maps

In this appendix, maps of the modeled velocities for the quasi-steady streamflow scenarios are provided. The 1,000-, 2,000-, 3,000-, 4,000-, 5,000-, 6,000-, and 7,000-cubic-foot-per-second streamflow scenarios are shown in figures 1.1, 1.2, 1.3, 1.4, 1.5, 1.6, and 1.7, respectively.

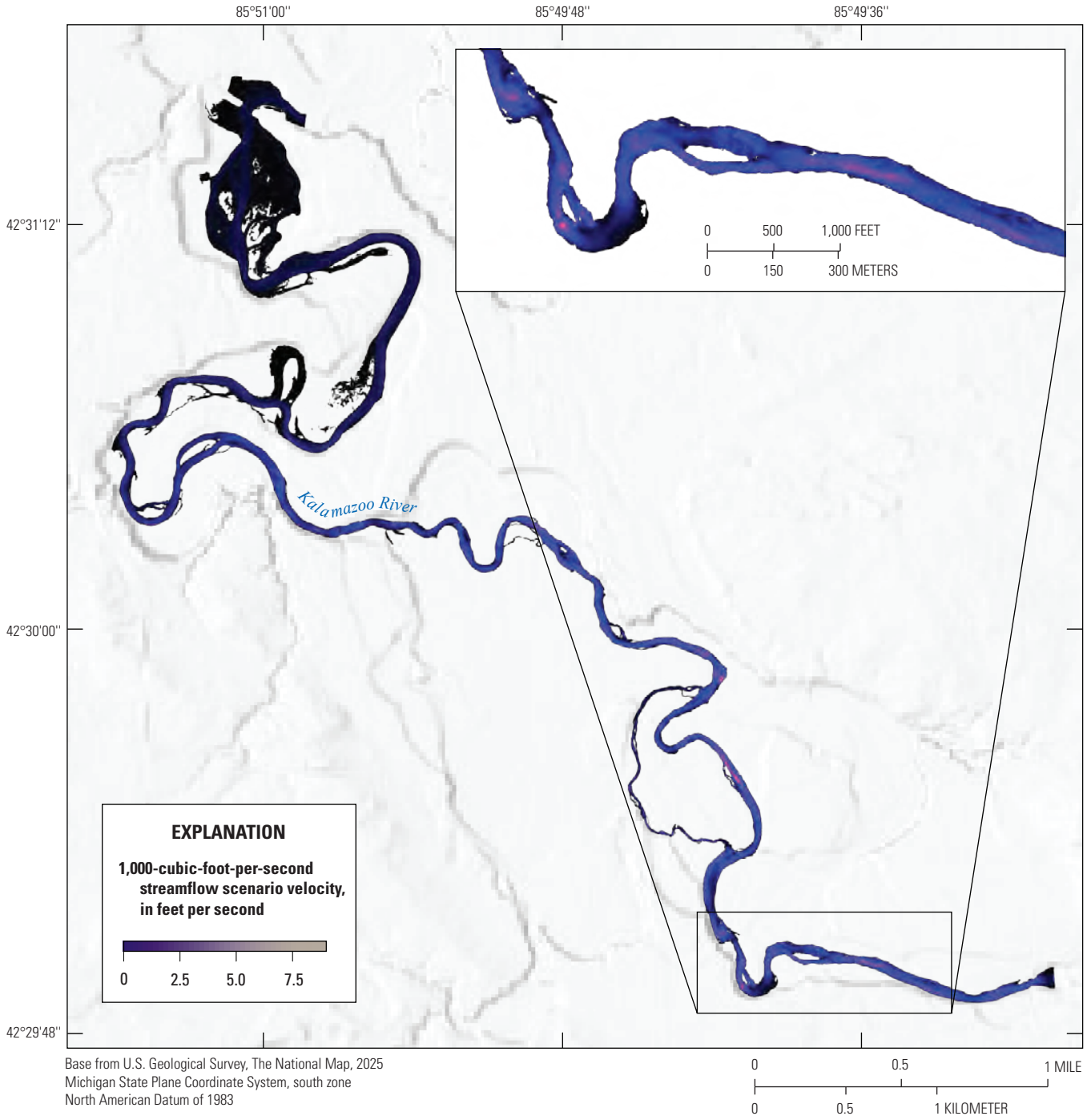

Figure 1.1. Map showing modeled velocities for the quasi-steady 1,000-cubic-foot-per-second streamflow scenario.

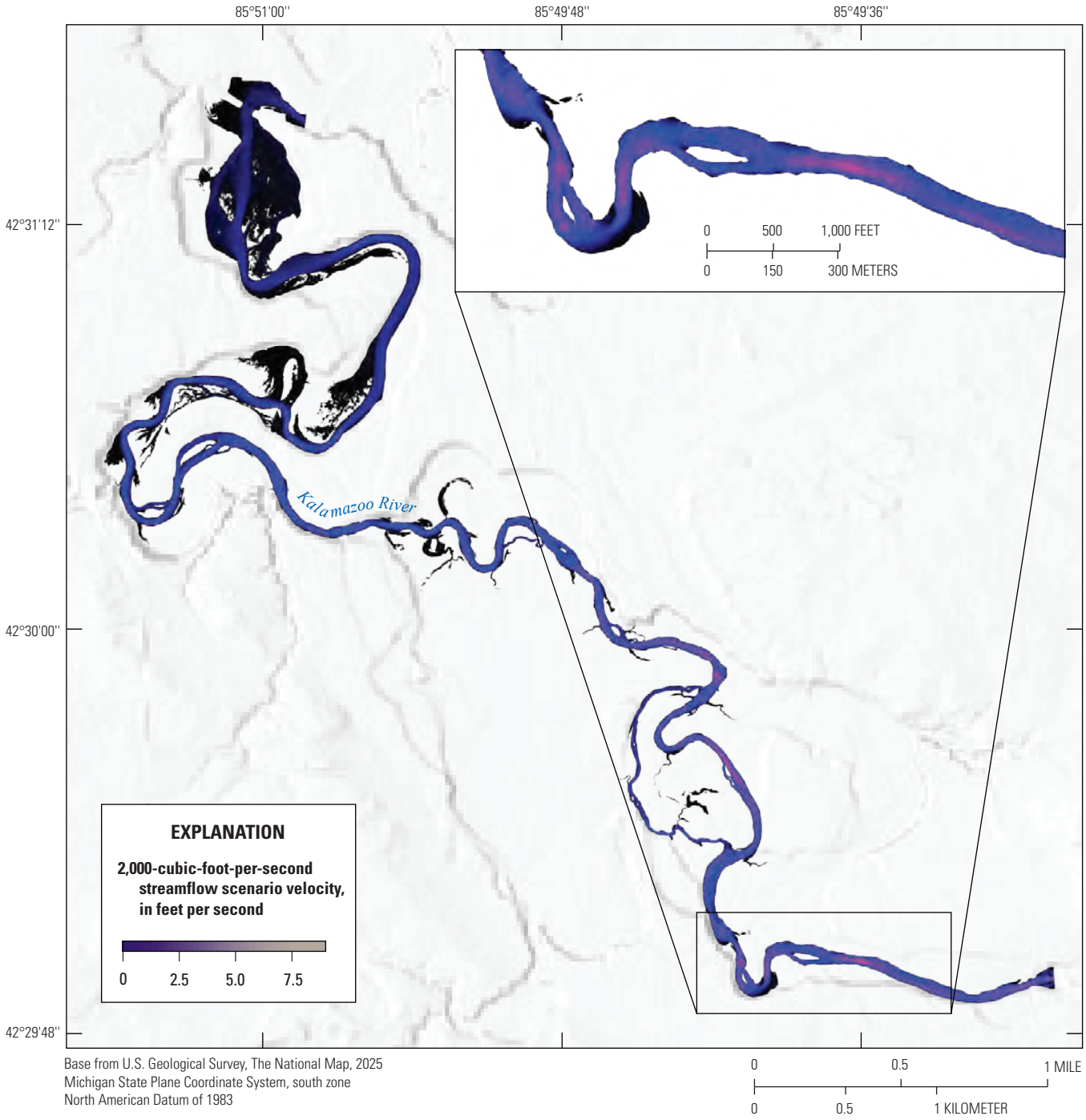

Figure 1.2. Map showing modeled velocities for the quasi-steady 2,000-cubic-foot-per-second streamflow scenario.

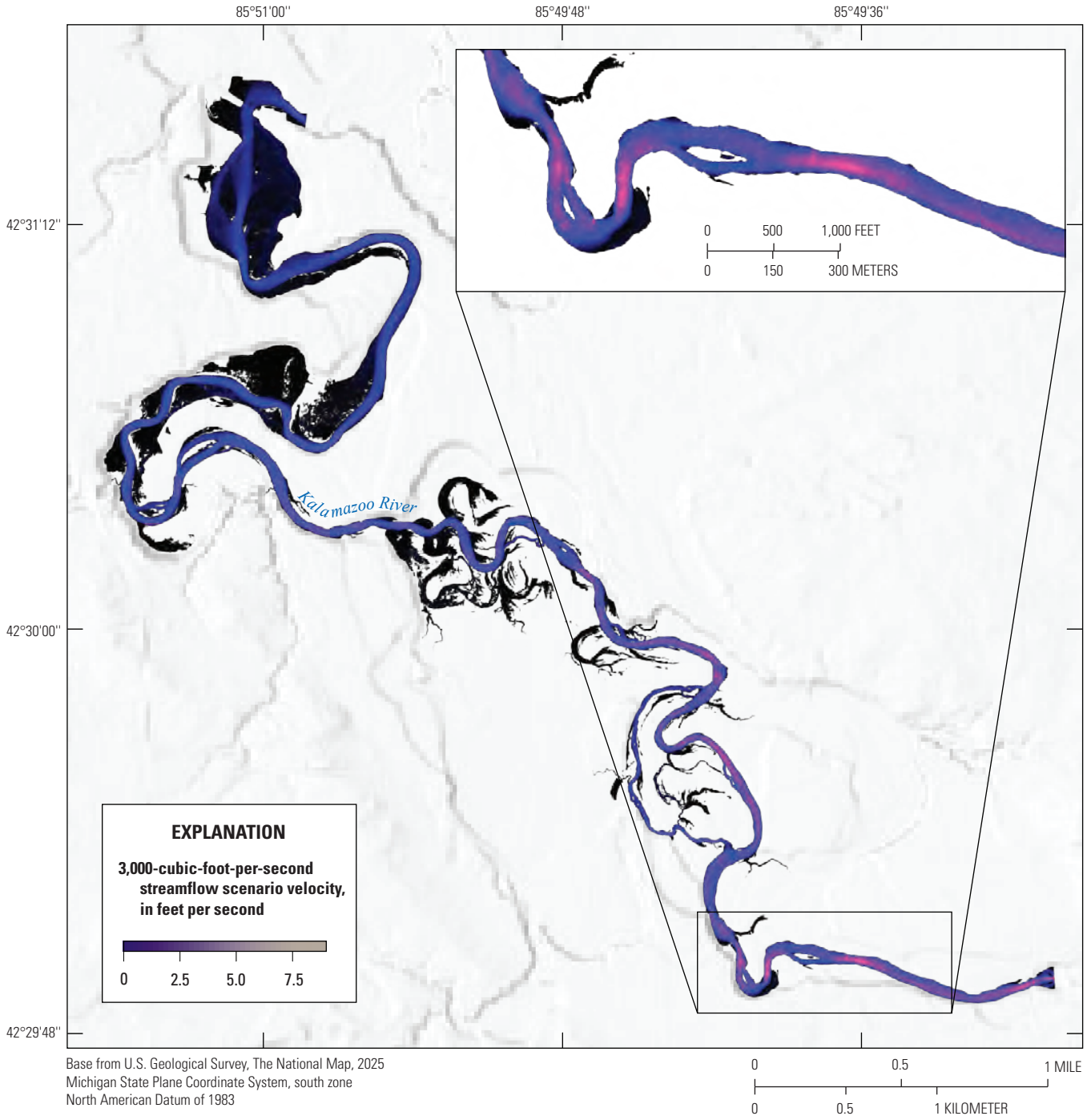

Figure 1.3. Map showing modeled velocities for the quasi-steady 3,000-cubic-foot-per-second streamflow scenario.

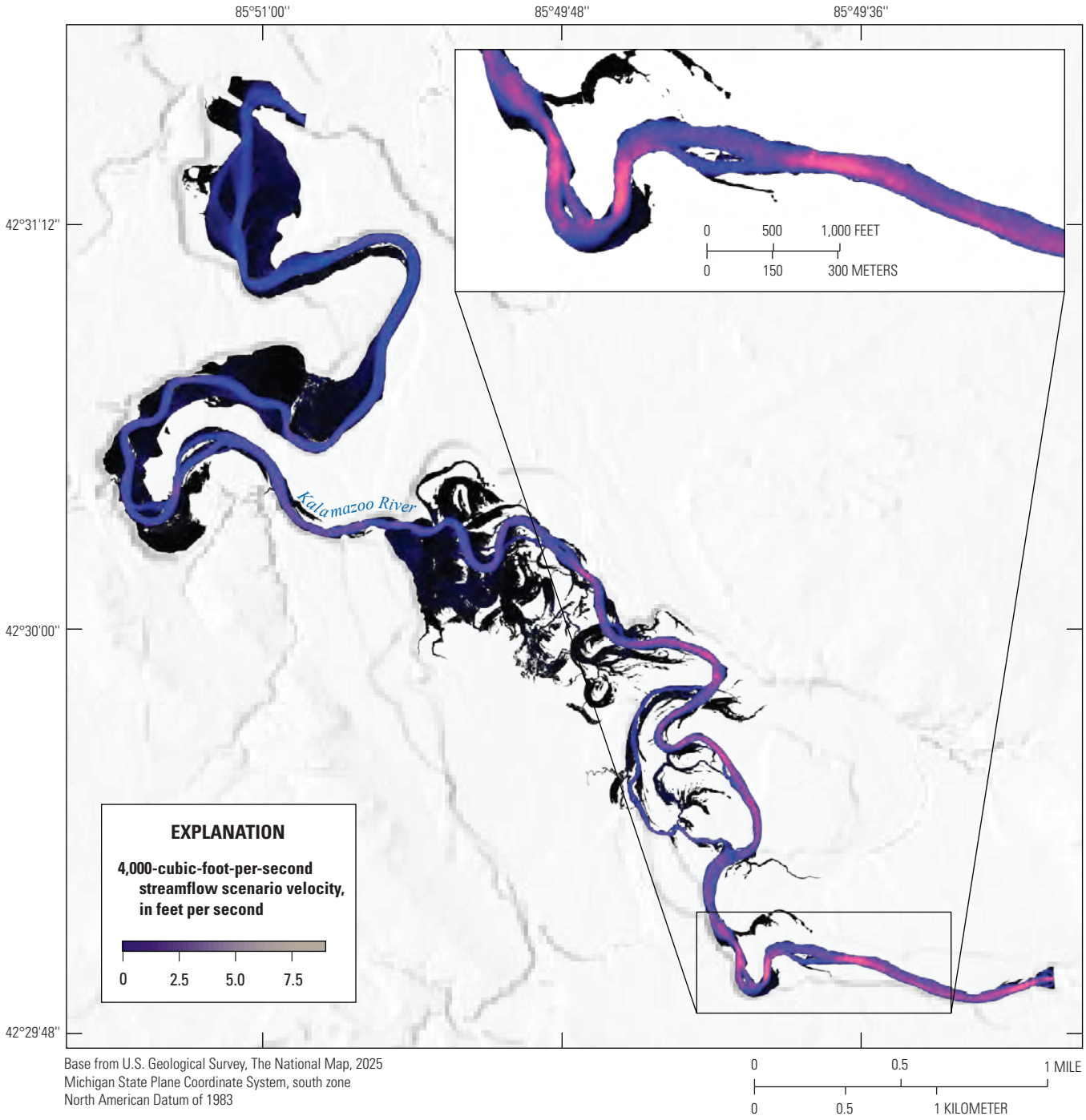

Figure 1.4. Map showing modeled velocities for the quasi-steady 4,000-cubic-foot-per-second streamflow scenario.

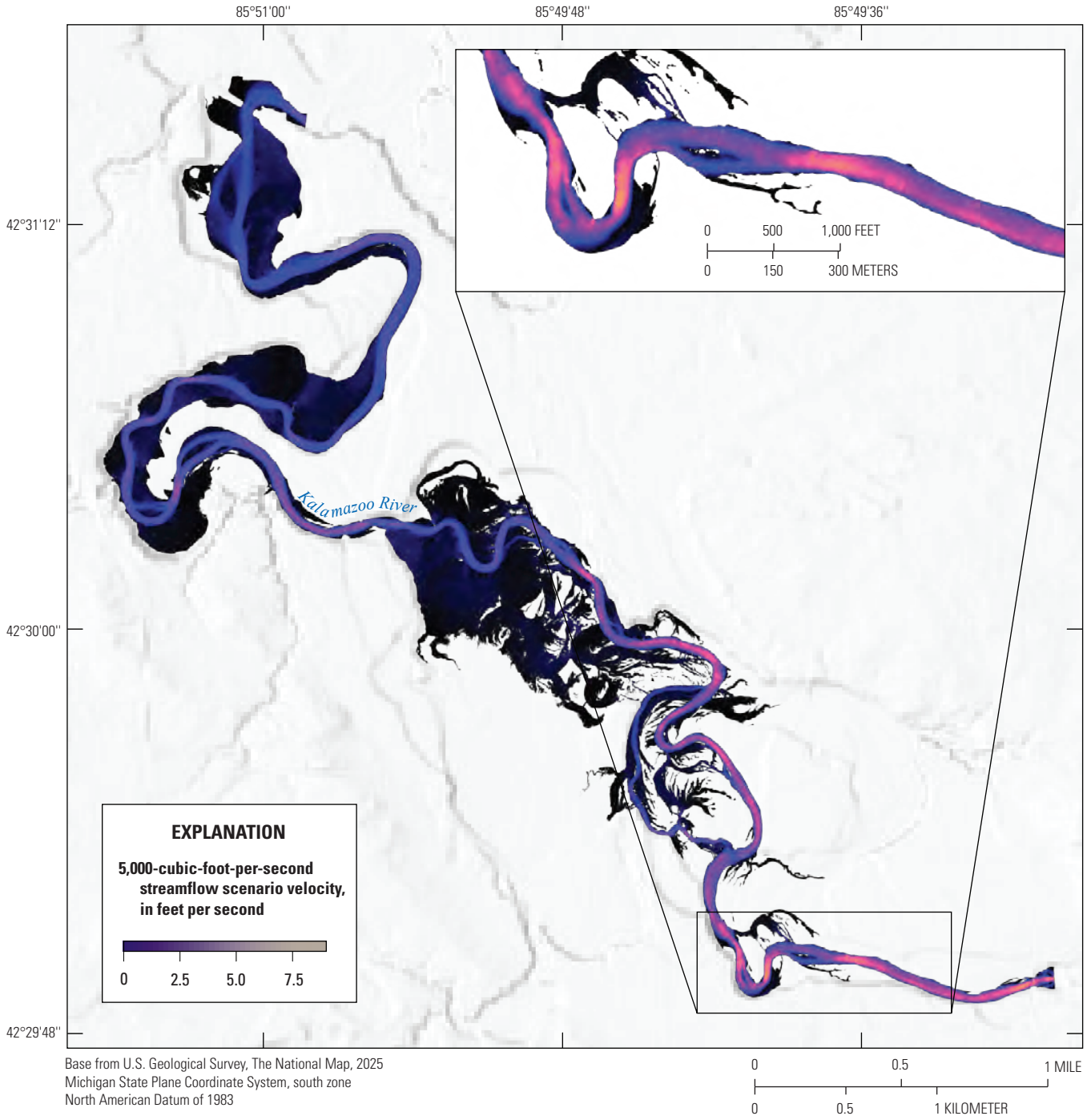

Figure 1.5. Map showing modeled velocities for the quasi-steady 5,000-cubic-foot-per-second streamflow scenario.

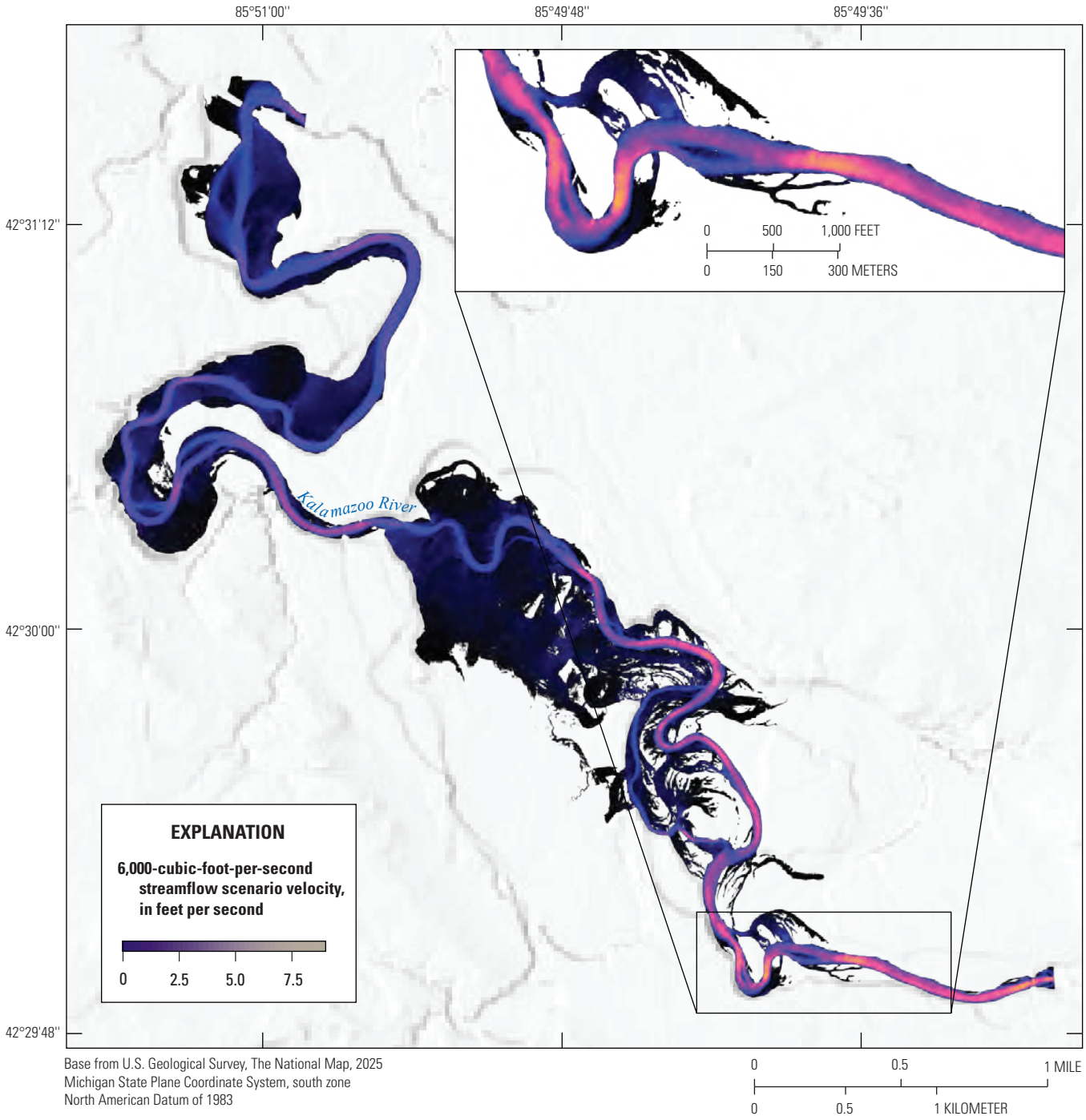

Figure 1.6. Map showing modeled velocities for the quasi-steady 6,000-cubic-foot-per-second streamflow scenario.

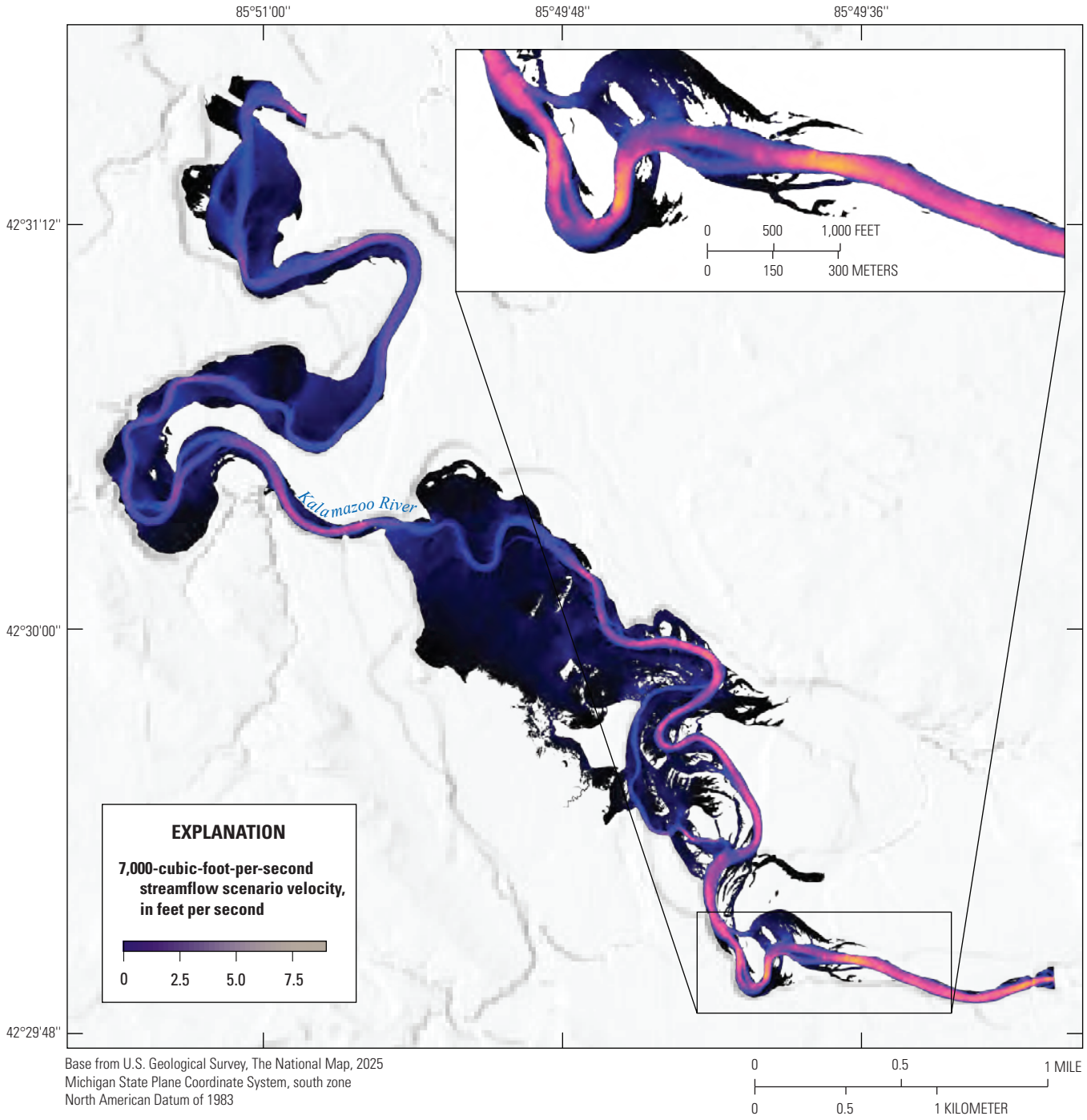

Figure 1.7. Map showing modeled velocities for the quasi-steady 7,000-cubic-foot-per-second streamflow scenario.

Appendix 2. Quasi-Steady Streamflow Scenario Depth Maps

In this appendix, maps of the modeled water depths for the quasi-steady streamflow scenarios are provided. The 1,000-, 2,000-, 3,000-, 4,000-, 5,000-, 6,000-, and 7,000-cubic-foot-per-second streamflow scenarios are shown in figures 2.1, 2.2, 2.3, 2.4, 2.5, 2.6, and 2.7, respectively.

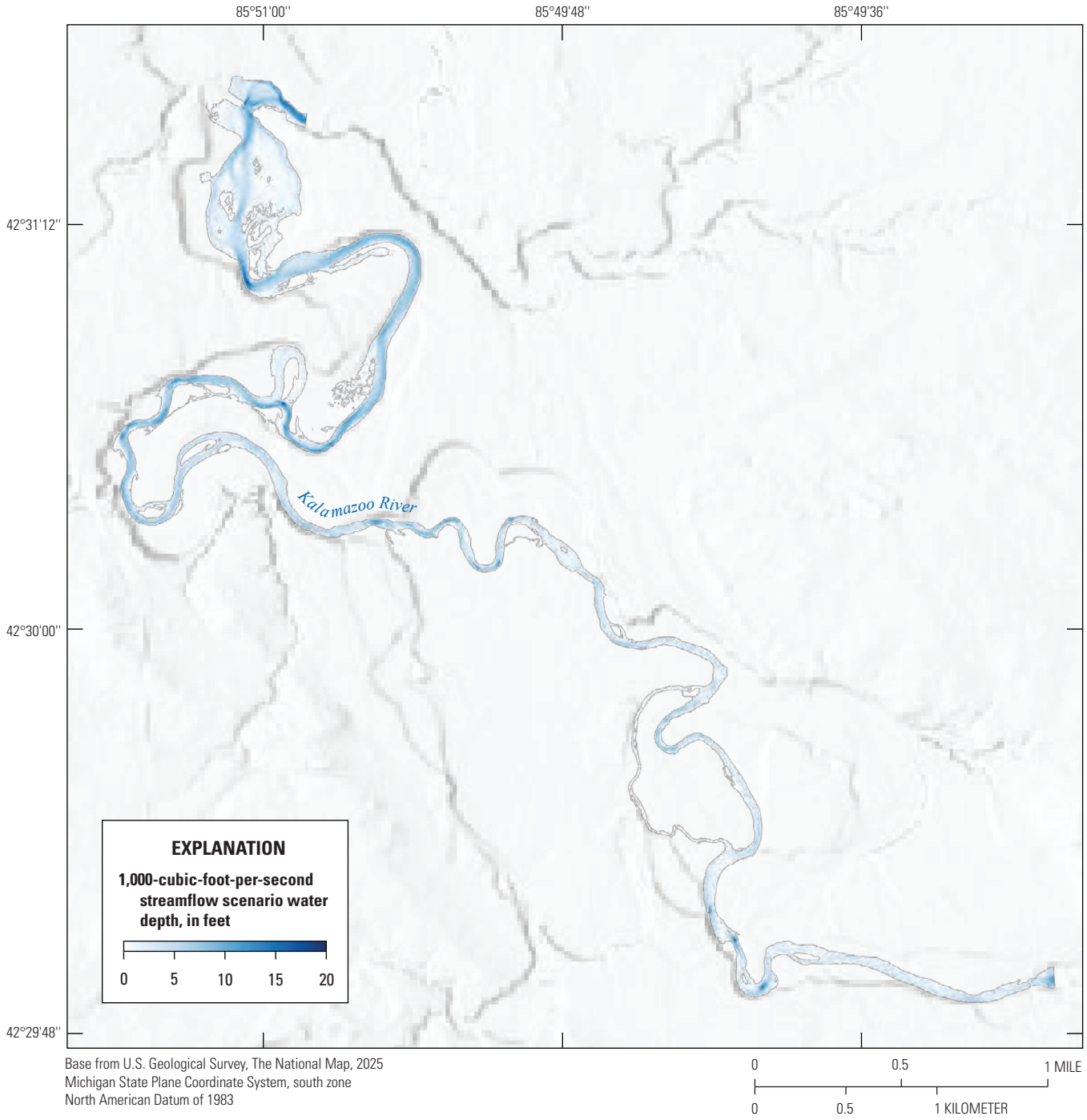

Figure 2.1. Map showing modeled water depths for the quasi-steady 1,000-cubic-foot-per-second streamflow scenario.

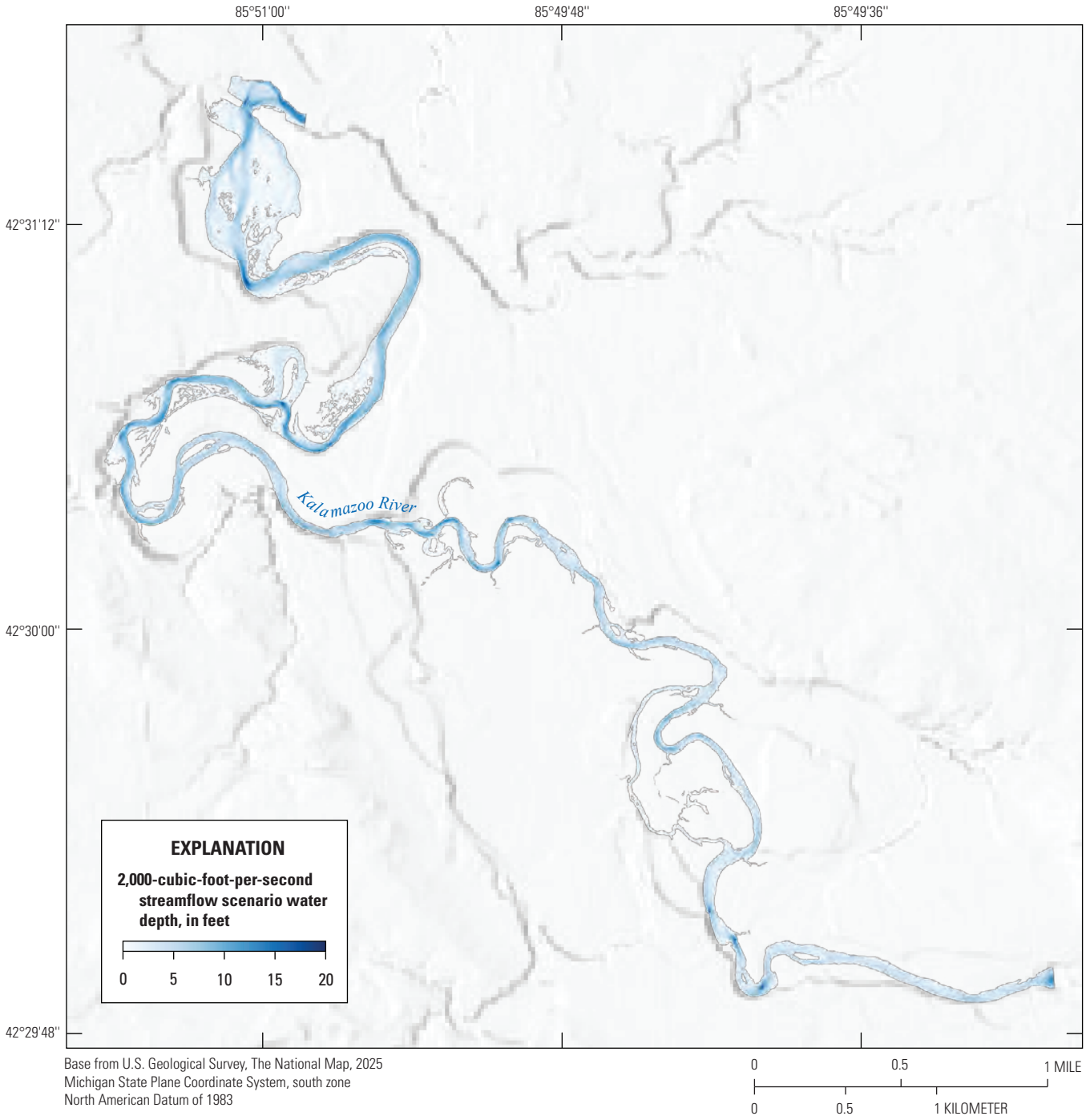

Figure 2.2. Map showing modeled water depths for the quasi-steady 2,000-cubic-foot-per-second streamflow scenario.

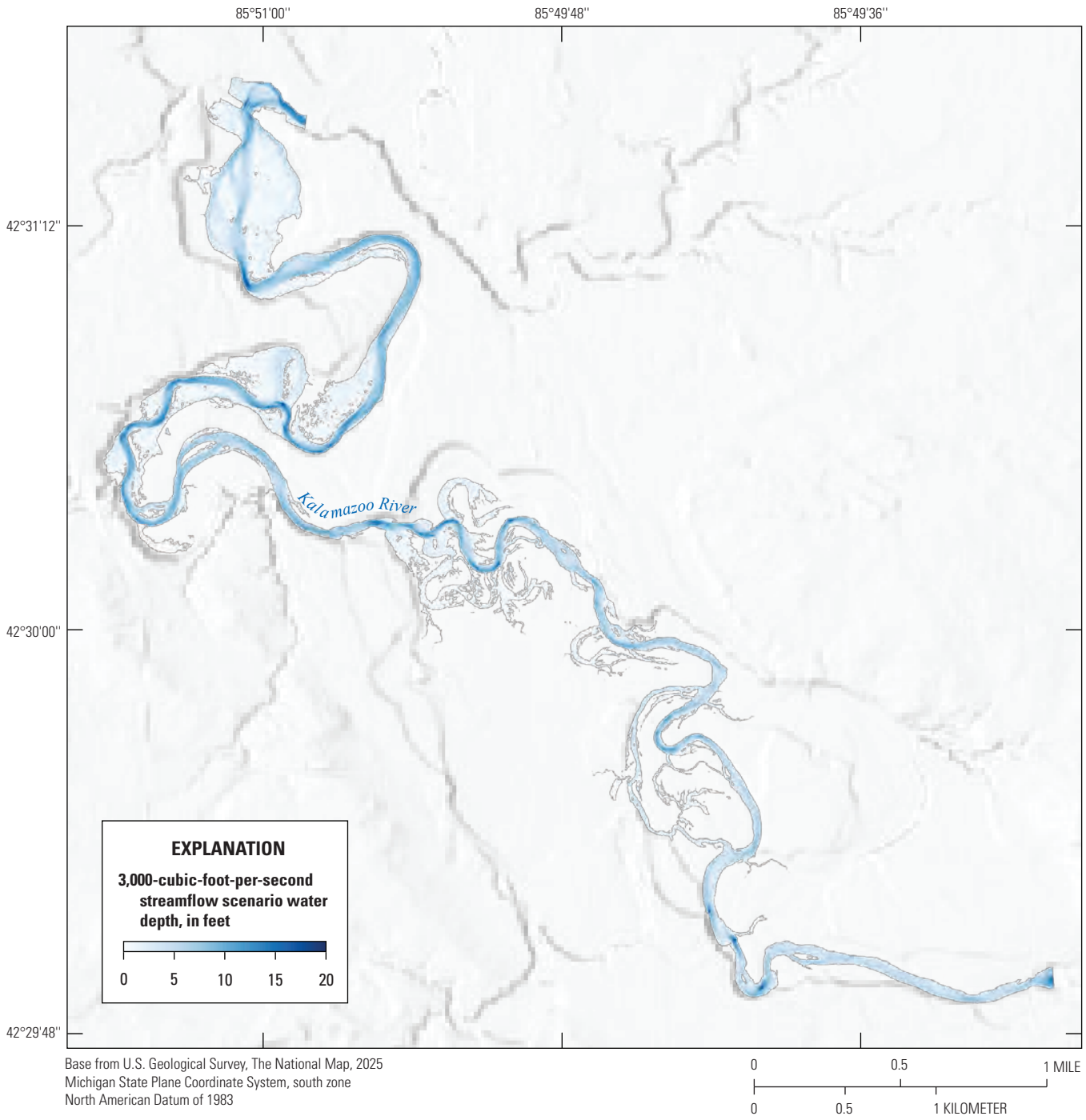

Figure 2.3. Map showing modeled water depths for the quasi-steady 3,000-cubic-foot-per-second streamflow scenario.

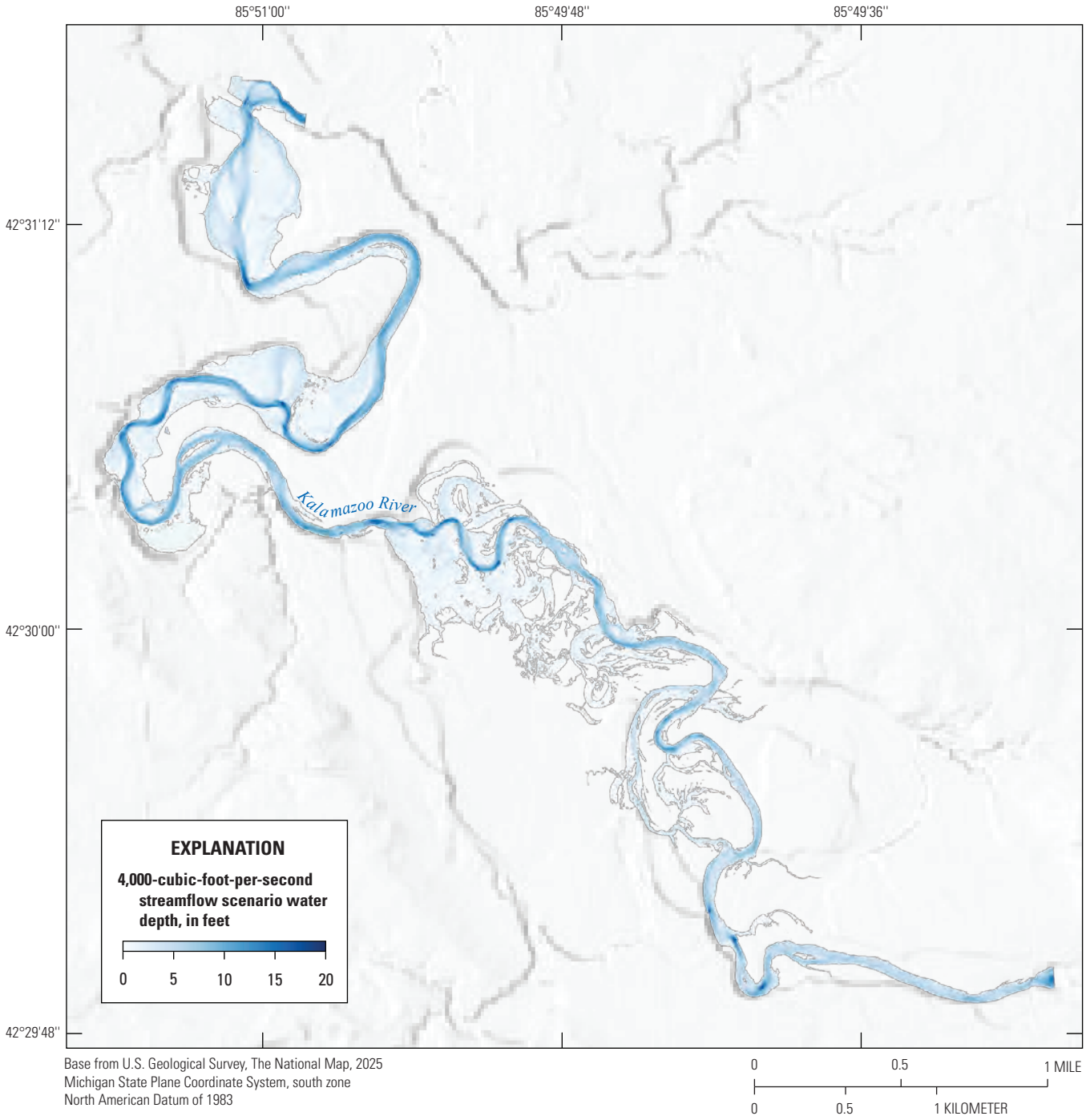

Figure 2.4. Map showing modeled water depths for the quasi-steady 4,000-cubic-foot-per-second streamflow scenario.

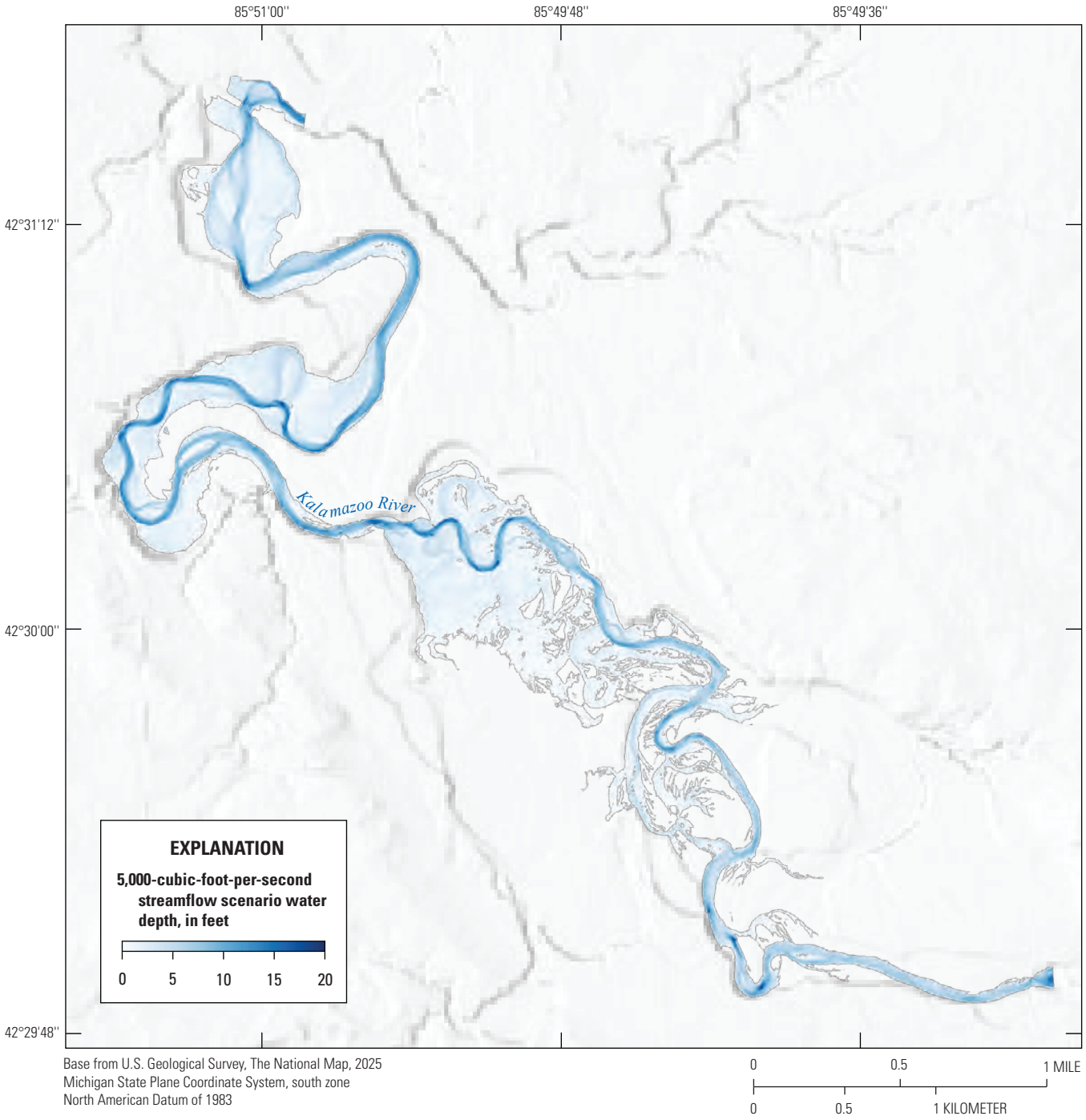

Figure 2.5. Map showing modeled water depths for the quasi-steady 5,000-cubic-foot-per-second streamflow scenario.

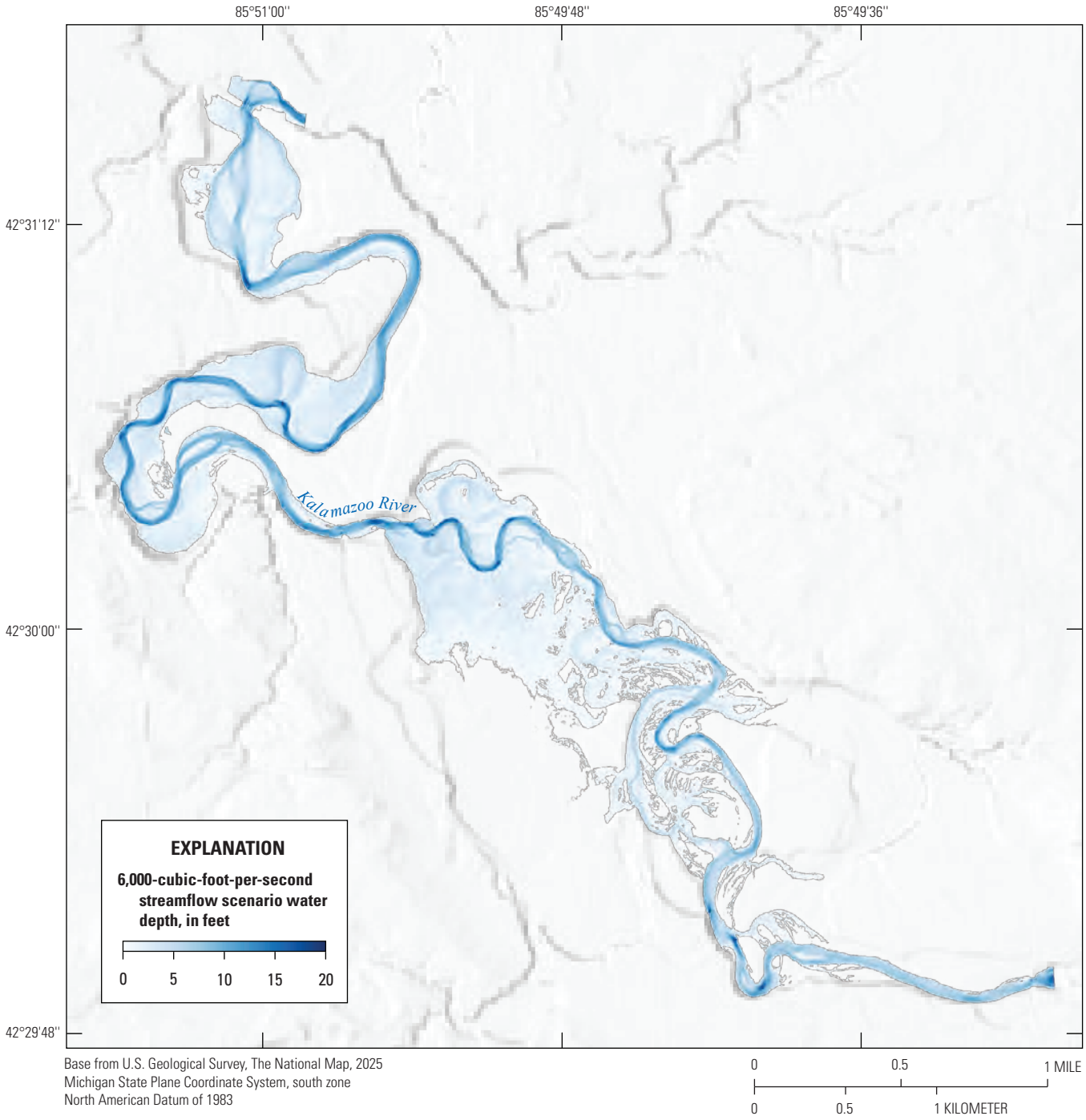

Figure 2.6. Map showing modeled water depths for the quasi-steady 6,000-cubic-foot-per-second streamflow scenario.

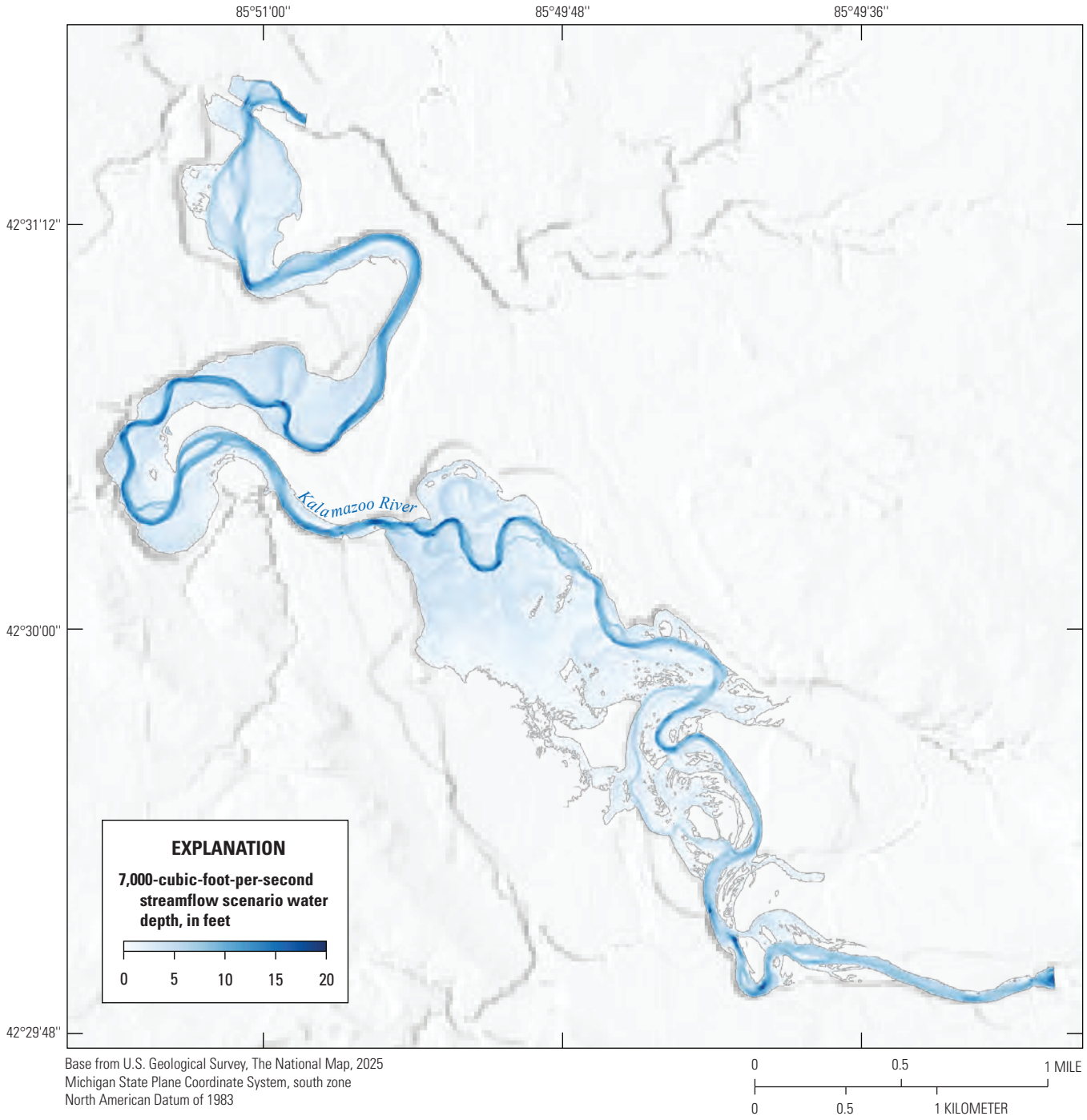

Figure 2.7. Map showing modeled water depths for the quasi-steady 7,000-cubic-foot-per-second streamflow scenario.

Appendix 3. Quasi-Steady Streamflow Scenario Basal Shear Stress Maps

In this appendix, maps of the modeled basal shear stress for the quasi-steady streamflow scenarios are provided. The 1,000-, 2,000-, 3,000-, 4,000-, 5,000-, 6,000-, and 7,000-cubic-foot-per-second streamflow scenarios are shown in figures 3.1, 3.2, 3.3, 3.4, 3.5, 3.6, and 3.7, respectively.

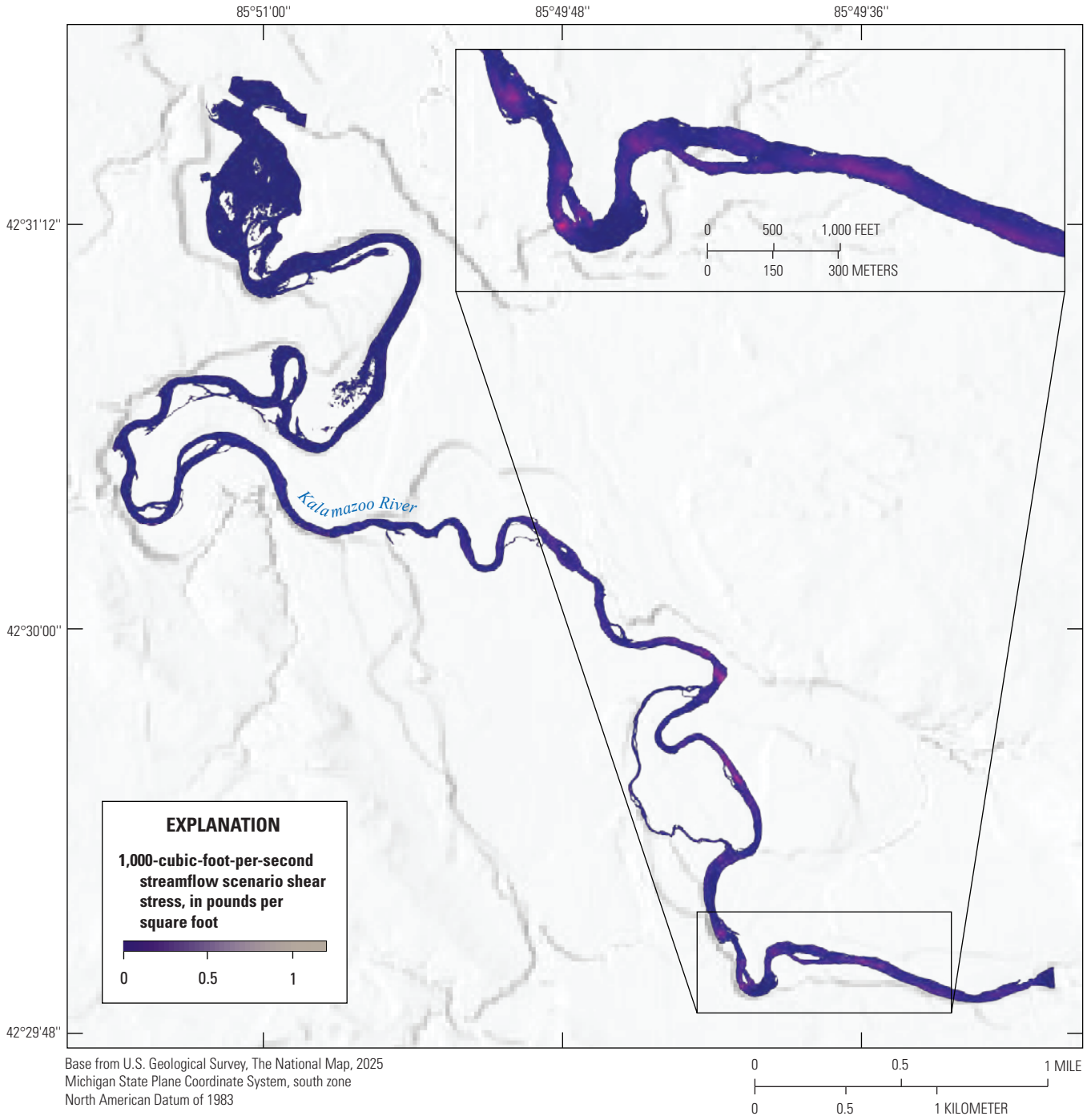

Figure 3.1. Map showing modeled basal shear stress for the quasi-steady 1,000-cubic-foot-per-second streamflow scenario.

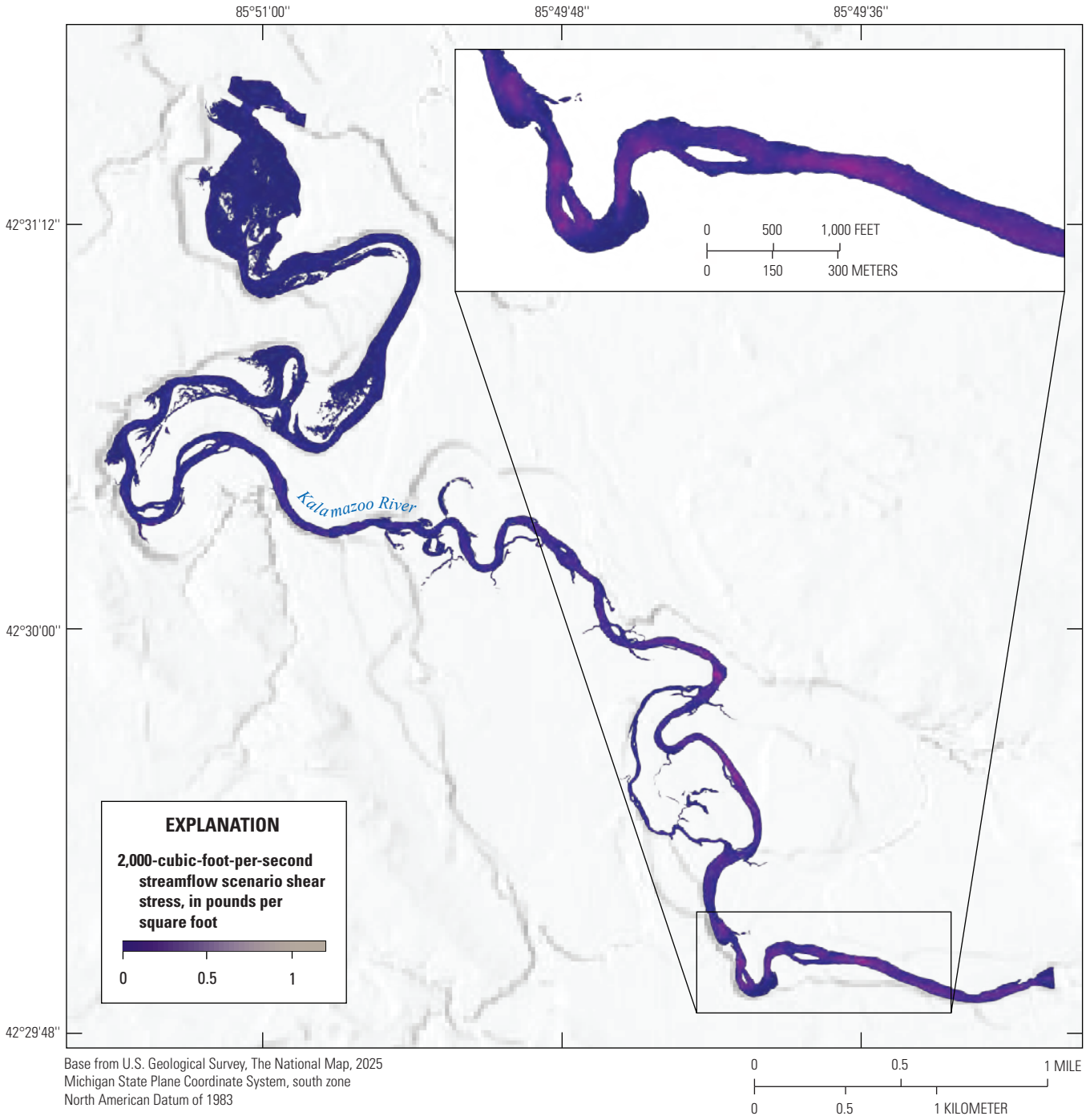

Figure 3.2. Map showing modeled basal shear stress for the quasi-steady 2,000-cubic-foot-per-second streamflow scenario.

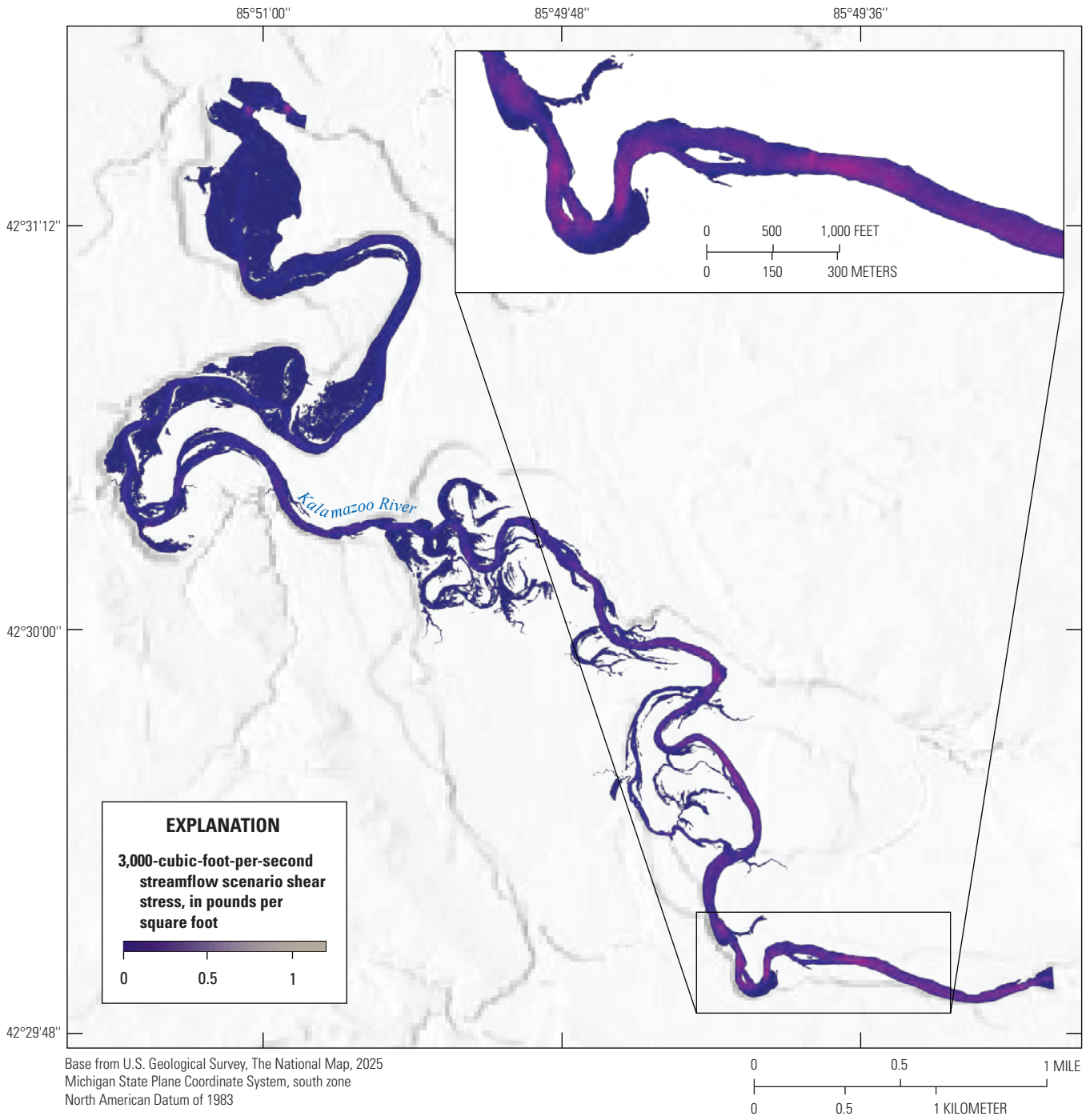

Figure 3.3. Map showing modeled basal shear stress for the quasi-steady 3,000-cubic-foot-per-second streamflow scenario.

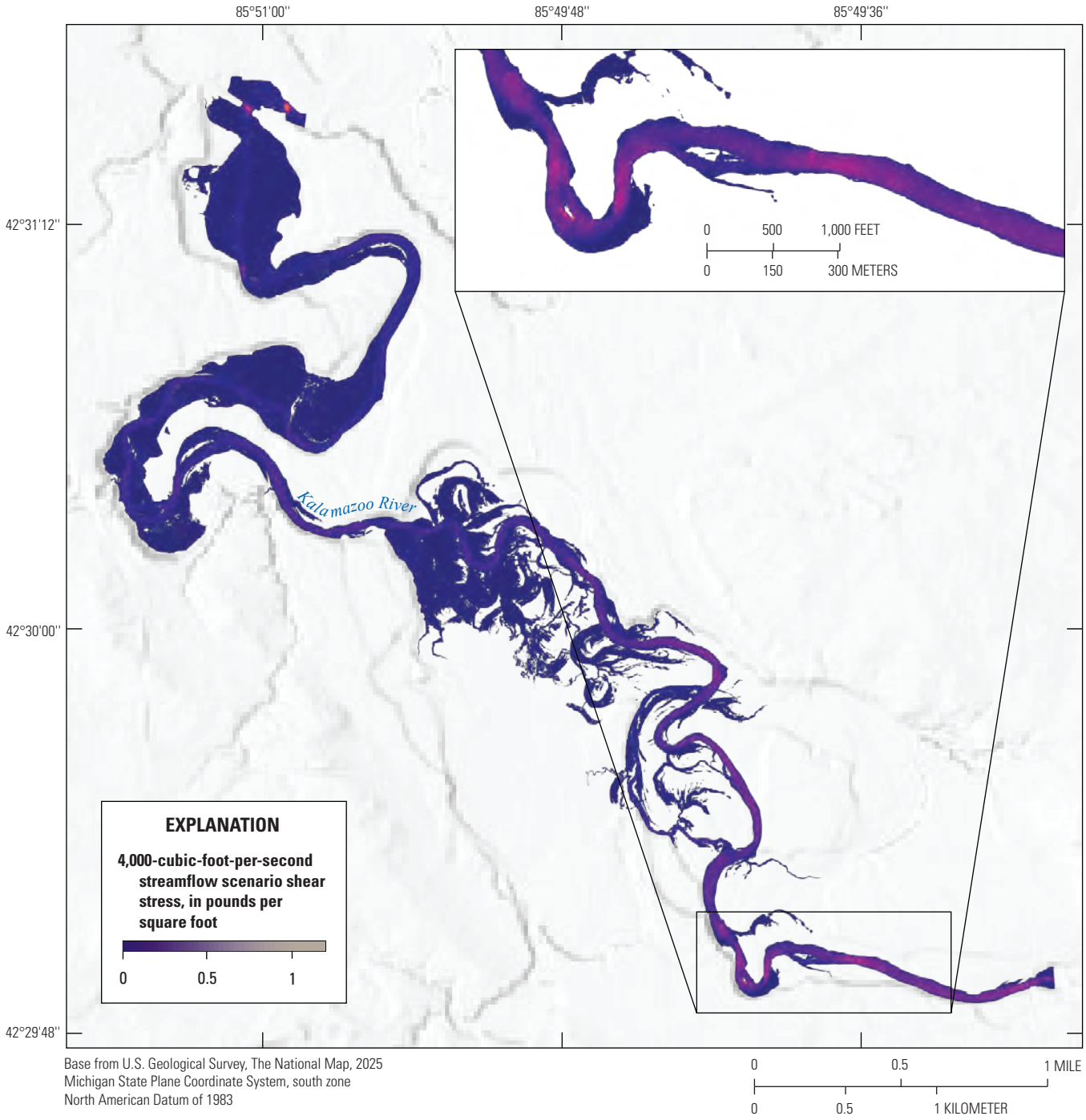

Figure 3.4. Map showing modeled basal shear stress for the quasi-steady 4,000-cubic-foot-per-second streamflow scenario.

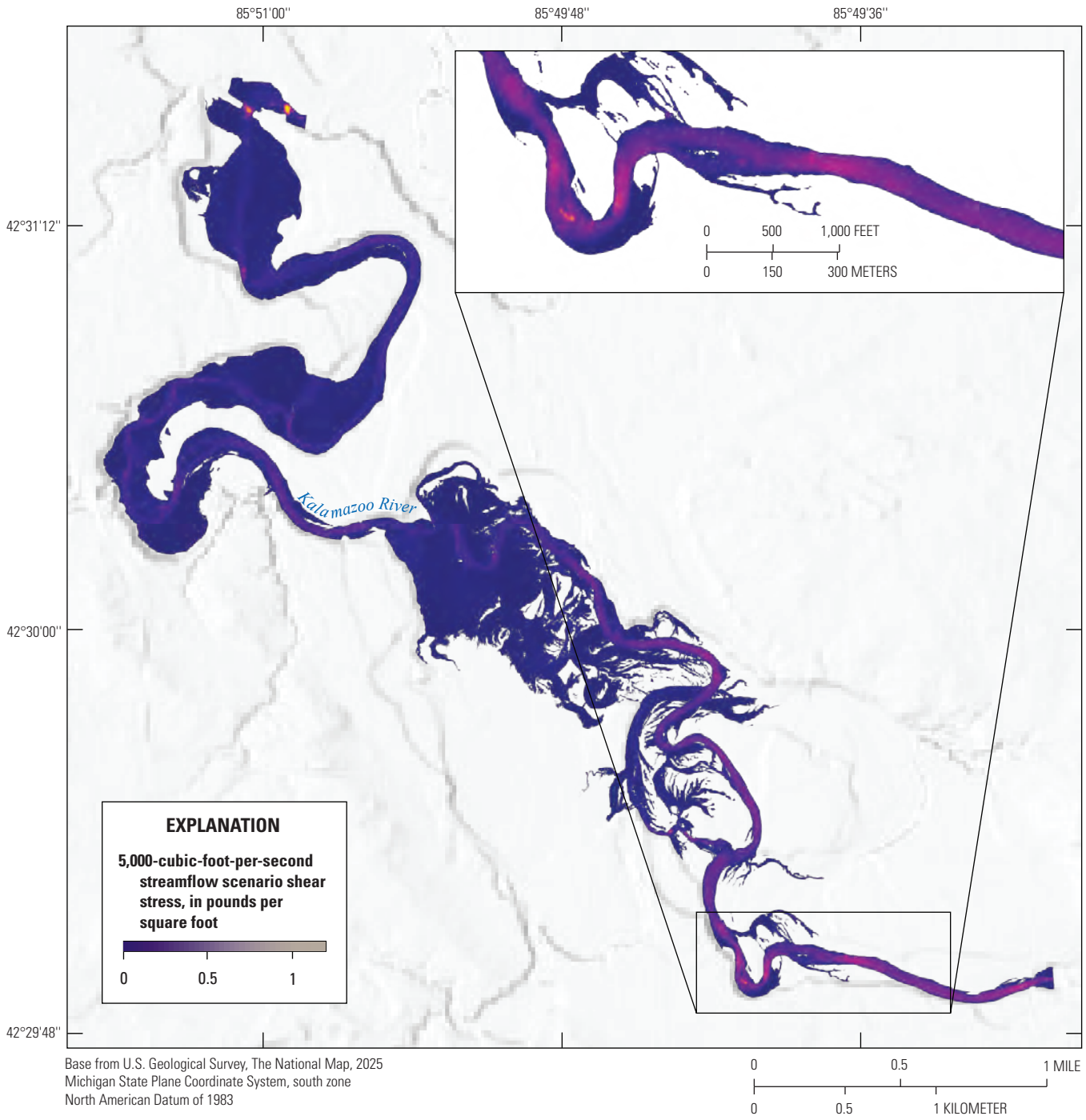

Figure 3.5. Map showing modeled basal shear stress for the quasi-steady 5,000-cubic-foot-per-second streamflow scenario.

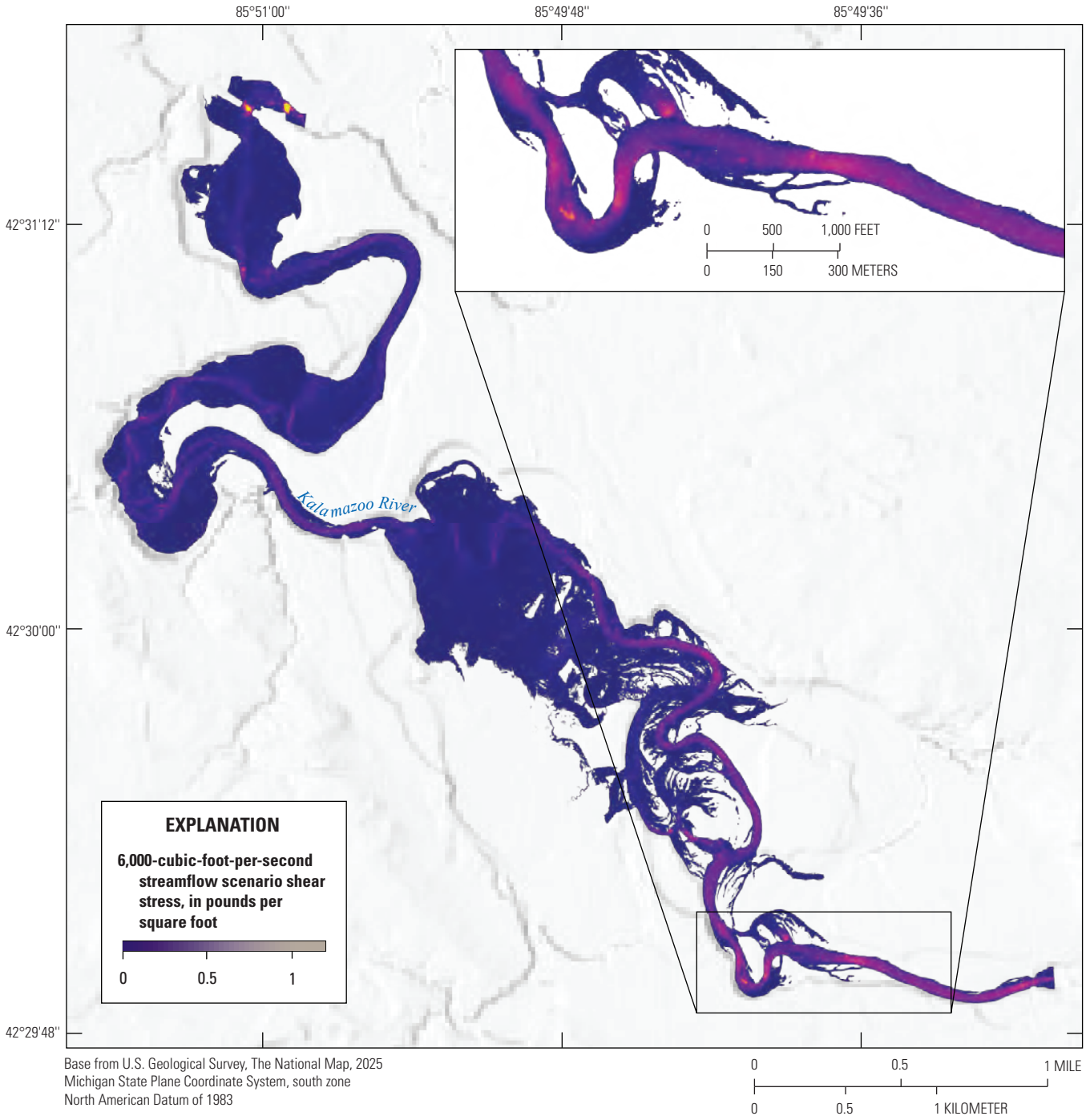

Figure 3.6. Map showing modeled basal shear stress for the quasi-steady 6,000-cubic-foot-per-second streamflow scenario.

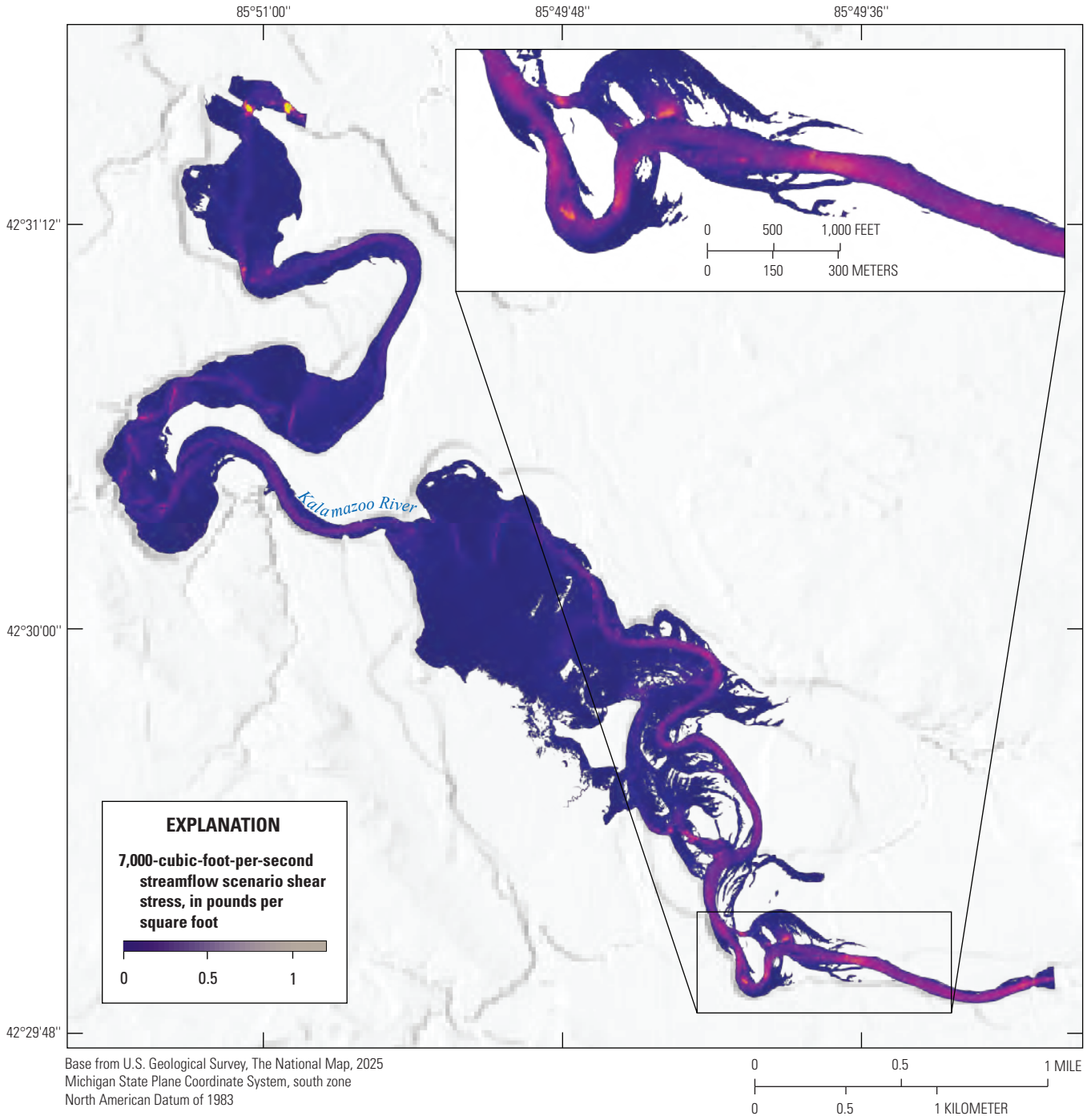

Figure 3.7. Map showing modeled basal shear stress for the quasi-steady 7,000-cubic-foot-per-second streamflow scenario.

Appendix 4. Quasi-Steady Streamflow Scenario Minimum Stable Grain Size Maps

In this appendix, maps of the modeled minimum stable grain size for the quasi-steady streamflow scenarios are provided. The 1,000-, 2,000-, 3,000-, 4,000-, 5,000-, 6,000-, and 7,000-cubic-foot-per-second streamflow scenarios are shown in figures 4.1, 4.2, 4.3, 4.4, 4.5, 4.6, and 4.7, respectively.

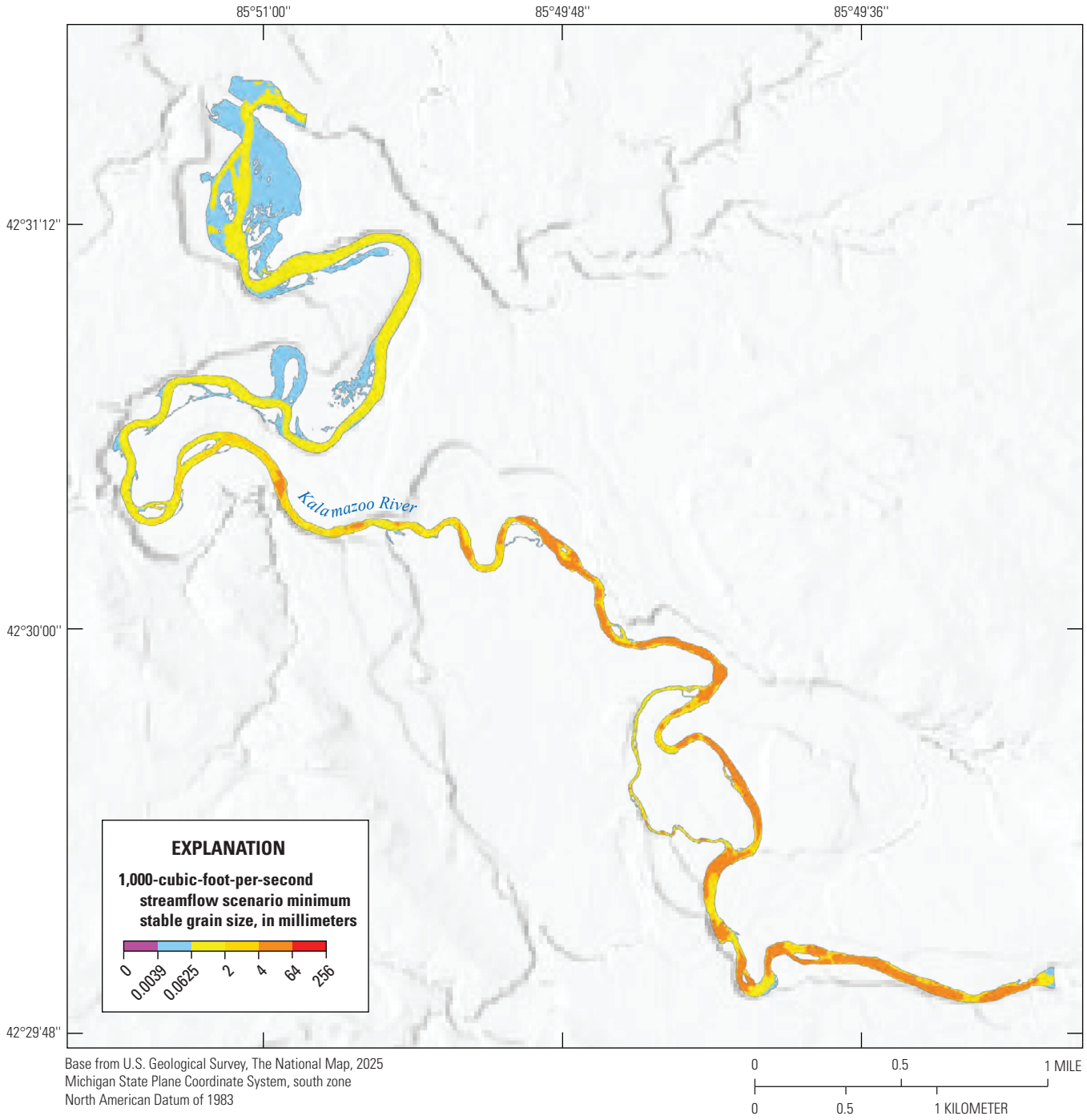

Figure 4.1. Map showing modeled minimum stable grain sizes for the quasi-steady 1,000-cubic-foot-per-second streamflow scenario.

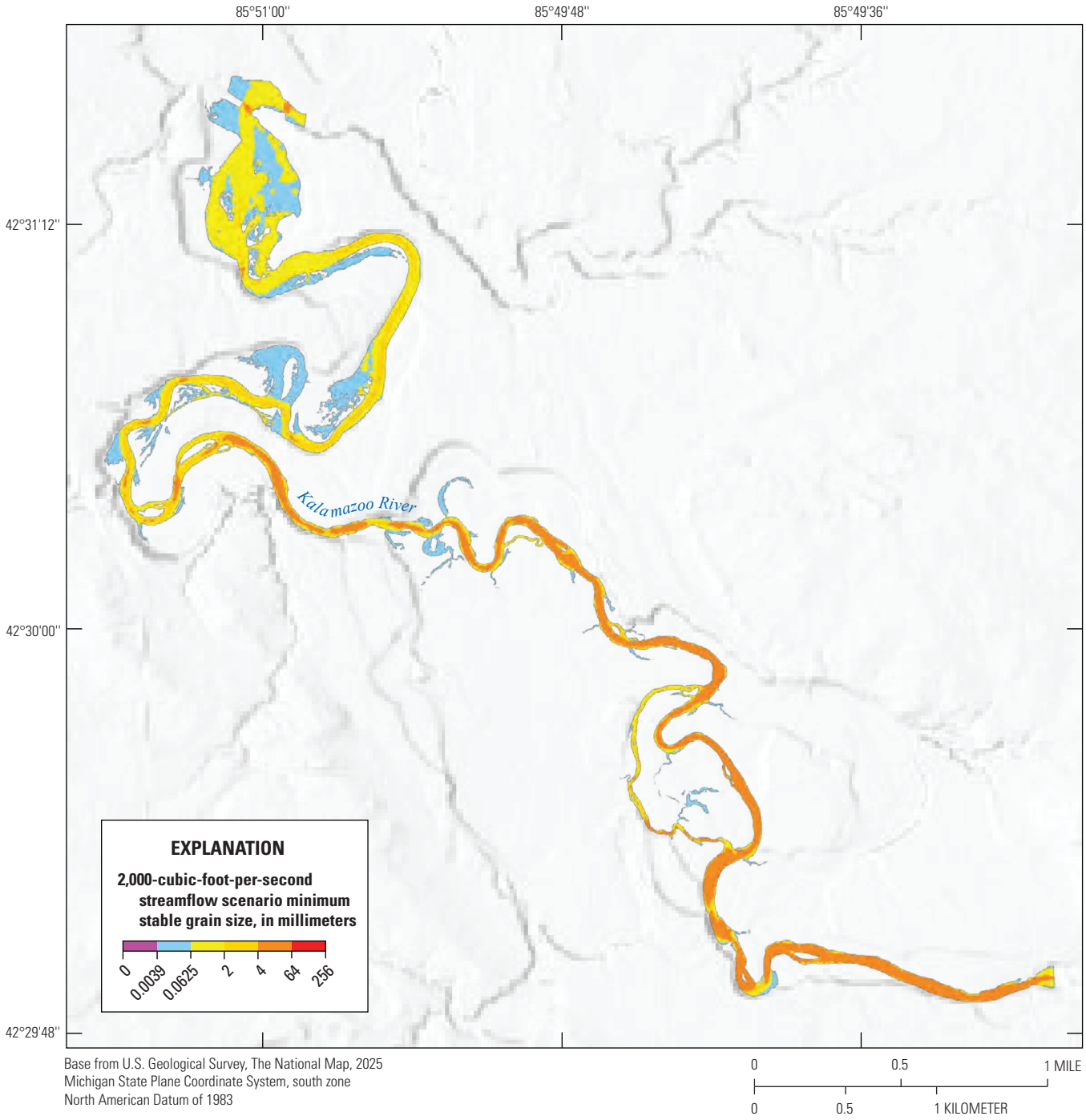

Figure 4.2. Map showing modeled minimum stable grain sizes for the quasi-steady 2,000-cubic-foot-per-second streamflow scenario.

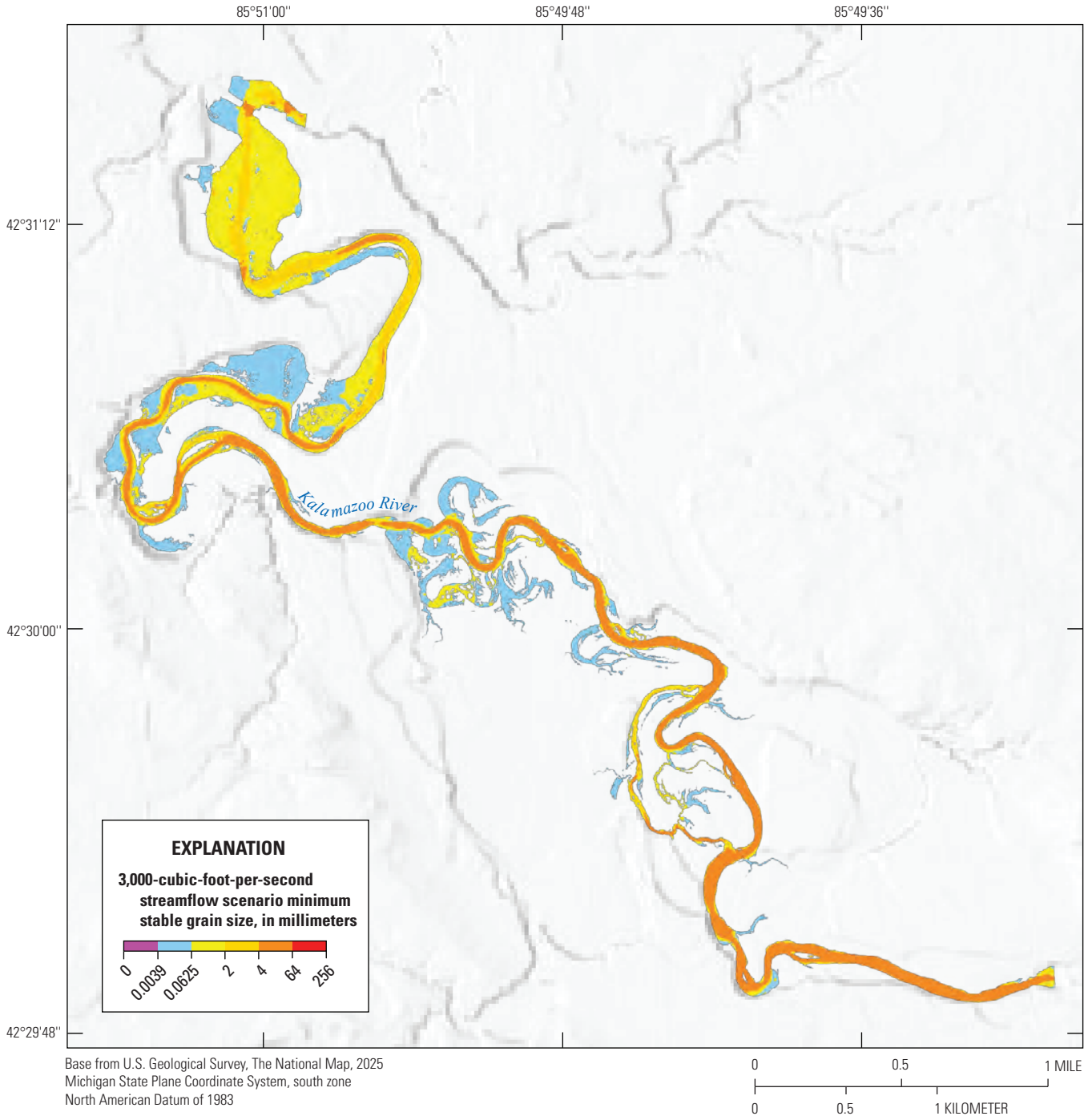

Figure 4.3. Map showing modeled minimum stable grain sizes for the quasi-steady 3,000-cubic-foot-per-second streamflow scenario.

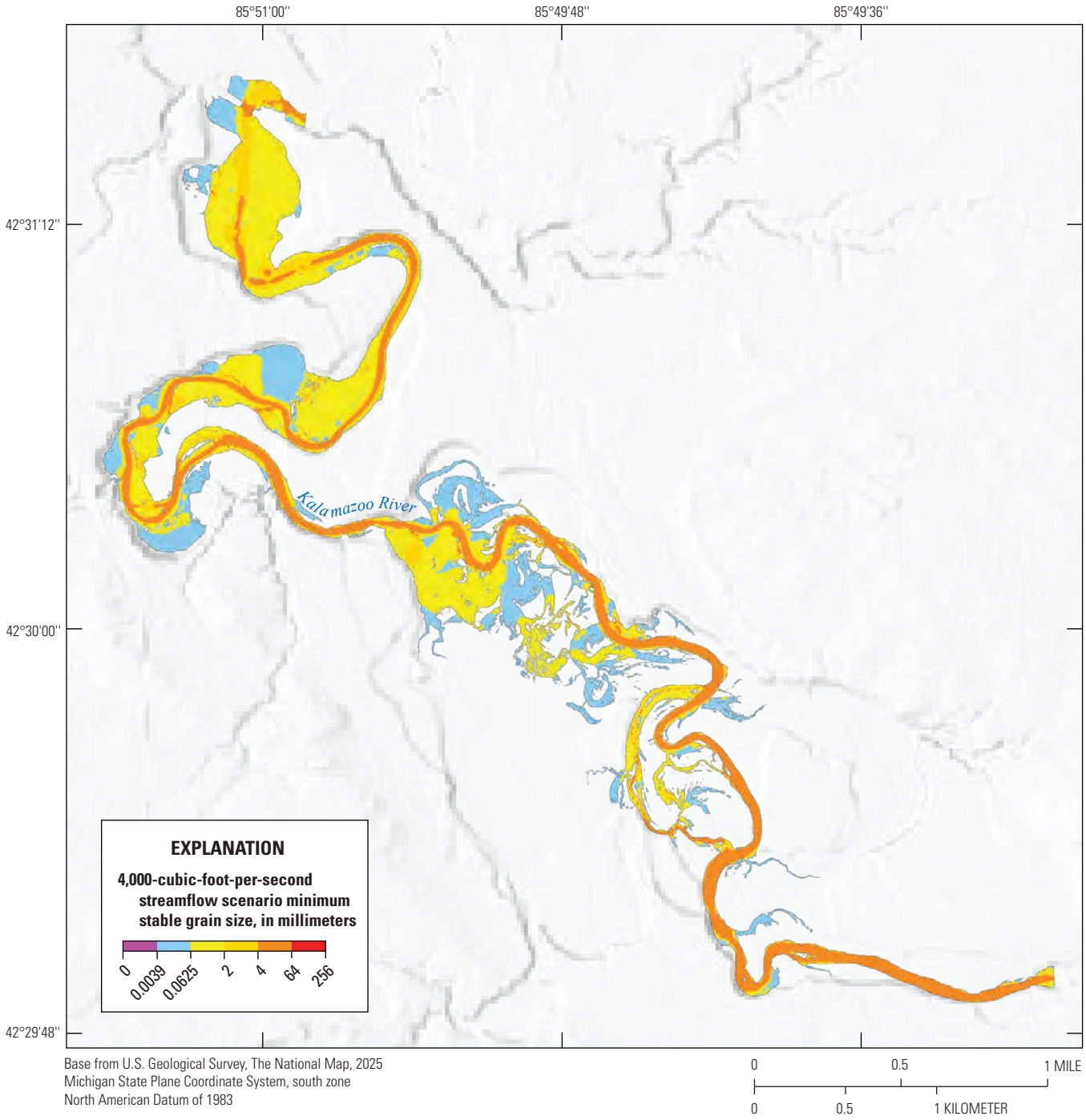

Figure 4.4. Map showing modeled minimum stable grain sizes for the quasi-steady 4,000-cubic-foot-per-second streamflow scenario.

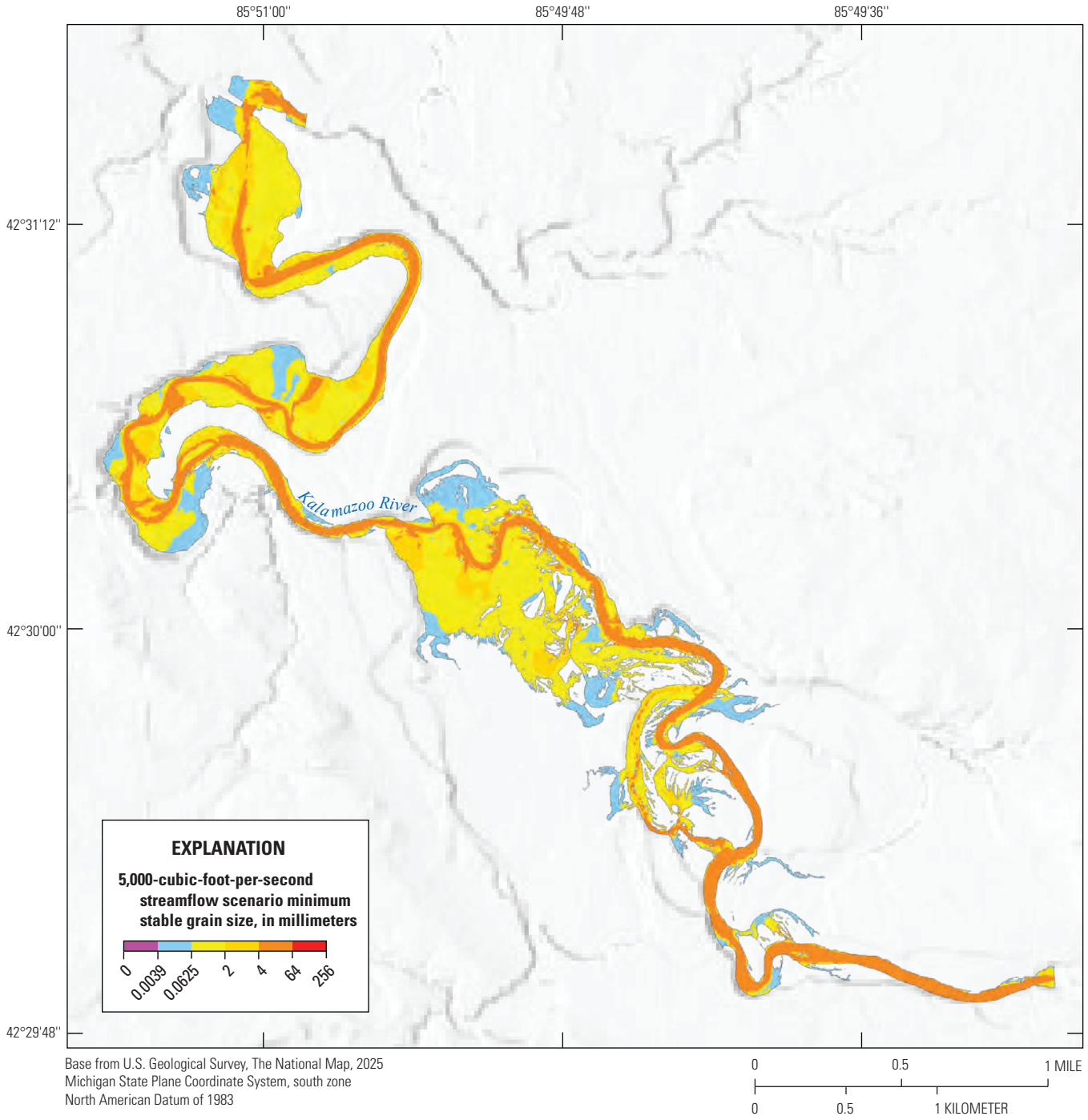

Figure 4.5. Map showing modeled minimum stable grain sizes for the quasi-steady 5,000-cubic-foot-per-second streamflow scenario.

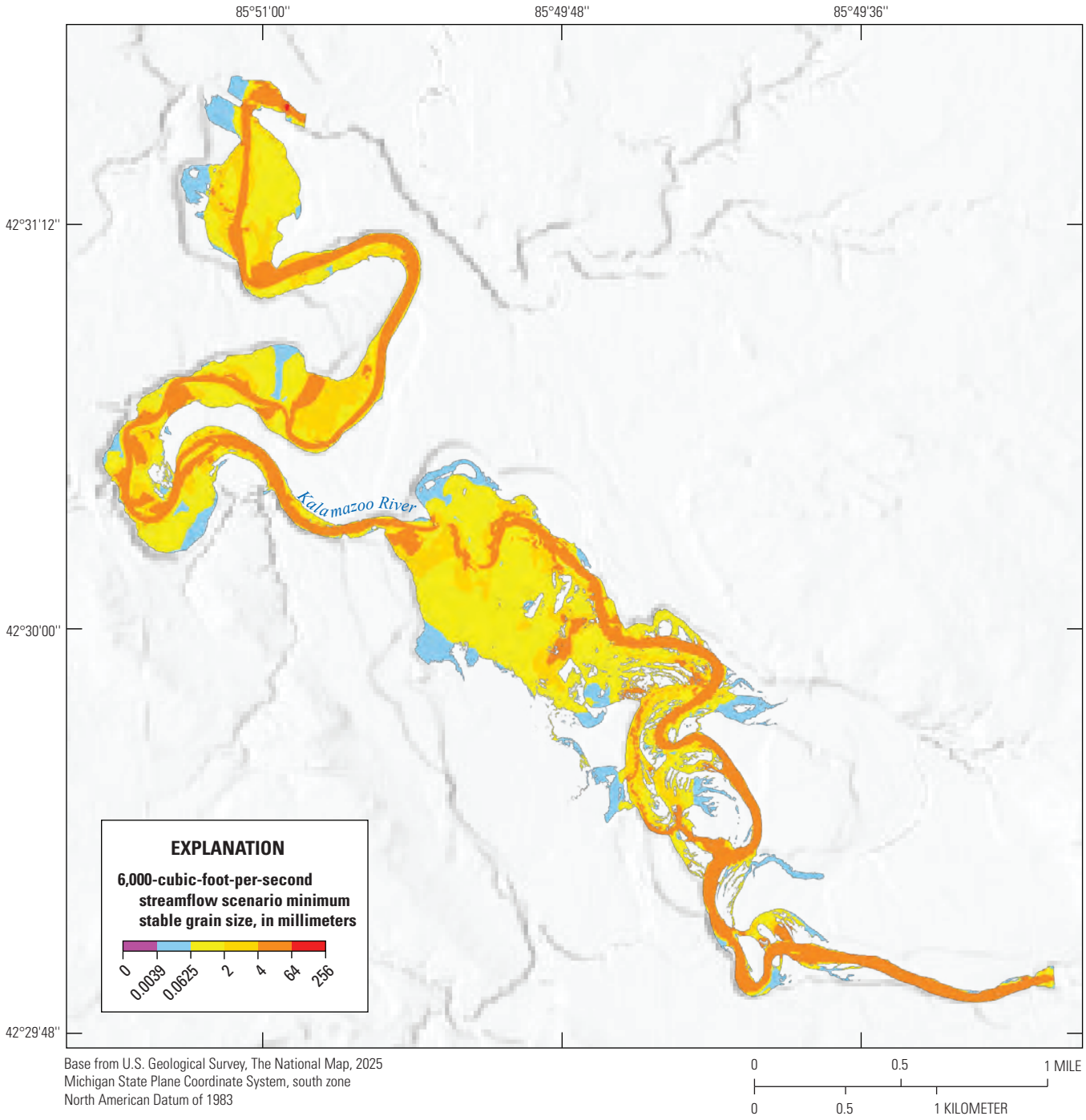

Figure 4.6. Map showing modeled minimum stable grain sizes for the quasi-steady 6,000-cubic-foot-per-second streamflow scenario.

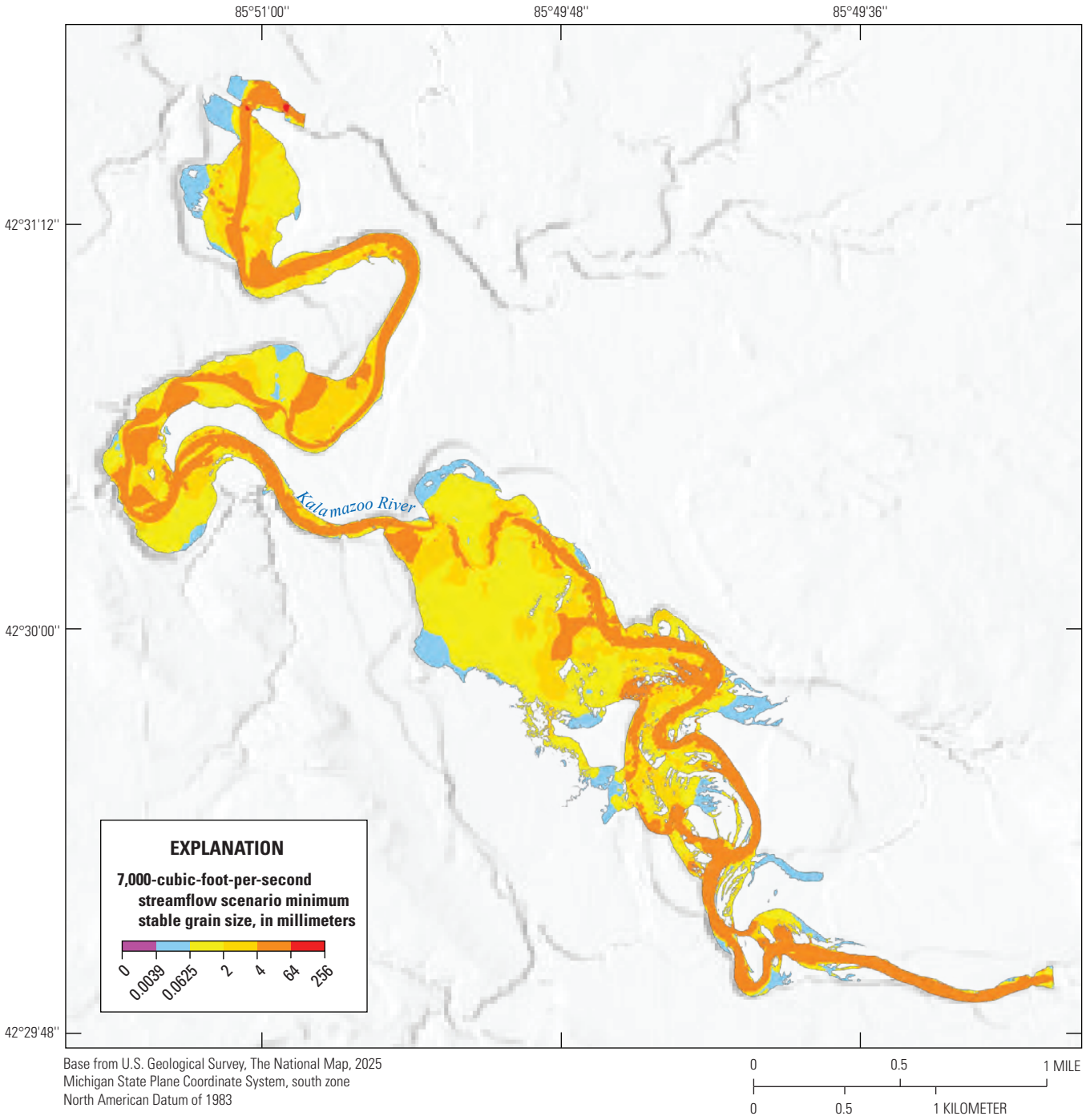

Figure 4.7. Map showing modeled minimum stable grain sizes for the quasi-steady 7,000-cubic-foot-per-second streamflow scenario.

For more information about this publication, contact:
Director, USGS Upper Midwest Water Science Center
1992 Folwell Avenue
St. Paul, MN 55108
763–783–3100

For additional information, visit: https://www.usgs.gov/centers/umid-water

Publishing support provided by the
USGS Science Publishing Network,
Rolla Publishing Service Center

USGS

Roland and others—**Development of a Two-Dimensional Hydraulic Model for the Kalamazoo River Between the Trowbridge and Allegan City Dams**—SIR 2026–5026

ISSN 2328-0328 (online)
https://doi.org/10.3133/sir20265026